CHALMERS UNIVERSITY OF TECHNOLOGY

Modeling and Comparison of Synchronous Condenser and SVC

Tarik Abdulahovic
Sercan Teleke

Examiner: Torbjörn Thiringer
Department of Energy and Environment
Electric Power Engineering Master Programme, 60p
Chalmers University of Technology, 2006
Göteborg, Sweden

Abstract

In this thesis, a synchronous condenser is modeled in PSCAD/EMTDC and compared with the PSCAD built-in model. After the model verification, a comparison between a conventional synchronous condenser and a superconducting synchronous condenser is made by simulating different cases in a grid setup. Finally, comparison between a conventional synchronous condenser, a superconducting synchronous condenser and an SVC is made in a grid setup by simulating different factors that affect the performance of reactive power compensation units.

The simulations have shown that the difference in the results between the implemented synchronous condenser model and the PSCAD built- in model was less than 5 %. Moreover, by increasing the order of the solver, more accurate results were obtained. Also, during the faults, injection of more reactive power by the superconducting synchronous condenser than the conventional synchronous condenser due to its low synchronous reactance was observed. As the SVC injects reactive power proportional to the square of its terminal voltage, during faults that cause less voltage drop on its terminals, such as the case observed in single phase to ground faults, it showed a better performance, whereas, during severe faults, such as two phase to ground and three phase to ground faults, synchronous condensers brought the load voltage to the nominal value quicker.

Preface

During the thesis, we have learned lots of valuable information about reactive power compensation. In addition to grasp working principles of synchronous condensers, details of control of an SVC was also an interesting experience to become familiar with. Also, the effect of different factors on the performance of reactive power compensation units is learned.

We would like to thank the staff of the R&D Department at ABB FACTS and especially our supervisor Jan Svensson, for their help and providing financial support for the thesis. Also, we would like to thank the staff at the Department of Electric Power Engineering, and especially our examiner Prof. Torbjörn Thiringer, for their suggestions. Moreover, we would like to thank Rob Rouse, industry marketing manager for American Superconductor Corporation, SuperMachines division, for providing figures of the superconducting synchronous condenser.

Sercan and Tarik,
Västerås,
25.10.2006

Contents

List of Figures

List of Tables

Chapter 1

Introduction

In this chapter, the aim and the structure of the thesis are explained.

1.1 Problem Overview

Reactive power compensation is an effective way to improve the utilization and stability of the electric power network. Controlled reactive power compensation can be done either by synchronous condensers which utilize synchronous generators or static voltage compensators (SVC) which utilize power electronic devices. According to the manufacturers of high-temperature superconductor (HTS) based machines, it is claimed that these newly developed HTS based machines are smaller, lighter, more efficient, and less expensive to manufacture and operate than conventional machines [1]. In addition, it is claimed that the synchronous condensers are comparable with static voltage compensators in terms of dynamic performance.

1.2 Aim

- Model a synchronous condenser and implement it into the simulation program PSCAD/EMTDC;
- Verify the implemented synchronous condenser model with the PSCAD/EMTDC built-in synchronous generator model;
- Compare the performance of a conventional synchronous condenser with a superconducting synchronous condenser;
- Compare the performance of synchronous condensers with SVCs.

1.3 Thesis structure

Chapter 2 - Literature Review: General information about reactive power compensation;

Chapter 3 - Modeling of Synchronous Condensers: State space equations for synchronous machines;

Chapter 4 - Modeling of a Static VAR Compensator: General description of the SVC and its control;

Chapter 5 - Model Implementation into PSCAD/EMTDC: Algorithms and numerical methods used for implementing the synchronous condenser into PSCAD/EMTDC;

Chapter 6 - Simulations of Synchronous Condenser: Different case studies for verification of synchronous condenser model.

Chapter 7 - Comparison of Superconducting Synchronous Condenser and Conventional Synchronous Condenser: Observing and comparing the performance of a superconducting synchronous condenser and a conventional synchronous condenser;

Chapter 8 - Comparison of SVCs and Synchronous Condensers: Observing and comparing the performance of a superconducting synchronous condenser, a conventional synchronous condenser and an SVC;

Chapter 9 - Conclusions and Suggestions: Ideas for future work.

Chapter 2

Literature Overview

In this chapter, different reactive power compensation methods are explained briefly by summarizing the literature.

2.1 Reactive power compensation

Reactive power compensation is defined as the reactive power management with the aim of improving the performance of AC power systems. The concept of reactive power compensation contains a wide and diverse field of system and customer problems, especially related with power quality issues, since most power quality problems can be attenuated or solved with an adequate control of reactive power [2]. In general, the problem of reactive power compensation is viewed from two aspects: load compensation and voltage support. In load compensation, the objectives are to increase the value of the system power factor, to balance the real power drawn from the ac supply and to eliminate current harmonic components produced by large and fluctuating nonlinear industrial loads [3], [4]. Voltage support is generally required to reduce voltage fluctuation at a given terminal of a transmission line [2]. Reactive power compensation in transmission systems also improves the stability of the AC system by increasing the maximum active power that can be transmitted. It also helps to maintain a substantially flat voltage profile at all levels of power transmission, it improves high-voltage DC (HVDC) conversion terminal performance, increases transmission efficiency, controls steady-state and temporary over-voltages [5], and helps to avoid catastrophic blackouts [6], [7].

Series- and shunt-reactive power compensation are used to modify the electrical characteristics of AC power systems. Series compensation modifies transmission or distribution system parameters, while shunt compensation changes the equivalent impedance of the load [2], [8]. In both cases, the reactive power that flows through the system can be effectively controlled to improve the performance of the overall AC power system.

Traditionally, for reactive power compensation, synchronous condensers and fixed or mechanically switched capacitors or inductors have been used. However, static VAr compensators (SVCs) employing thyristor-switched capacitors (TSCs) and thyristor-controlled reactors (TCRs) to provide or absorb the required reactive power have been developed [8]-[10]. Also, the use of self-commutated pulse-width modulated (PWM) converters with a suitable control scheme permits the implementation of static compensators capable of generating or absorbing reactive current components with a time response faster than the fundamental power network cycle [11]-[13].

Based on the use of reliable high-speed power electronics, powerful analytical tools, advanced control and microcomputer technologies, flexible AC transmission systems (FACTS) have been developed and represent a new concept for the operation of power transmission systems [14], [15]. In these systems, the use of SVCs with fast response times play an important role, allowing to increase the amount of apparent power transfer through an existing line, close to its thermal capacity, without compromising its stability limits. These opportunities arise through the ability of special SVCs to adjust the parameters that govern the operation of transmission systems, including shunt impedance, current, voltage, phase angle and damping of oscillations [16].

2.1.1 Reactive power compensation principles

In general, the reactive power is defined as the AC component of the instantaneous power. The reactive power generated by the source is stored in a capacitor or a reactor during a quarter of a cycle, and in the next quarter, it is sent back to the power source. In other words, the reactive power oscillates between the source and the capacitor or reactor, and also between them, at a frequency that equals to two times the rated grid frequency. For this reason it can be compensated using reactive power generators, avoiding its circulation between the load (inductive or capacitive) and the source, and hence, improving voltage stability of the power system. Reactive power compensation can be implemented with reactive power generators connected in parallel or in series with the grid.

The principles of both shunt and series-reactive power compensation techniques are described below.

Shunt compensation

Figure 2.1 shows principles and theoretical effects of shunt reactive power compensation in a basic AC system, which comprises a voltage source U_1, a power line, and a typical inductive load.

Figure 2.1 a) shows the system without compensation and its related phasor diagram. In the phasor diagram, the phase angle of the current has been related to the load side, which means that the active current I_{P} is in phase with the load voltage U_2. Since the load is assumed inductive, it requires reactive power for proper operation that the source must supply. This is done by increasing the current from the generator and through the power lines. If reactive power is supplied near the load, the line current can be reduced or minimized, resulting in less power losses and improving voltage regulation at the load terminals.

In Figure 2.1 b), a shunt-connected current source is being used to compensate the reactive component of the load current (I_{Q}). As a result, the system voltage regulation is improved and the reactive current component from the source is abated or almost eliminated.

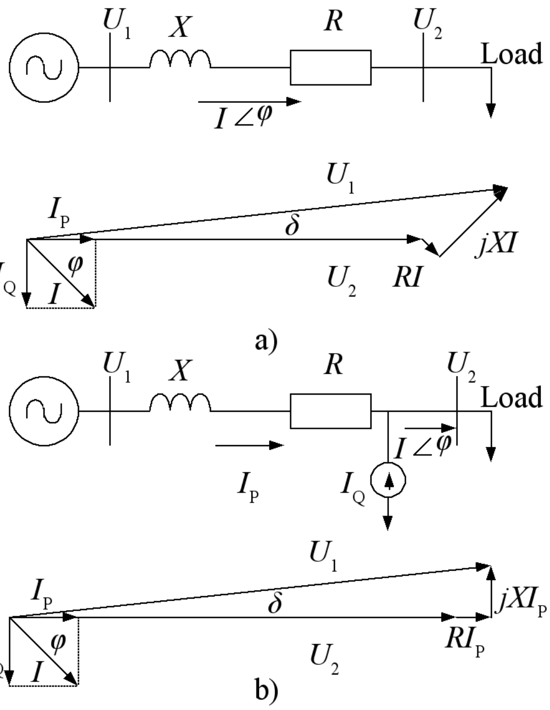

Figure 2.1: Principles of shunt compensation in a radial AC system. a)Without reactive compensation. b) Shunt compensation with a current source I_{Q}.

Series compensation

Reactive power compensation can also be of series type. Typical series compensation systems use capacitors to decrease the equivalent reactance of a power line at rated grid frequency. The connection of a series capacitor generates reactive power that balances a fraction of the line's transfer reactance. The result is an improved operation of the power transmission system through:

- increased angular stability;
- improved voltage stability;
- optimized power sharing between parallel circuits.

Figure 2.2 a) shows the same power system as in Figure 2-1 a), with the reference voltage U_2. Figure 2.2 b) shows results obtained with the series compensation through a voltage source that has been adjusted to have a unity power factor operation at U_2. However, the compensation strategy is different compared to the shunt compensation. In this case, voltage U_{COMP} has been added between the line and the load to change the angle of U_2', which represents now the voltage at the load side. With the appropriate magnitude adjustment of U_{COMP}, unity power factor can be reached at U_2. As it is seen from the phasor diagram of Figure 2.2 b), U_{COMP} generates a voltage with the opposite direction to the voltage drop in the line inductance since it lags the current I_{P}.

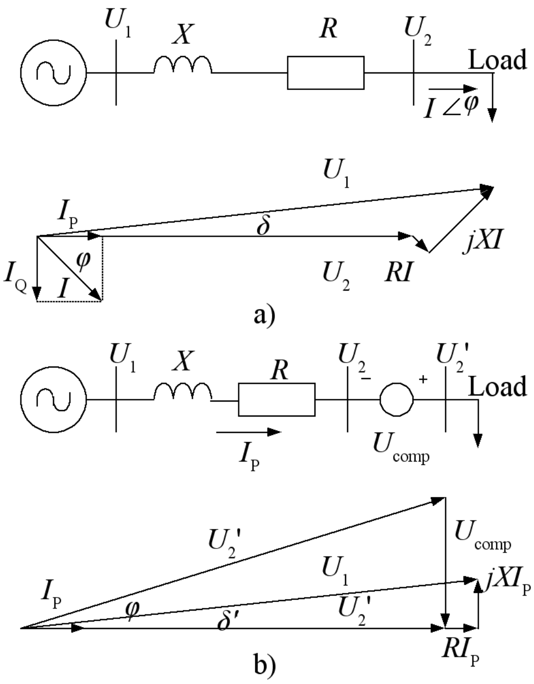

Figure 2.2: Principles of series compensation. a) The system without compensation. b) Series compensation with a voltage source.

Independent of the source type or system configuration, different requirements have to be taken into consideration for a successful operation of reactive power generators. Some of these requirements are simplicity, controllability, dynamics, cost, reliability, and harmonic distortion. Following sections describe different solutions used for reactive power generation with their related principles of operation and compensation characteristics.

2.2 Synchronous Condensers

2.2.1 Traditional Synchronous Condenser

Synchronous condensers have played a major role in voltage and reactive power control for more than 50 years. In this section, conventional and superconducting synchronous condensers are described.

A synchronous condenser is fundamentally an AC synchronous motor that is not attached to any driven equipment. Its field is controlled by a voltage regulator either to generate or to absorb reactive power as needed by the system. It operates at full leading power factor and puts VArs onto the network as required to support a system's voltage or to keep the system power factor at a specified level. Synchronous condensers installation and operation are identical to large electric motors. A single-phase scheme with a synchronous condenser is shown in Figure 2.3. After the unit is synchronized, the field current is adjusted either to generate or to absorb reactive power as required by the AC system. The machine can provide continuous reactive power control when used with the suitable automatic exciter.

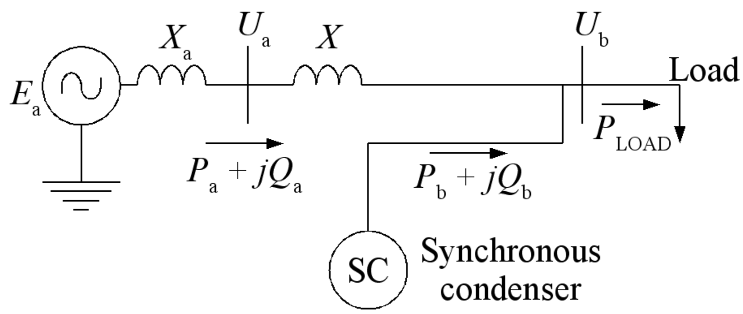

Figure 2.3: Single phase diagram with a synchronous condenser connected to grid.

An increase of the device's field excitation results in providing magnetizing power (kVArs) to the system. Its main advantage is the ease in the adjustment of amount of correction.

Synchronous condensers are also useful for supporting voltage in situations such as starting large motors, or where power must travel long distances from where it is generated to where it is used, which is the case with power wheeling (distribution of electric power from one geographical location to another within an electric power distribution system).

According to [17], it is mentioned that synchronous condensers have been used at both distribution and transmission voltage levels to improve stability and to maintain voltages within desired limits under changing load conditions and contingency situations. Moreover, it is claimed that synchronous condensers also contribute to the short-circuit current, and can not be controlled fast enough to compensate for rapid load changes. Furthermore, their losses are much higher than those related with static compensators, and the cost is much higher compared with static compensators. Their advantage lies in their high temporary overload capability.

2.2.2 Superconducting synchronous condenser

According to [1], the development of high-temperature superconductivity is expected to have a big effect in the technology of large electric machines due to the expectation of high-temperature superconductor (HTS) based motors and generators being smaller, lighter, more efficient, and less expensive to manufacture and to operate than conventional machines. One prototype is shown in Figure 2.4.

The advancements in the HTS wire technology in the last decades have resulted in superconducting electromagnets that can operate at higher temperatures than those made of low-temperature superconductor (LTS) materials, and as a consequence, these electromagnets can utilize relatively simpler, less costly, and more efficient cooling systems. These advantages make the HTS wire technically suitable and also economically feasible for use in the development of motor and generator applications at power ratings lower than that could be done with the LTS wire [1].

Components of a rotating machine utilizing HTS winding is shown in Figure 2.5. Only the field winding of the machine uses HTS cooled with a cryocooler subsystem to about 35-40 K. The cryocooler modules are placed in a stationary frame and a gas, such as helium, is used to cool components of the rotor of the machine. The stator winding uses conventional

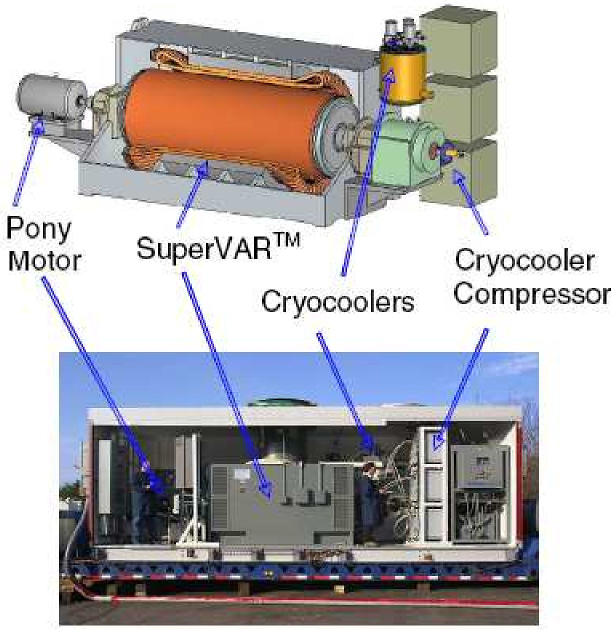

Figure 2.4: Dynamic synchronous condenser prototype (Photo courtesy of American Superconductor).

copper winding but with some differences. The stator winding is not placed in conventional iron core teeth because of the fact that iron core saturates due to the high magnetic field imposed by the HTS winding.

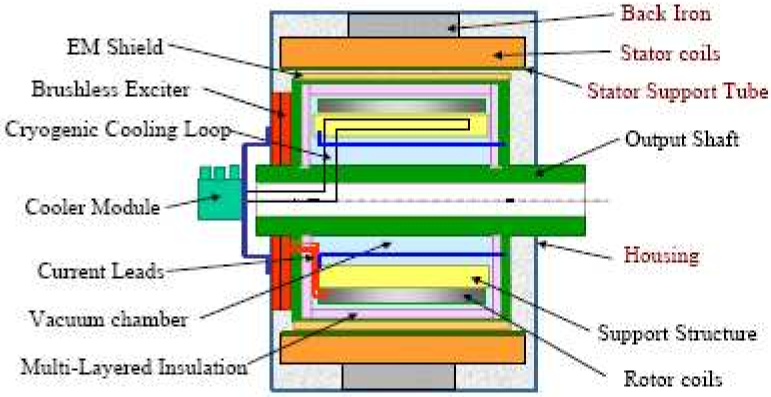

Figure 2.5: HTS Synchronous generator (Design courtesy of American Superconductor).

According to [18], a conventional magnetic iron core is generally not used for a superconducting (SC) rotor, since the high magnetic field generated by the SC windings can saturate the iron core easily. For instance, the magnetic field in the air gap of an SC machine is typically 1.5-2.0 T, which is twice the value of the magnetic field in a conventional machine. This field can saturate the iron teeth and can produce excessive heating and noise. Only the stator yoke (back iron) uses magnetic iron to provide shielding and to carry flux between adjacent poles. The absence of iron in most of the magnetic circuit in these machines results in a very low synchronous reactance (typically 0.3-0.5 per unit). It is claimed that SC machines are more robust than conventional machines during transient system faults, whereas, transient and sub-transient reactances are similar to those of conventional machines. The lower synchronous reactance allows operation of these machines at lower load angles than conventional machines.

2.2.3 Excitation System Models

The basic function of an excitation system is to provide direct current to the synchronous machine field winding. Moreover, the excitation system performs control and protective functions essential to the satisfactory performance of the power system by controlling the field voltage and hence, the field current [19].

When the behavior of synchronous machines is to be simulated accurately in power system stability studies, it is essential that the excitation systems of the synchronous machines are modeled in sufficient detail. The desired models must be suitable for representing the actual excitation equipment performance for large, severe disturbances as well as for small perturbations.

The general functional block diagram shown in 2.6 indicates various synchronous machine excitation subsystems. These subsystems may include a terminal voltage transducer and a load compensator, excitation control elements, an exciter, and in many instances, a power system stabilizer [20].

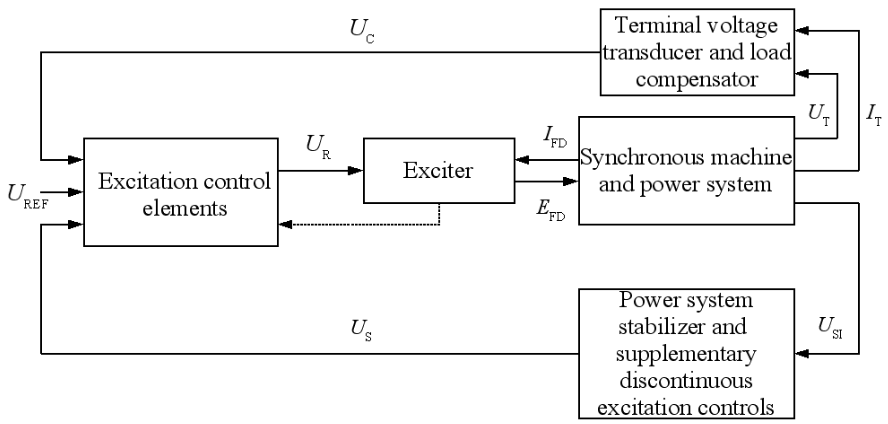

Figure 2.6: General functional block diagram for synchronous machine excitation control system.

The per unit (p.u.) system is used for modeling the excitation systems. Three distinctive types of excitation systems are identified on the basis of excitation power source, as follows:

- Type DC excitation systems, which utilize a direct current generator with a commutator as the source of excitation system power;
- Type AC excitation systems, which use an alternator and either stationary or rotating rectifiers to produce the direct current needed for the synchronous machine field;
- Type ST excitation systems, in which excitation power is supplied through transformers or auxiliary generator windings and rectifiers.

Type DC-Direct current commutator exciters

Type DC exciters utilize DC generators as sources of excitation power and provide current to the rotor of the machine via slip rings. The exciter may be driven by a motor or the shaft of the generator. It can be either separately or self excited. When separately excited, the exciter field is supplied by a pilot exciter utilizing a permanent magnet generator.

DC excitation systems represent early systems such as used in the years from 1920's to 1960's. Few new synchronous machines are being equipped with Type DC exciters, which have been superseded by Type AC and ST systems. However, many such systems are still in service.

The voltage regulators for these systems range all the way from the early non-continuously acting rheostatic type to the later systems using many stages of magnetic amplifiers and rotating amplifiers [21], [22].

Type AC-Alternator-supplied rectifier excitation systems

The excitation system of this type uses an AC alternator and either stationary or rotating rectifiers to produce the DC field requirements. When using stationary rectifiers, the DC output is fed to the field winding of the main generator via slip rings, whereas, with rotating rectifiers, the need for slip rings and brushes is eliminated, and the DC output is directly fed to the main generator field.

Loading effects on such exciters are significant, and the use of generator field current as an input to the models allows these effects to be represented accurately. These systems do not allow the supply of negative field current.

Type ST-Static excitation systems

Components in these systems are static or stationary. Static rectifiers, controlled or uncontrolled, supply the excitation current directly to the field of the main synchronous generator via slip rings. The supply of power to the rectifiers is from the main generator (or the station auxiliary bus) through a transformer to step down the voltage to an appropriate level, or in some cases from an auxiliary winding in the generator [19].

While many of these systems allow negative field-voltage, most do not supply negative field current. For specialized studies where negative field current is needed, it is required to have a more detailed model.

For many of the static systems, the exciter ceiling voltage is very high. For such systems, additional field current limiter circuits may be used to protect the exciter and the generator rotor. These frequently include both instantaneous and time delayed elements [20].

2.3 Static VAr Compensators (SVC)

A typical shunt-connected SVC, composed of thyristor-switched capacitors (TSCs) and thyristor-controlled reactors (TCRs), is shown in Figure 2.7. With proper coordination of the capacitor switching and reactor control, the VAr output can be varied continuously between the capacitive and inductive ratings of the equipment.

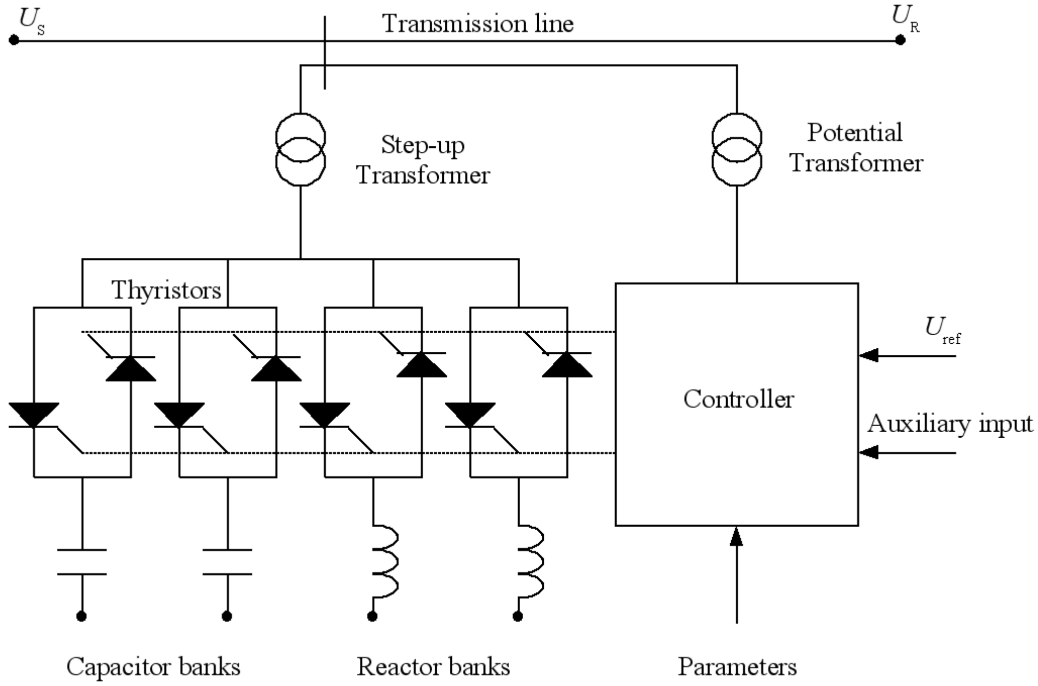

Figure 2.7: Conventional thyristor-controlled SVC.

The compensator is operated to regulate the voltage of the transmission system at a selected terminal. The U-I characteristic of the SVC, shown in Figure 2.8, indicates that the regulation with a given slope around the nominal voltage can be achieved in the normal operating range defined by the maximum capacitive and inductive currents of the SVC. However, the maximum obtainable capacitive current is decreasing linearly with the system voltage since the SVC becomes a fixed capacitor when the maximum capacitive output is reached. Therefore, the conventional thyristor-controlled SVC rapidly deteriorates its voltage support capability with the decrease of system voltage.

In addition to the voltage support, SVCs are also used for dynamic stability improvements by damping power oscillations. The dynamic stability improvement can be obtained by alternating the output of the SVC between appropriate capacitive and inductive values in order to oppose the angular acceleration and deceleration of machines involved. The idea is to increase the transmitted electrical power by increasing the voltage (via capacitive VArs) when the machines accelerate and to decrease it by decreasing the voltage (via inductive VArs) when the machines decelerate. The effectiveness of the SVC in power oscillation damping is a function of the voltage variation it is able, or allowed, to produce [23].

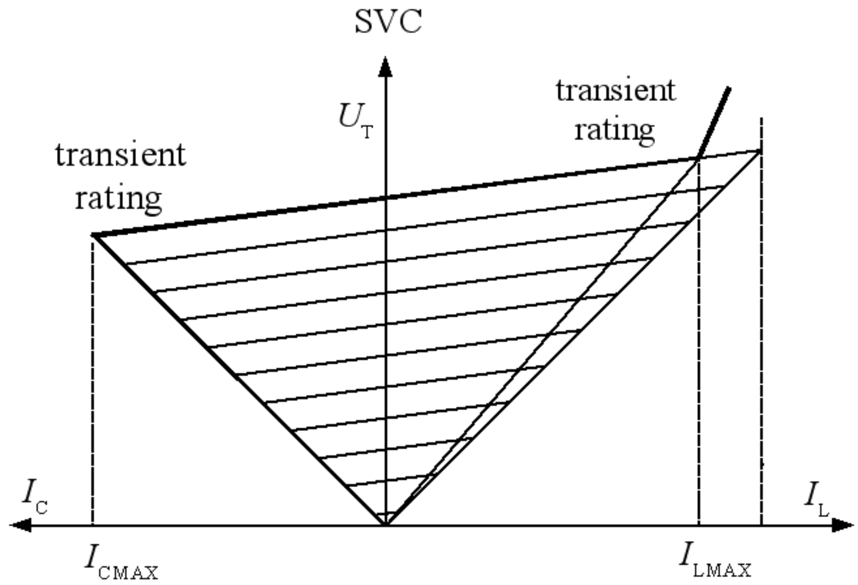

Figure 2.8: U-I characteristic of thyristor-controlled SVC.

2.4 Static Synchronous Compensators (STATCOM)

The STATCOM is based on a solid-state voltage source, implemented with an inverter and connected in shunt with the power system through a coupling reactor, in analogy with a synchronous machine, generating a balanced set of three sinusoidal voltages at the fundamental frequency, with a controllable amplitude and phase-shift angle [17]. The major system component of the STATCOM is a three phase PWM forced commutated voltage sourced inverter shown in Figure 2.9 [24].

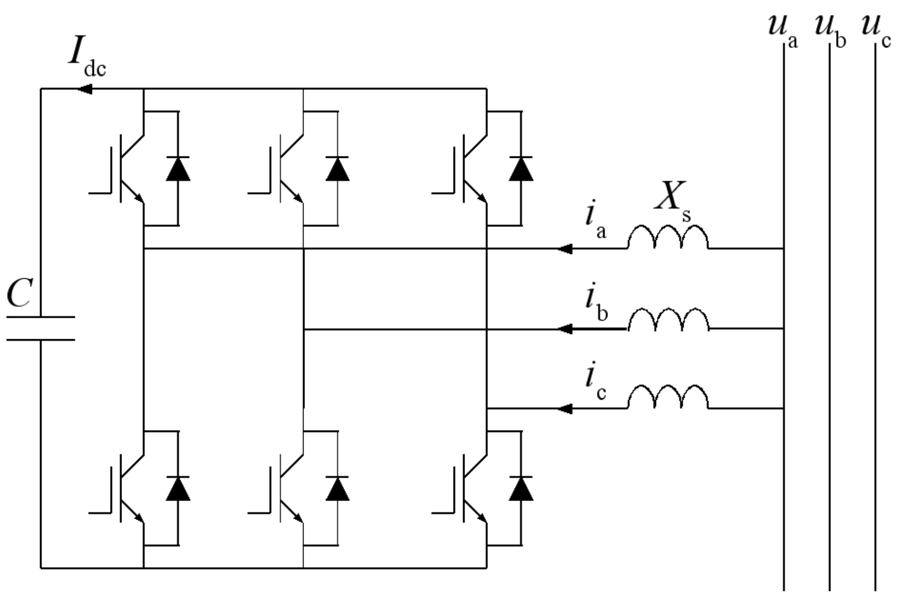

Figure 2.9: Main Circuit of STATCOM.

If the line voltage is in phase with the converter output voltage and has the same magnitude, then there can be no current flow into or out of the STATCOM. If the converter voltage is increased, then the voltage difference between the converter output and the line voltage appears on the reactance. As a result, a leading current with respect to the line voltage is drawn and the STATCOM behaves as a capacitor and generates VArs. Conversely, if the converter output voltage becomes less than the line voltage, then the STATCOM draws a lagging current, behaving as an inductor, and absorbs VArs. A STATCOM operates essentially like a synchronous condenser where the excitation may be greater or less than the terminal voltage [25]. The U-I characteristics of a STATCOM is shown in Figure 2.10.

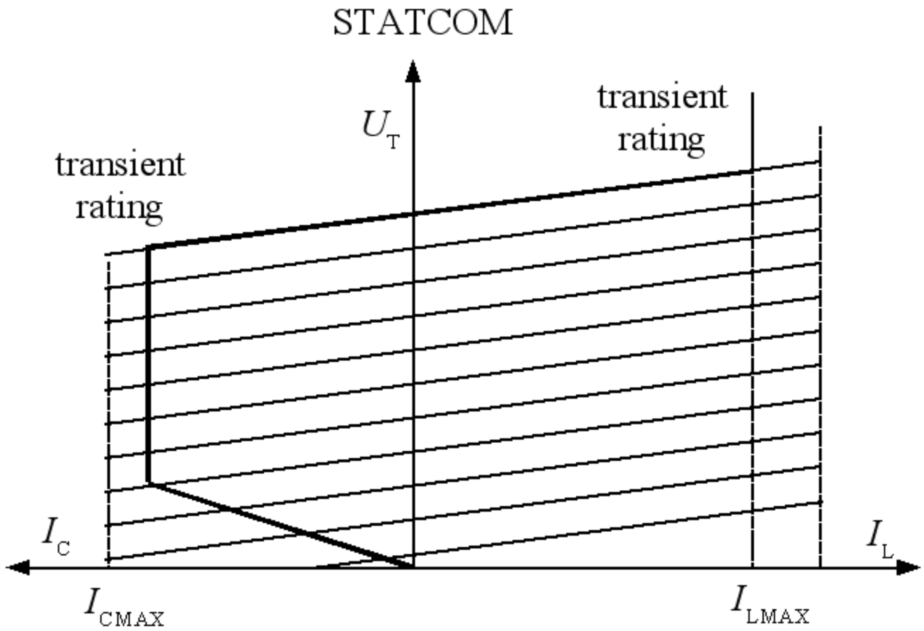

Figure 2.10: U-I characteristic of STATCOM.

Chapter 3

Modeling of Synchronous Condensers

Synchronous machines have a significant role in electric power systems. Most of the energy generated is produced in synchronous generators. However, the ability of the synchronous machine to control the reactive power production also made it suitable for reactive power compensation and voltage control. Before power electronics were available for reactive power compensation and voltage control, this was a good way of controllable reactive power compensation.

For reactive power compensation and voltage control, it is essential to understand the transient phenomena occurring in a synchronous machine. Transient phenomena occur frequently in electrical machines during the start or in case of faults. To analyze the transient phenomena, it is common to use the two axis model of synchronous machine.

3.1 Mathematical Modeling of Synchronous Condensers

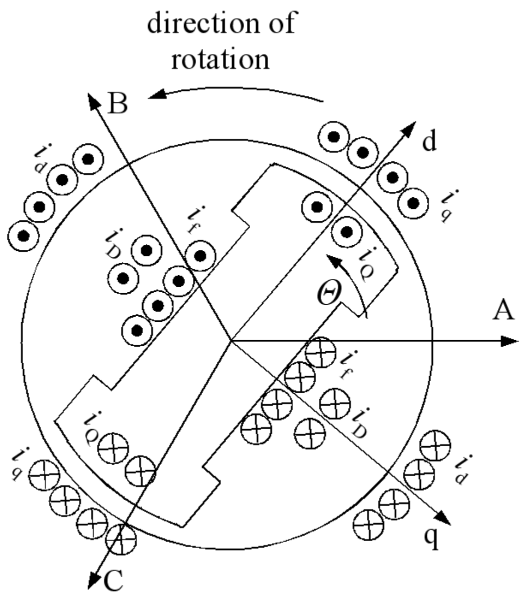

Figure 3.1: Two axis model of a synchronous machine.

Figure 3.1 shows the two-axis model of the synchronous machine. In the two axis model, the d-axis is placed in the direction of pole and the q-axis is placed in the direction between the poles. The field winding F is placed on the direct axis of the rotor (d-axis). The damper winding in the rotor is replaced by two perpendicular windings (D and Q) which are aligned with the d-axis and q-axis. The three phase stator winding is replaced by a two phase winding (d and q) which rotates with the rotor. Hence, the model consists of two groups of perpendicular windings: d, f and D on the direct axis, and q and Q on the quadrature axis which is shown in Figure 3.2.

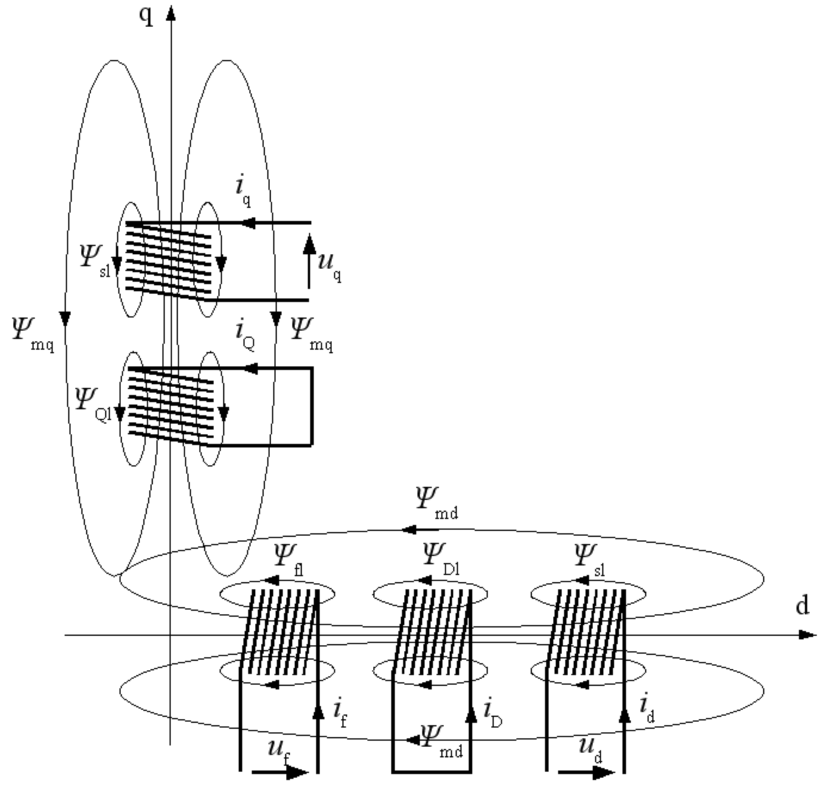

Figure 3.2: Windings of a synchronous machine.

As can be seen from Figure 3.2, the D and Q windings are short circuited. In dq rotor reference frame, the synchronous machine voltage equations become:

$$u_{\mathrm{d}} = R_{\mathrm{s}} i_{\mathrm{d}} + \frac{d\psi_{\mathrm{d}}}{dt} + \omega\psi_{\mathrm{q}} \tag{3.1}$$

$$u_{\mathrm{q}} = R_{\mathrm{s}} i_{\mathrm{q}} + \frac{d\psi_{\mathrm{q}}}{dt} + \omega\psi_{\mathrm{d}} \tag{3.2}$$

$$u_{\mathrm{f}} = R_{\mathrm{f}} i_{\mathrm{f}} + \frac{d\psi_{\mathrm{f}}}{dt} \tag{3.3}$$

$$0 = R_{\mathrm{D}} i_{\mathrm{D}} + \frac{d\psi_{\mathrm{D}}}{dt} \tag{3.4}$$

$$0 = R_{\mathrm{Q}} i_{\mathrm{Q}} + \frac{d\psi_{\mathrm{Q}}}{dt} \tag{3.5}$$

Where, u_{d} is d component of stator voltage, u_{q} is q component of stator voltage, u_{f} is field winding voltage, R_{s} is armature resistance, R_{f} is field winding resistance, R_{D} and R_{Q} damper winding resistances, i_{d} and i_{d} are stator currents in d and q directions respectively, i_{f} is field current and i_{D} and i_{Q} are damper winding currents in d and q directions respectively.

The flux linkage equations are given by:

$$\psi_{\mathrm{d}} = L_{\mathrm{d}} i_{\mathrm{d}} + L_{\mathrm{df}} i_{\mathrm{f}} + L_{\mathrm{dD}} i_{\mathrm{D}} \tag{3.6}$$

$$\psi_{\mathrm{f}} = L_{\mathrm{df}} i_{\mathrm{d}} + L_{\mathrm{f}} i_{\mathrm{f}} + L_{\mathrm{fd}} i_{\mathrm{D}} \tag{3.7}$$

$$\psi_{\mathrm{D}} = L_{\mathrm{dD}} i_{\mathrm{d}} + L_{\mathrm{fD}} i_{\mathrm{f}} + L_{\mathrm{D}} i_{\mathrm{D}} \tag{3.8}$$

$$\psi_{\mathrm{q}} = L_{\mathrm{q}} i_{\mathrm{q}} + L_{\mathrm{qQ}} i_{\mathrm{Q}} \tag{3.9}$$

$$\psi_{\mathrm{Q}} = L_{\mathrm{qQ}} i_{\mathrm{q}} + L_{\mathrm{Q}} i_{\mathrm{Q}} \tag{3.10}$$

where, ψ_{d} is the flux linkage in d direction in the stator winding, ψ_{f} is the field winding flux linkage, ψ_{D} is the damper winding flux linkage in d direction, ψ_{q} is the flux linkage in the stator winding in q direction, ψ_{Q} is the damper winding flux linkage in q direction, L_{d} is the direct axis synchronous inductance, L_{q} is the quadrature axis synchronous inductance, L_{D} is the damper winding inductance in d direction, L_{Q} is the damper winding inductance in q direction, L_{f} is the field winding inductance and L_{df}, L_{dD}, L_{fD}, L_{qQ} are the mutual inductances of corresponding windings.

The equation of motion is given by:

$$\frac{3}{2} p \left(\psi_{\mathrm{d}} i_{\mathrm{q}} - \psi_{\mathrm{q}} i_{\mathrm{d}} \right) = \frac{J}{p} \frac{d\omega}{dt} + T_{\mathrm{m}} \tag{3.11}$$

where, J is inertia of the machine, T_{m} is the torque and p is the pole-pair number.

In order to obtain rotor position the following equation is used:

$$\omega = \frac{d\theta}{dt} \tag{3.12}$$

where, ω is the rotor speed and θ is the rotor position. However, it is also necessary to use load angle equation:

$$\frac{d\delta}{dt} = \omega - \omega_{\mathrm{s}} \tag{3.13}$$

where, δ is the load angle and ω_{s} is the synchronous speed.

As the field and damper winding are both placed on the rotor, L_{fD} is slightly higher than L_{df} and L_{dD}, but due to the small difference in these mutual inductances and to simplify the modeling, it can be assumed that:

$$L_{\mathrm{df}} = L_{\mathrm{dD}} = L_{\mathrm{fD}} = L_{\mathrm{md}} \tag{3.14}$$

$$L_{\mathrm{qQ}} = L_{\mathrm{mq}} \tag{3.15}$$

where, L_{md} is the direct axis magnetizing inductance and L_{mq} is the quadrature axis magnetizing inductance. After this simplification,the d-axis and q-axis inductances can be written as follows:

$$L_{\mathrm{d}} = L_{\mathrm{md}} + L_{\mathrm{sl}} \tag{3.16}$$

$$L_{\mathrm{q}} = L_{\mathrm{mq}} + L_{\mathrm{sl}} \tag{3.17}$$

$$L_{\mathrm{f}} = L_{\mathrm{md}} + L_{\mathrm{fl}} \tag{3.18}$$

$$L_{\mathrm{D}} = L_{\mathrm{md}} + L_{\mathrm{Dl}} \tag{3.19}$$

$$L_{\mathrm{Q}} = L_{\mathrm{mq}} + L_{\mathrm{Ql}} \tag{3.20}$$

By inserting flux linkage equations in voltage equations we obtain:

$$u_{\mathrm{d}} = R_{\mathrm{s}} i_{\mathrm{d}} + L_{\mathrm{d}} \frac{di_{\mathrm{d}}}{dt} + L_{\mathrm{md}} \frac{di_{\mathrm{f}}}{dt} + L_{\mathrm{md}} \frac{di_{\mathrm{D}}}{dt} - \omega L_{\mathrm{q}} i_{\mathrm{q}} - \omega L_{\mathrm{mq}} i_{\mathrm{Q}} \tag{3.21}$$

$$u_{\mathrm{q}} = R_{\mathrm{s}} i_{\mathrm{q}} + L_{\mathrm{q}} \frac{di_{\mathrm{q}}}{dt} + L_{\mathrm{mq}} \frac{di_{\mathrm{Q}}}{dt} + \omega L_{\mathrm{d}} i_{\mathrm{d}} + \omega L_{\mathrm{md}} i_{\mathrm{f}} + \omega L_{\mathrm{md}} i_{\mathrm{D}} \tag{3.22}$$

$$u_{\mathrm{f}} = R_{\mathrm{f}} i_{\mathrm{f}} + L_{\mathrm{md}} \frac{di_{\mathrm{d}}}{dt} + L_{\mathrm{md}} \frac{di_{\mathrm{D}}}{dt} + L_{\mathrm{f}} \frac{di_{\mathrm{f}}}{dt} \tag{3.23}$$

$$0 = R_{\mathrm{D}} i_{\mathrm{D}} + L_{\mathrm{md}} \frac{di_{\mathrm{d}}}{dt} + L_{\mathrm{md}} \frac{di_{\mathrm{f}}}{dt} + L_{\mathrm{D}} \frac{di_{\mathrm{D}}}{dt} \tag{3.24}$$

$$0 = R_{\mathrm{D}} i_{\mathrm{D}} + L_{\mathrm{md}} \frac{di_{\mathrm{d}}}{dt} + L_{\mathrm{md}} \frac{di_{\mathrm{f}}}{dt} + L_{\mathrm{D}} \frac{di_{\mathrm{D}}}{dt} \tag{3.25}$$

In matrix form these electrical and motion equations choosing currents as state variables can be given as:

$$\begin{bmatrix} u_{\mathrm{d}} \\ u_{\mathrm{q}} \\ u_{\mathrm{f}} \\ 0 \\ 0 \\ T_{\mathrm{m}} \\ \omega_{\mathrm{s}} \\ 0 \end{bmatrix} = R \begin{bmatrix} i_{\mathrm{d}} \\ i_{\mathrm{q}} \\ i_{\mathrm{f}} \\ i_{\mathrm{D}} \\ i_{\mathrm{Q}} \\ \omega \\ \delta \\ \theta \end{bmatrix} + L \frac{d}{dt} \begin{bmatrix} i_{\mathrm{d}} \\ i_{\mathrm{q}} \\ i_{\mathrm{f}} \\ i_{\mathrm{D}} \\ i_{\mathrm{Q}} \\ \omega \\ \delta \\ \theta \end{bmatrix} \tag{3.26}$$

where, R and L matrices are equal to:

$$R = \begin{bmatrix} R_{\mathrm{s}} & -\omega L_{\mathrm{q}} & 0 & 0 & -\omega L_{\mathrm{mq}} & 0 & 0 & 0 \\ \omega L_{\mathrm{d}} & R_{\mathrm{s}} & \omega L_{\mathrm{md}} & \omega L_{\mathrm{md}} & 0 & 0 & 0 & 0 \\ 0 & 0 & R_{\mathrm{f}} & 0 & 0 & 0 & 0 & 0 \\ 0 & 0 & 0 & R_{\mathrm{D}} & 0 & 0 & 0 & 0 \\ 0 & 0 & 0 & 0 & R_{\mathrm{Q}} & 0 & 0 & 0 \\ -p\frac{3}{2}\psi_{\mathrm{q}} & p\frac{3}{2}\psi_{\mathrm{d}} & 0 & 0 & 0 & 0 & 0 & 0 \\ 0 & 0 & 0 & 0 & 0 & 1 & 0 & 0 \\ 0 & 0 & 0 & 0 & 0 & 1 & 0 & 0 \end{bmatrix} \tag{3.27}$$

$$L = \begin{bmatrix} L_{\mathrm{d}} & 0 & L_{\mathrm{md}} & L_{\mathrm{md}} & 0 & 0 & 0 & 0 \\ 0 & L_{\mathrm{q}} & 0 & 0 & L_{\mathrm{mq}} & 0 & 0 & 0 \\ L_{\mathrm{md}} & 0 & L_{\mathrm{f}} & L_{\mathrm{md}} & 0 & 0 & 0 & 0 \\ L_{\mathrm{md}} & 0 & L_{\mathrm{md}} & L_{\mathrm{D}} & 0 & 0 & 0 & 0 \\ 0 & L_{\mathrm{mq}} & 0 & 0 & L_{\mathrm{Q}} & 0 & 0 & 0 \\ 0 & 0 & 0 & 0 & 0 & -\frac{J}{p} & 0 & 0 \\ 0 & 0 & 0 & 0 & 0 & 0 & -1 & 0 \\ 0 & 0 & 0 & 0 & 0 & 0 & 0 & -1 \end{bmatrix} \tag{3.28}$$

In the state-space form our system is described using following equations:

$$\frac{dX}{dt} = X' = AX + BU \tag{3.29}$$

Where $A = -L^{-1}R$ and $B = L^{-1}$.

In general, the information about synchronous machines is given in reactances in p.u. and time constants in seconds. Hence, to use them in the state-space model, Eqs. (3.30) to (3.35) are used to calculate the inductances and resistances:

$$L_{\mathrm{d}}^{''} = L_{\mathrm{d}} - \frac{L_{\mathrm{md}}^2 L_{\mathrm{f}} + L_{\mathrm{md}}^2 L_{\mathrm{D}} - 2L_{\mathrm{md}}^3}{L_{\mathrm{D}} L_{\mathrm{f}} - L_{\mathrm{md}}^2} \tag{3.30}$$

$$\omega T_{\mathrm{do}}^{'} = \frac{L_{\mathrm{f}}}{R_{\mathrm{f}}} \tag{3.31}$$

$$\omega T_{\mathrm{do}}^{''} = \frac{L_{\mathrm{D}} - \frac{L_{\mathrm{md}}^2}{L_{\mathrm{D}}}}{R_{\mathrm{D}}} \tag{3.32}$$

$$\omega T_{\mathrm{d}}^{'} = \left(1 - \frac{L_{\mathrm{md}}^2}{L_{\mathrm{d}} L_{\mathrm{f}}}\right) \frac{L_{\mathrm{f}}}{R_{\mathrm{f}}} \tag{3.33}$$

$$\omega T_{\mathrm{qo}}^{''} = \frac{L_{\mathrm{Q}}}{R_{\mathrm{Q}}} \tag{3.34}$$

$$L_{\mathrm{q}}^{''} = L_{\mathrm{q}} - \frac{L_{\mathrm{mq}}^2}{L_{\mathrm{Q}}} \tag{3.35}$$

where, all inductance values are given in per unit and time constants are in seconds, L_{d}'' is the direct axis sub-transient inductance, T_{d0}' is the direct axis open-circuit time constant, T_{d0}'' is the direct axis sub-transient open-circuit time constant, T_{d}' is the direct axis short-circuit time constant, T_{q0}'' is the quadrature axis sub-transient open-circuit time constant, L_{q}'' is the quadrature axis sub-transient inductance, and it is assumed that L_{df}=L_{dD}=L_{fD}, L_{qQ}=L_{mq}. To utilize these equations in the state-space model, the known values of L_{q} and L_{sl} is used in Eq.(3.17), to find the value of L_{mq}, the known value of L_{d} is used in Eq.(3.16) to find the value of L_{md}. Then L_{Q} is calculated using Eq.(3.35) with the known values of L_{q}, L_{mq} and L_{q}''. After it, R_{Q} is calculated using Eq.(3.34) with the known values of T_{q0}'' and L_{Q}''. The value of L_{f} is calculated using Eq.(3.33) with the known values of T_{d}', L_{md}, L_{d} and $L_{\mathrm{f}}/R_{\mathrm{f}}$ which is equal to T_{d0}'. The value of L_{D} is calculated using Eq.(3.30) with the known values of L_{md}, L_{d}, L_{d}'' and L_{f}. Finally, the value of R_{D} is calculated using Eq.(3.32) with the known values of L_{D}, L_{md} and T_{d0}''. After these calculations, for finding inertia from the inertia constant, following equation is used:

$$H = \frac{1}{2} \frac{J \omega_{\mathrm{m}}^2}{S_{\mathrm{n}}} \tag{3.36}$$

where, J is the inertia of the machine, ω_{m} is the machine mechanical speed, S_{b} is the rated apparent power of the machine and H is the inertia constant.

3.2 Main Flux Saturation modeling

If saturation is neglected, the inductances described in Section 3.1 are constant. To take saturation into account new inductance matrix has to be calculated for each time step [26]. Only main-flux saturation is to be considered in the synchronous machine modeling and saturation in q direction is assumed to be equal in d direction. This assumption is reasonably accurate because during the synchronous condenser operation flux in q direction is very low.

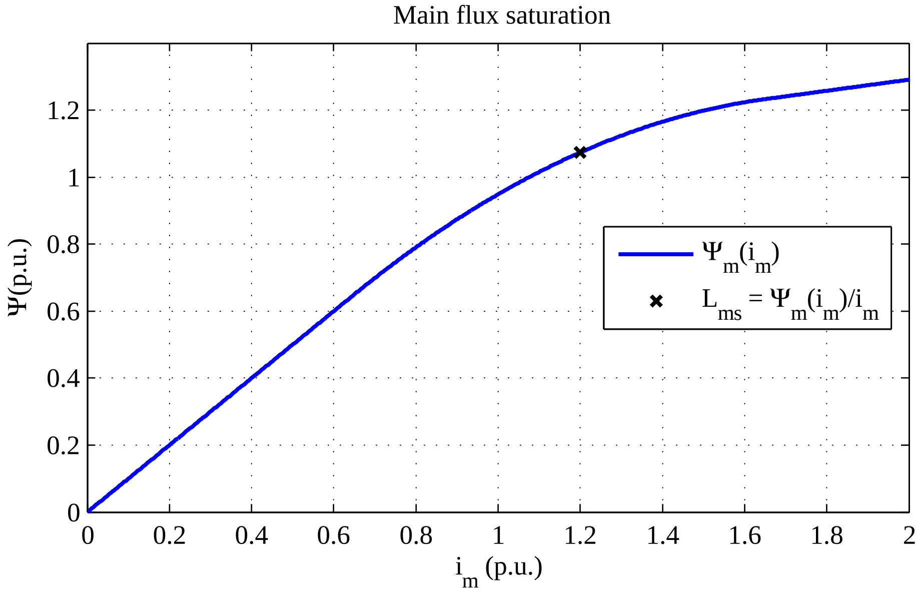

Figure 3.3: Ψ_{m} as a function of i_{m}.

In Figure 3.3 the saturation of flux Ψ_{m} is shown as a function of magnetizing current i_{m} which is equal to $\sqrt{(i_{\mathrm{f}} + i_{\mathrm{d}} + i_{\mathrm{D}})^2 + (i_{\mathrm{q}} + i_{\mathrm{Q}})^2}$. New values of inductances will be calculated as follows:

$$L_{\mathrm{mt}} = \frac{d\psi_{\mathrm{m}}}{di_{\mathrm{m}}} \tag{3.37}$$

$$\psi_{\mathrm{m}} = \int L_{\mathrm{mt}} di_{\mathrm{m}} \tag{3.38}$$

$$L_{\mathrm{ms}} = \frac{\psi_{\mathrm{m}}}{i_{\mathrm{m}}}. \tag{3.39}$$

where, L_{ms} is the magnetizing inductance and L_{mt} is the tangential magnetizing inductance. Since values of unsaturated inductances in d-axis and q-axis are different, L_{msD} which is the saturated inductance in d direction and L_{msQ} which is the saturated inductance in q direction are given using equations:

$$L_{\mathrm{msD}} = L_{\mathrm{ms}} \tag{3.40}$$

$$L_{\mathrm{msQ}} = L_{\mathrm{ms}} \frac{L_{\mathrm{mq}}}{L_{\mathrm{md}}}. \tag{3.41}$$

In order to account for saturation phenomena in synchronous machine modeling, the state space equations have to be modified by recalculating magnetizing inductances both in d and q direction. For that purpose the following equations are used:

$$L_{\mathrm{mds}} = L_{\mathrm{msD}} + \frac{i_{\mathrm{md}}^2}{i_{\mathrm{m}}} \frac{dL_{\mathrm{msD}}}{di_{\mathrm{m}}} \tag{3.42}$$

$$L_{\mathrm{mqs}} = L_{\mathrm{msQ}} + \frac{i_{\mathrm{mq}}^2}{i_{\mathrm{m}}} \frac{dL_{\mathrm{msQ}}}{di_{\mathrm{m}}} \tag{3.43}$$

where, i_{md}, i_{mq} are the d-axis and q-axis components of the magnetizing current, L_{mds} is the new value of magnetizing inductance in d-axis direction, L_{mqs} is the new value of magnetizing inductance in q-axis direction. These new values of magnetizing inductances are put in Eqs. (3.16) - (3.28) instead of L_{md} and L_{mq}.

The values of L_{msD} and L_{msQ} calculated using equations 3.39 and 3.41 and the values of $dL_{\mathrm{msD}}/di_{\mathrm{m}}$ and $dL_{\mathrm{msQ}}/di_{\mathrm{m}}$ are shown in Figure 3.4.

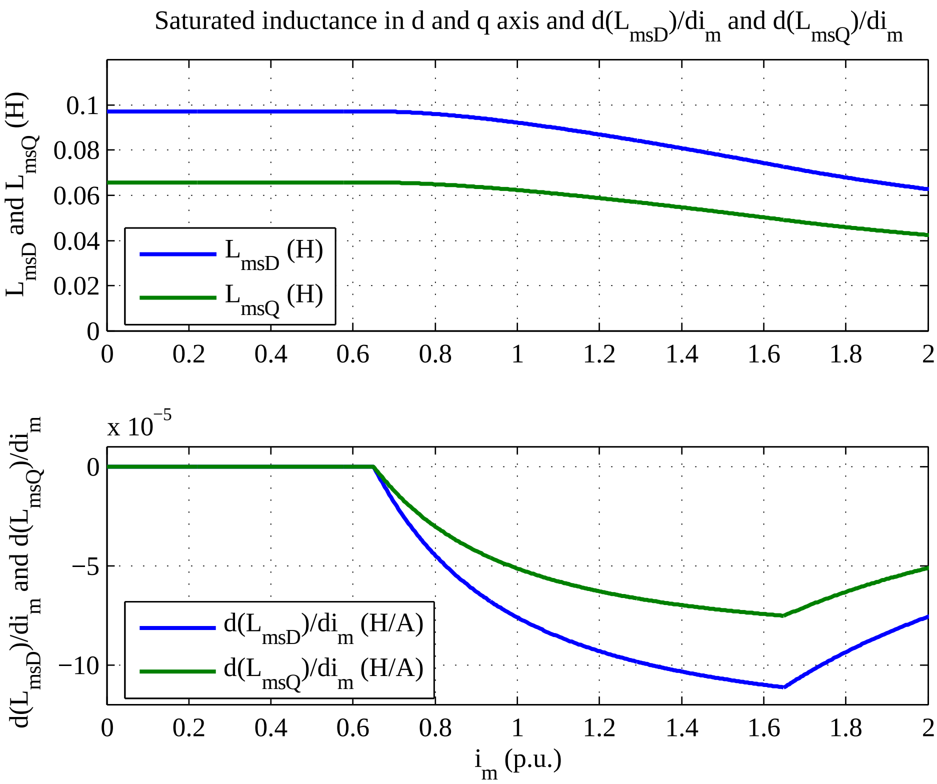

Figure 3.4: Calculated values of L_{msD}, L_{msQ}, dL_{msD}/di_{m} and dL_{msQ}/di_{m} during saturation.

3.3 Exciter modeling

As the DC excitation system has widely been implemented by the industry [21], for our conventional synchronous condenser model, type DC2A excitation system shown in Figure 3.5 is used to represent the field-controlled DC commutator exciters with continuously acting voltage regulators having supplies obtained from the generator or the auxiliary bus.

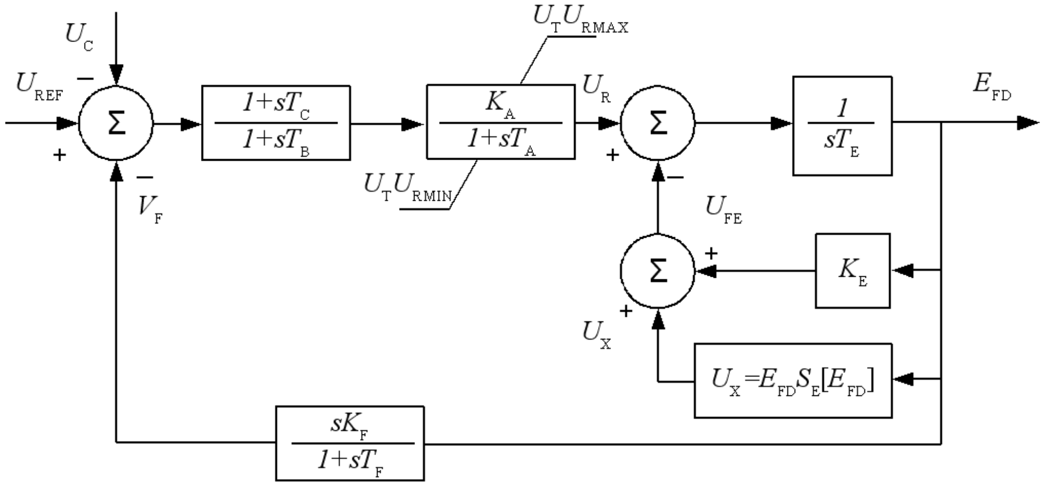

Figure 3.5: Type DC2A - DC commutator exciter with bus-fed regulator.

The principal input to this model is the output, U_C, from the synchronous machine terminal voltage transducer. At the summing junction, terminal voltage transducer output, U_C, is subtracted from the set point reference, U_{REF}. The stabilizing feedback, U_F, is subtracted and the power system stabilizing signal, U_S, is added to produce an error voltage. In the steady state, these last two signals are zero, leaving only the terminal voltage error signal. The resulting signal is amplified in the regulator. The major time constant, T_A, and gain, K_A, associated with the voltage regulator are shown incorporating non-windup limits typical of saturation or amplifier power supply limitations. These voltage regulators utilize power sources that are essentially unaffected by brief transients on the synchronous machine or auxiliary buses. The time constants, T_B and T_C, may be used to model equivalent time constants inherent in the voltage regulator.

The output of the voltage regulator, U_R, is used to control the exciter, which may be either separately excited or self-excited. When a self-excited shunt field is used, the value of K_E reflects the setting of the shunt field rheostat. In some instances, the resulting value of K_E can be negative and allowance should be made for this. If a nonzero value for K_E is provided, the program should not recalculate K_E, as a fixed rheostat setting is implied. For such systems, the rheostat is frequently fixed at a value that would produce self-excitation near rated conditions. Systems with fixed field rheostat settings are in widespread use on units that are remotely controlled. A value for $K_E = 1$ is used to represent a separately excited exciter.

The term $S_E[E_{FD}]$ is a nonlinear function with values defined at two or more chosen values of E_{FD}. The output of this saturation block, U_X, is the product of the input, E_{FD}, and the value of the nonlinear function $S_E[E_{FD}]$ at this exciter voltage.

A signal derived from the field voltage is normally used to provide excitation system stabilization, U_F, via the rate feedback with gain, K_F, and the time constant, T_F [20].

As new synchronous machines are mostly equipped with type AC or ST systems [20], for our superconducting synchronous condenser model, type ST1A excitation system shown in Figure 3.6 is used to represent systems in which excitation power is supplied through a transformer from the generator terminals (or the unit's auxiliary bus) and is regulated by a controlled rectifier. The maximum exciter voltage that can be obtained from such systems is directly related to the generator terminal voltage.

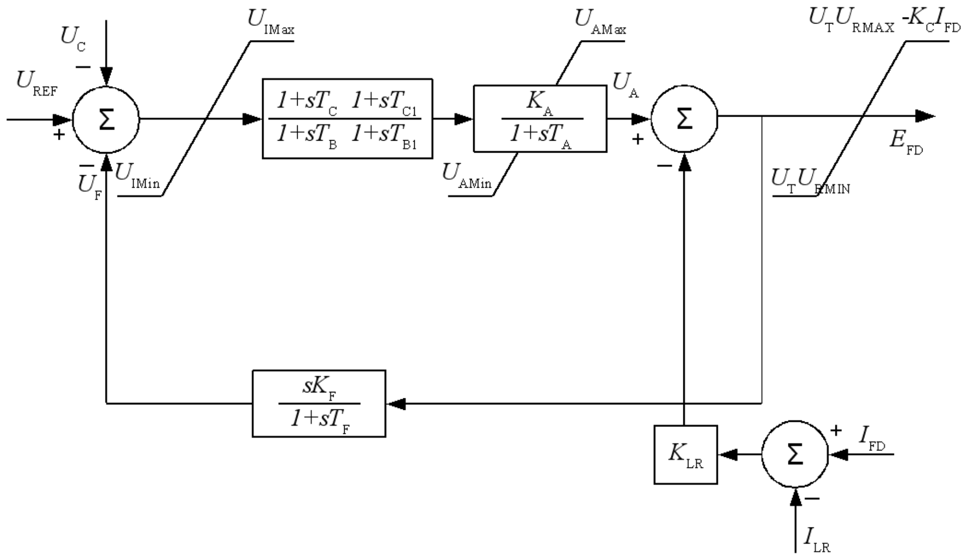

Figure 3.6: Type ST1A - Potential-source, controlled-rectifier exciter.

In Type ST1A system, as the inherent exciter time constants are very small, exciter stabilization may not be required. In contrast, it may be advantageous to reduce the transient gain of these systems for other reasons. The model shown is sufficiently flexible to represent transient gain reduction implemented either in the forward path via time constants, T_B and T_C (where K_F would normally be set to zero), or in the feedback path by suitable choice of rate feedback parameters, K_F and T_F. Voltage regulator gain and any inherent excitation system time constant are represented by K_A and T_A, respectively.

Due to the very high forcing capability of these systems, a field current limiter is sometimes employed to protect the generator rotor and exciter. The limit start setting is defined by I_LR and the gain is represented by K_LR. To allow this limit to be ignored, provision should be made to allow K_LR to be set to zero.

While for the majority of these excitation systems, a fully controlled bridge is employed, this model is also applicable to systems in which only half of the bridge is controlled, in which, the negative field voltage limit is set to zero ($U_\mathrm{RMIN} = 0$) [20].

Chapter 4

Modeling of Static VAR Compensator

Static VAR compensators (SVCs) are used primarily in power systems for different applications such as increasing the steady-state power-transfer capability, enhancement of transient stability, prevention of voltage instability and improvement of HVDC link performance [27]-[30].

In the modeling of the SVC, the model taken from ABB FACTS is used in simulations which employs two Thyristor Switched Capacitor (TSC) banks each of which supplies 35.8 % of the rated reactive power, two 3^{rd} and 5^{th} harmonic filters each of which supplies 10.2 % of the rated reactive power and two 7^{th} and 11^{th} harmonic filters each of which supplies 4 % of the rated reactive power. For reactive power consumption, one Thyristor Controlled Reactor (TCR) unit with size of 38.3 % of the rated reactive power is employed. In the connection of the SVC to the network, $Y\Delta$ coupling transformer with the size of rated reactive power is used where the high voltage side is connected with Y grounded.

The control system of the SVC consists of various systems such as a measurement system, a voltage regulator, a gate pulse-generator, a synchronizing system and supplementary control and protection functions [30]. The general schematic diagram of an SVC control system is shown in Figure 4.1.

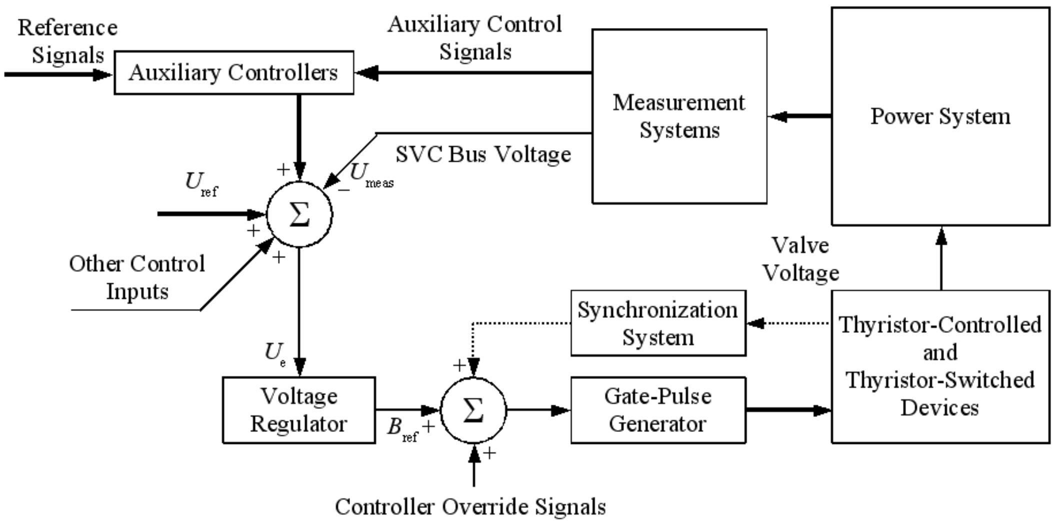

Figure 4.1: General schematic diagram of SVC control System.

4.1 Measurement system

Measurement systems provide necessary inputs to the SVC controller to perform its functions. Depending on the function that the SVC controller is intended to perform, different inputs are required for an SVC such as, voltage measurement, current measurement and power measurement.

When the voltage control is based on individual phase voltage control, the voltage measurement system is used with the purpose of generating a DC signal proportional to the root mean square (rms) value of the 3-phase balanced voltages at fundamental frequency. In the SVC model used in the simulations, this DC signal is obtained after $\alpha\beta$-coordinate transformation which is given in Appendix A.

4.2 Voltage regulator

The voltage regulator of the SVC processes the measured system variables and generates an output signal in order to establish the required reactive power output from the compensator [31]. Different control variables and transfer functions of the voltage regulator can be used depending on the application of the SVC. The measured control variables are compared with the reference signal and then, an error signal is given as input to the controller transfer function. The output of the controller is a per-unit susceptance reference, B_{ref}, which is generated to reduce the error signal to zero in the steady state. This signal is, in principle, a measure of the reactive power generation or absorption needed to maintain the network voltage at the desired value [32]. The susceptance signal is subsequently transmitted to the gate pulse generation circuit.

A small slope or droop (3-5 %) is generally incorporated into the steady-state characteristics of SVCs to achieve specific advantages, such as reduction of the SVC rating and prevention of frequent operation at reactive power limits.

4.3 Gate-Pulse Generation

The susceptance reference output from the voltage regulator is transmitted to the gate-pulse generation block, which produces appropriate firing pulses for all the thyristor valves of the SVC in order to produce the required reactive power output from the compensator.

In a general SVC configuration with TSC and TCR, the Gate Pulse Generation unit performs functions such as [33]:

- Ascertaining the number of TSC banks to be switched in order to meet the capacitive susceptance demand;
- Calculating the magnitude of TCR inductive susceptance in order to offset the surplus capacitive susceptance;

- Determining the order in which the TSC connections should be actuated, depending on the existing polarity of charges on the different capacitors, and hence ensuring transient-free capacitor switching;
- Computing the firing angle for TCR thyristors in order to implement the desired TCR inductive susceptance at the SVC terminals.

As there is a highly non-linear relationship between the firing angle and the equivalent susceptance of the controlled reactors, a linearizing function is employed in the model in order to ensure that B_{ref} is equal to B_{SVC}, the actual installed susceptance.

4.4 Synchronizing System

The purpose of the synchronizing system is to generate reference pulses in synchronism with the fundamental component of the system voltage. While the reference pulses are synchronized to the system voltage, the timing of these pulses must be sufficiently insensitive to distortions in supply voltage in order to minimize the generation of non-characteristics harmonics which can lead to amplification of voltage distortion and also to a form of control instability. Another important attribute that a synchronizing system must possess is the accurate tracking of the system frequency and the phase angle. Also, a synchronizing system must operate unhindered during severe system faults and have a quick resynchronizing capability on reappearance of the system voltage after clearing the fault.

A common method of generating the necessary timing pulses is through the use of phase-locked oscillators which are employed in the model used. This is a good method of producing equally spaced timing pulses synchronized to the system, and it is highly insensitive to harmonic voltage distortions.

Unlike the TCR, the TSC is not phase controlled, but just switched on or off. Therefore, the TSC trigger pulses are given at the natural zero crossings of the current.

4.5 Suplementary Control and Protection Functions

The voltage regulator is usually improved by certain special control and protection functions depending on the nature of the study [34].

In the model used, an undervoltage strategy is implemented. In this strategy, a logic is incorporated in the SVC control to block the SVC during instances of severe undervoltages, such as three phase to ground faults. If the SVC continues to operate under these conditions, the voltage regulator act to make the SVC output highly capacitive which may lead to excessive overvoltages as soon as the fault is cleared. However, as no overvoltage is observed after faults during simulations, undervoltage strategy is disabled during the simulations.

Another control function employed in the model is the secondary-overvoltage limiter which ensures that the secondary (low voltage) side of the SVC coupling transformer does not exceed the design limits during an abnormal situation when the SVC output is highly capacitive and the voltage regulator is out of use.

The TCR overcurrent limiter is also employed in the model in order to restrict the TCR current during periods of high voltage, such as those caused by load rejections, to prevent any damage to thyristors.

Chapter 5

Model implementation into PSCAD/EMTDC

In this chapter, details of the implementation of the model into PSCAD/EMTDC are explained.

5.1 Model description

The synchronous machine model is written in FORTRAN following both FORTRAN 77 and FORTRAN 90 standards. This ensured portability of the written code to all compilers available for PSCAD/EMTDC. The program itself consists of the main program and four subroutines. This provides easier overview of the written code and easier updating of changes made during the development process. Saturation is modeled as separate subroutine which is very suitable for testing and analyzing of different extrapolation and interpolation methods available for the main flux saturation curve modeling.

The graphical user interface (GUI) of the model was designed in a user friendly fashion. The intention was to keep the design of the GUI as simple as possible while giving the user the power of changing all important parameters of the model and solver. The model implemented into PSCAD/EMTDC is given in Figure 5.1.

Interfaces to the EMTDC/PSCAD network and to the exciter are kept in the same arrangement as those of the built-in PSCAD model. This enables use of the model in a way that PSCAD users are used to. On the right side of the model, there are three electrical nodes A, B and C that represent the terminals of the machine. Synchronous machine model is interfacing electrical network through these nodes. Connection of the windings of the synchronous machine is arranged in Y connection. Other types of connections are not observed since the construction of the synchronous machine and it's impact on performance is not observed in this work.

Output signals for exciter are given in per unit and can interface with any exciter given in PSCAD main library. All outputs for the exciter are provided and user cannot turn off any of the exciter outputs although not all of them are needed for some exciters.

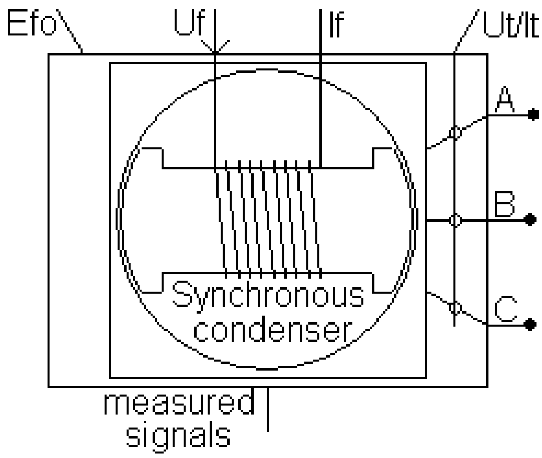

Figure 5.1: The synchronous machine model designed in PSCAD/EMTDC.

This model does not provide interface for torque input since this synchronous machine is intended to run as a synchronous condenser. On the other hand, on the bottom of the model some signals are internally measured and provided as twelve dimension signal called "Measured signals". The "Measured signals" consists of:

- Signals from 1 to 5 - currents in dq reference frame i_{d}, i_{q}, i_{f}, i_{D} and i_{Q} in Amperes;
- Signal 6 - angular mechanical speed ω in radians per second;
- Signal 7 - load angle δ in radians;
- Signal 8 - rotor position θ in radians;
- Signals 9 and 10 - active and reactive power P and Q respectively given in Watts and Volt-Amperes;
- Signals 11 and 12 - voltages in dq reference frame u_{d} and u_{q} given in Volts.

These signals provide most of the informations needed for observation of the transients that occur in the synchronous machine. To observe these signals user has to arrange a line with twelve data taps that acts as a demultiplexer and place output channels for plotting.

Machine parameters and solver parameters are set in the properties of the machine. Properties of the synchronous machine model consists of six categories. The first category is called ”configuration” and the general data for the machine and the solver parameters are entered here. Window of the main configuration widow of the synchronous machine model is given in Figure 5.2.

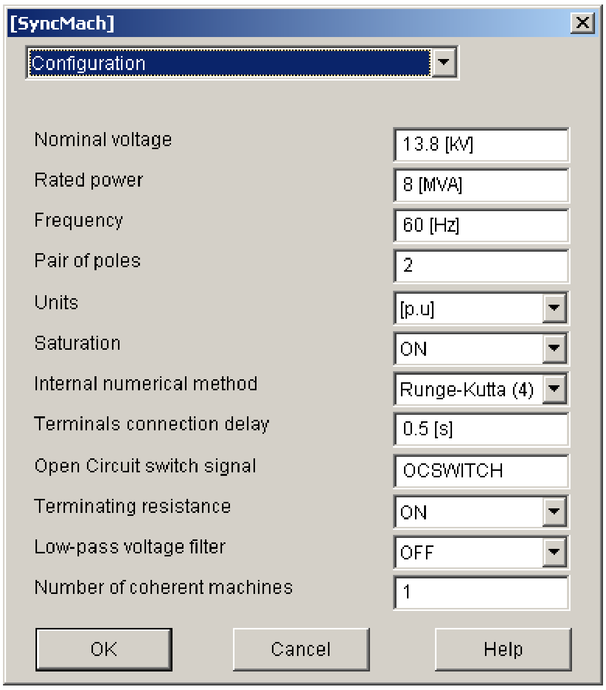

Figure 5.2: The synchronous machine model - main configuration window.

General data of the machine is entered in the first four fields. Nominal voltage, rated power, frequency and the number of pair of poles are used for recalculations of the parameters if they are given in per unit. Depending on the selection of units, corresponding window for machine parameters data entry is enabled. This also affects the calculation part of the PSCAD script which uses proper procedure for different type of units selected. If the model with saturation is simulated then the saturation should be set to ”ON”. This enables saturation window where the saturation parameters are entered.

The second part of the parameters entered in the main configuration window is mainly solver related parameters. The user can choose between five different types of solver. Solvers are given in increasing order starting with forward Euler method and ending with Runge-Kutta 5 as the highest order solver. Terminals connection delay is entered as time in seconds and provides very useful feature of ”skipping” initial transients in the electric network. During this time stator currents are set to zero, while other state variables are calculated. For instance, if the electric grid gets close to steady state in 0.5 s, then the terminals connection delay is set at that value and machine is connected at that time. Open circuit signal switch acts the same way with exception that machine stator currents are set to zero by timed breaker logic signal. This acts as an open circuit switch and is the only way of disconnecting machine from the grid if the terminating resistance is set to ”OFF”. The user can enter zero value if the machine is going to be connected whole time. If it is going to be disconnected from the grid using a regular breaker from PSCAD library, the terminating resistance has to be set to ”ON”. Two following two fields, terminating resistance and low-pass voltage filter are used to increase the stability of calculations. Number of coherent machines is a feature that provides simulation of several machines connected to the same bus. This value should be entered as a positive integer.

Machine parameters data entry windows are simple and very much straight forward. Window for synchronous machine parameters in SI units is shown in Figure 5.3.

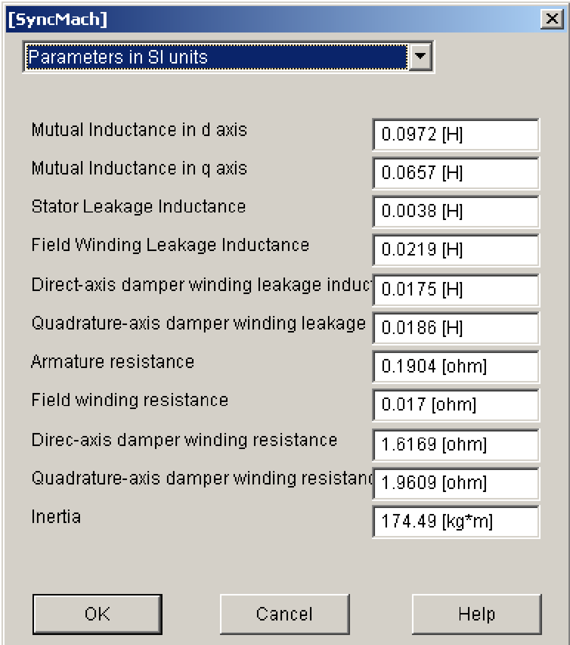

Figure 5.3: The synchronous machine model - SI unit parameters.

Data entry fields start by entering the parameters of the mutual and leakage inductances. After this, resistances and inertia of the machine is entered. The same structure of the data entry window is given for per unit parameters which can be observed in Figure 5.4.

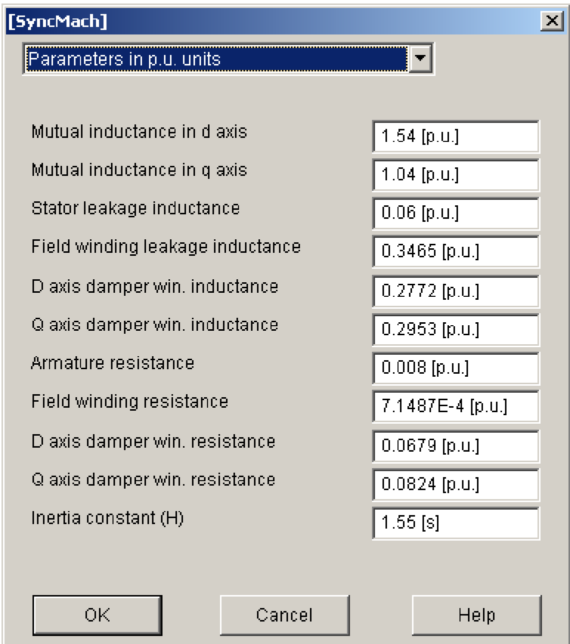

Figure 5.4: The synchronous machine model - per unit parameters.

Standard parameters data entry window differs from previous two and the structure of the window starts by entering the values of reactances in d-axis and q-axis. Then, stator leakage reactance and stator resistance are entered. This is followed by time constant data entry fields. The standard unit data form is given in Figure 5.5.

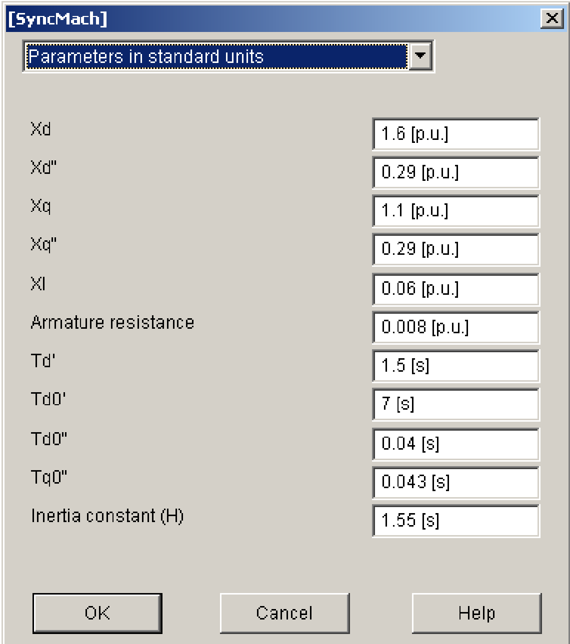

Figure 5.5: The synchronous machine model - standard parameters.

After this data category, the saturation parameters can be set if the saturation on the main configuration window is set to "ON". The data form given in saturation window corresponds to the saturation parameters given in Appendix D where is explained how to determine these extrapolation parameters observing the main flux saturation curve. The data entry form for saturation parameters is given in Figure 5.6.

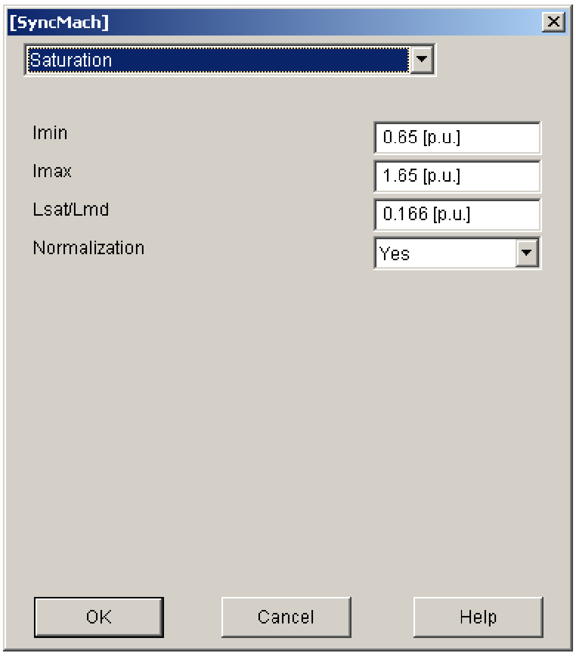

Figure 5.6: The synchronous machine model - saturation parameters.

The last data entry category is reserved for initial conditions settings. Currents are entered in Amperes except for the field current which is given in per unit. Rotor angular speed initial condition is entered in per unit while the load angle δ and the rotor position angle Θ are entered in degrees. This form with recommended values of initial conditions is given in Fig. 5.7.

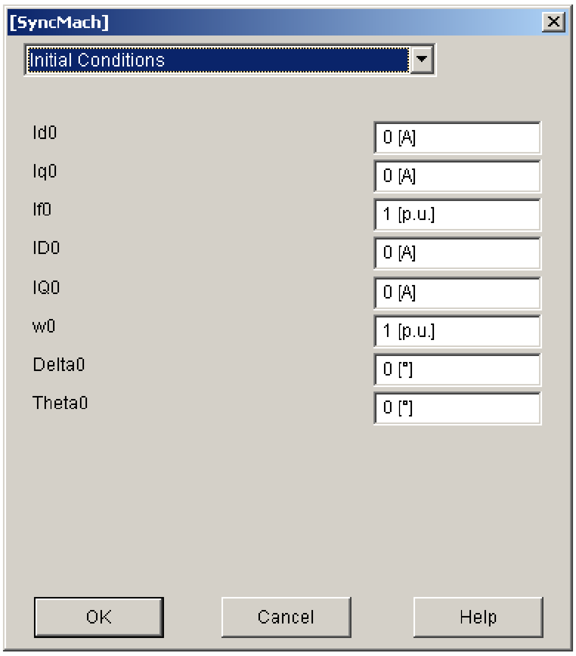

Figure 5.7: The synchronous machine model - Initial conditions with recommended settings.

5.2 Algorithm

To implement model in PSCAD/EMTDC following algorithm given in Figure 5.8 is used.

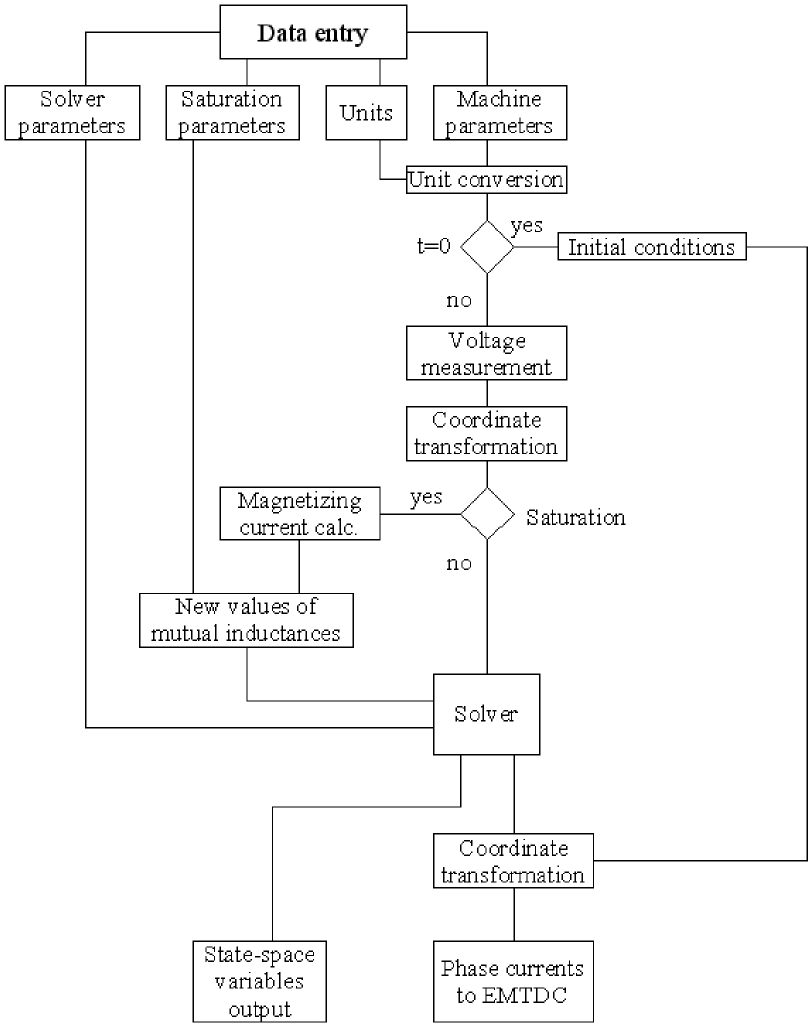

Figure 5.8: Algorithm for the synchronous machine model.

For the given model, data can be entered in three different ways, such as SI, p.u. or standard units. Unit calculation is performed before any other calculations of state variables and is performed in calculations segment of the PSCAD script.

In the first time step when t=0, the state variables takes value from initial conditions. Voltage measurement is skipped, coordinate transformation is performed and currents are injected into the electrical nodes by interfacing the model to EMTDC. In the following steps, the voltages from the electrical nodes at synchronous machine terminals are measured. Since the synchronous machine model is modeled in the dq-coordinate system, coordinate transformation is performed as the next step. After this step, all of the control variables are measured and transformed to the proper form so the solver can start calculating state variables. However, depending on the data entry for the saturation parameters synchronous machine model has to perform additional calculations. For the saturation option switched on, synchronous machine model performs the calculation of the magnetizing current. Depending on the value of this current, new values for mutual inductances L_{mds} and L_{mqs} are calculated. After this step, the implemented solver can calculate new values of the state variables depending on the entered solver parameters. Currents in the *dq*-coordinate system, other state variables, active and reactive power injected into the node and measured terminal voltage in the *dq*-coordinate system are given as the "measured signals" from the synchronous machine model block.

However, more important is the fact how will the synchronous machine model "inject" these new values of the phase currents into its voltage terminals.New values of the currents first have to be transformed to ABC coordinate system. After coordinate transformation block, phase currents can be "injected" into the corresponding phase. This "injection" is performed using node interface to the PSCAD/EMTDC electric network. It can be represented by simple Norton current injection and the synchronous machine model acts as an ideal current source. The scheme of the synchronous machine model interface to EMTDC can be observed in Figure 5.9. Interface of the synchronous machine to the EMTDC electric grid is presented in Figure 5.9 a) while in Figure 5.9 b) can be observed that i_a,i_b and i_c are injected using Norton current sources.

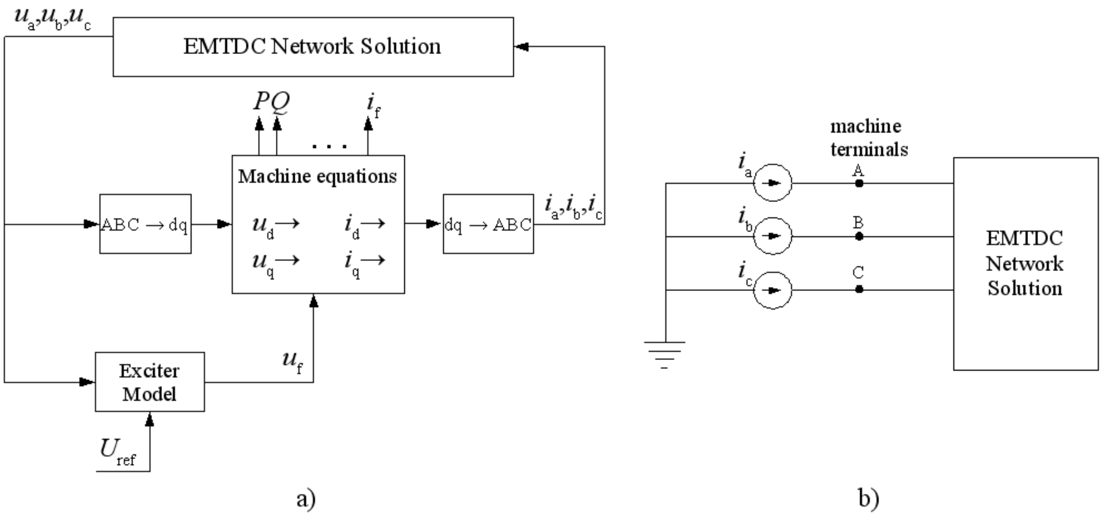

Figure 5.9: Synchronous Machine Model Interface to EMTDC.

5.3 Numerical methods for solution of state space equations

To solve the differential equations in the state space model two different numerical methods were used:

1 - Forward Euler Method

In Forward-Euler method, numerical integration is presented by step-by-step algorithm that gives solution going from the solution point (t_i, y_i) to the point (t_{i+1}, y_{i+1}). This stepping procedure is illustrated in Figure 5.10.

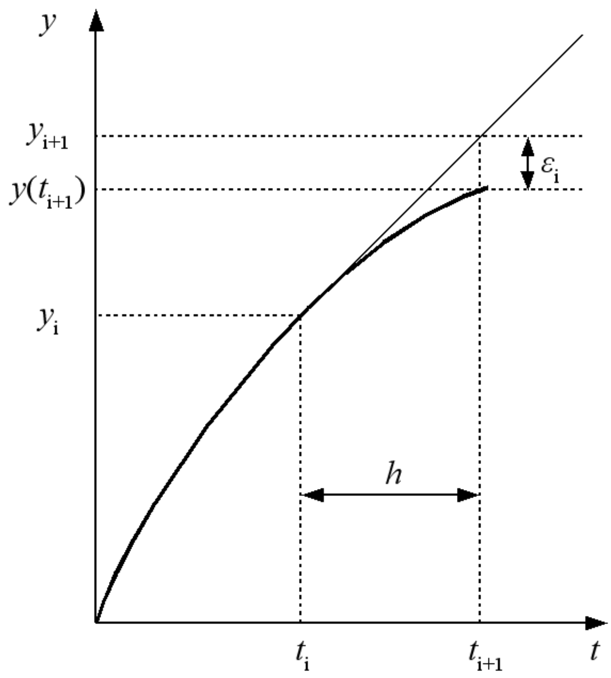

Figure 5.10: Stepping along the solution with Euler's method.

and can be represented mathematically by a Taylor series:

$$y_{i+1} = y_i + \frac{dy_i}{dt}h + \frac{d^2y_i}{dt^2}\frac{h^2}{2!} + ... \tag{5.1}$$

Where h = t_{i+1} - t_i. This series can be truncated after the linear term in h

$$y_{i+1} \approx y_i + \frac{dy_i}{dt}h \tag{5.2}$$

and can be used with this approximation to step along the solution from y_0 to y_1 (with $i = 0$), then from y_1 to y_2 (with $i = 1$), etc. This is the Euler's method. Note that "Euler" equation is equivalent to projecting along a tangent line from i to i+1. In other words, the solution, $y(t)$, is represented by a linear approximation. As indicated in Figure 5.10, an error ε_i will occur, which in the case of Figure 5.10 appears to be excessive. However, this apparently large error is only for purposes of illustration in Figure 5.10. By taking a small enough step, h, the error can, at least in principle, be reduced to any acceptable level.

2- Runge-Kutta Method

In order to increase the accuracy of the calculations, higher order terms are needed. Therefore, the Runge-Kutta method which consists of a series of algorithms of increasing order is used. There is only one first order Runge-Kutta method, which is the Forward Euler method, fits the underlying Taylor series of the solution up to and including the first derivative term, as indicated by:

$$y_{\mathrm{i}\,+\,1} \approx y_{\mathrm{i}} + \frac{dy_{\mathrm{i}}}{dt}h \tag{5.3}$$

The second-order Runge-Kutta method is actually a family of second-order methods where, a particular member is selected by choosing an arbitrary constant in the general second-order Runge-Kutta formulas. The origin of these formulas is illustrated by the following development. The analysis starts with a general Runge-Kutta stepping formula of the form:

$$y_{\mathrm{i}\,+\,1} = y_{\mathrm{i}} + c_1k_1 + c_2k_2 \tag{5.4}$$

where k_1 and k_2 are Runge-Kutta constants of the form:

$$\begin{aligned} &k_1 = f\left(y_{\mathrm{i}}, t_{\mathrm{i}}\right)h \\ &k_2 = f\left(y_{\mathrm{i}} + a_2k_1\left(y_{\mathrm{i}}, t_{\mathrm{i}}\right), t_{\mathrm{i}} + a_2h\right)h = f\left(y_{\mathrm{i}} + a_2f\left(y_{\mathrm{i}}, t_{\mathrm{i}}\right)h, t_{\mathrm{i}} + a_2h\right)h \end{aligned} \tag{5.5}$$

and c_1, c_2 and a_2 are constants to be determined using Taylor series expansion where terms of third order and higher are neglected. Using this expansion the following relations obtained for constants:

$$\begin{aligned} &c_1 + c_2 = 1 \\ &c_2a_2 = \tfrac{1}{2} \end{aligned} \tag{5.6}$$

This is a system of two equations in three unknowns or constants (c_1, c_2, a_2). Therefore, one constant can be selected arbitrarily. For the choice of $c_1 = 0$, $c_2 = 1$, $a_2 = 1/2$, the resulting second order Runge-Kutta method is:

$$\begin{aligned} &y_{\mathrm{i}\,+\,1} = y_{\mathrm{i}} + c_1k_1 + c_2k_2 = y_{\mathrm{i}} + k_2 \\ &k_1 = f\left(y_{\mathrm{i}}, t_{\mathrm{i}}\right)h \\ &k_2 = f\left(y_{\mathrm{i}} + \tfrac{1}{2}k_1, t_{\mathrm{i}} + \tfrac{1}{2}h\right)h \end{aligned} \tag{5.7}$$

Which is the midpoint method shown in Figure 5.11.

For 3^{rd}, 4^{th} and 5^{th} order Runge-Kutta methods 3^{rd}, 4^{th} and 5^{th} order terms of Taylor series expansion are required to calculate the coefficients. For 3^{rd} order Runge-Kutta method in particular Nystrom method is used. For Runge-Kutta(4,5) pair Runge-Kutta Fehlberg (RKF) method is used [35].

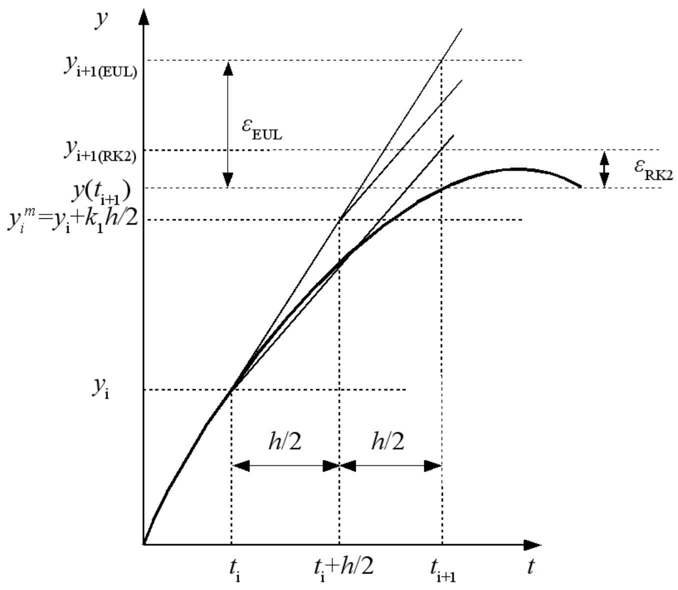

Figure 5.11: Midpoint method.

5.4 Effect of Terminating Resistance

Representing machines as a Norton current source in PSCAD has some drawbacks. For example, each machine must be computationally far from the other machines for stable operation [36]. As the machine is represented by a simple current source (which depends on the voltages from previous time step), any sudden change in voltage will cause a current response in the next time step. Hence, for the previous time step, the machine looked like an open circuit and spikes, which are not proceeding from the true source, appeared on the machine terminal voltages. According to [36], the cumulative effect of many machines causing this problem simultaneously in the same subsystem is proved to be destabilizing. Also, it is found that when the machine is simulated near open circuit conditions, a smaller time step is required to keep computational stability. Alternatively, a small capacitance or large resistance can be placed between the machine terminals and ground to prevent the machine from being totally open-circuited. Even if the physical meaning of parasitic capacitance or leakage resistance can be applied to these elements, it is not a satisfactory solution.

This idea led to terminate the machine to the network through a terminating "characteristic impedance" as shown in Figure 5.12. The effect of this added impedance is then corrected by an adjustment to the current injected.

Using this technique, a uniformly good machine model behavior is obtained. It combines the compensation-based model and the non-compensated model, while eliminating the restriction of adjacent machines and the necessity of calculating the network Thevenin equivalent circuit.

Since the synchronous machine model is observed, its "characteristic impedance" can be approximated by sub-transient synchronous reactance in d-axis. Furthermore, synchronous condenser during sub-transients can be represented with a Norton current source and a resistor with its value calculated using Eq.(5.9) which is machine "characteristic impedance".

According to Figure 5.12 the variables are calculated as follows:

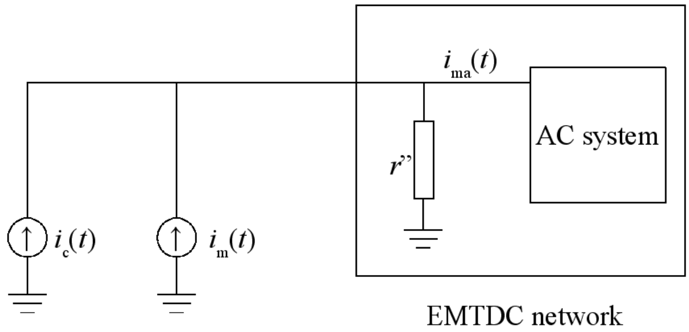

Figure 5.12: Interface with terminating resistance.

$$i_c = \frac{u(t - \Delta t)}{r''} \tag{5.8}$$

$$r'' = \frac{2L''}{N\Delta t} \tag{5.9}$$

The impedance r'' is calculated using the direct axis sub-transient inductance of the synchronous machine L'', number of coherent machines in parallel N and EMTDC time step Δt. This resistance is placed from each node of the machine terminal to ground within the EMTDC network. Instead of injecting only the calculated machine current $i_m(t)$, a compensated current and calculated machine current $i_m(t) + i_c(t)$ is injected, where $u(t - \Delta t)$ is the terminal voltage in the previous time-step, to the network. Therefore, the actual current injected into the network is:

$$i_{ma}(t) = i_m(t) + \frac{u(t - \Delta t) - u(t)}{r''} \tag{5.10}$$

Terminating resistance r'' is usually quite large, due to the Δt in its denominator. Also, for a small time step $u(t - \Delta t) = u(t)$, and hence, $i_{ma}(t) = i_m(t)$, and the error introduced vanishes in the limit with a small Δt. However, for a sudden voltage change, as $i_m(t) + i_c(t)$ is not calculated until the next time step, the network sees the impedance r'' for this instant (instead of the open circuit discussed earlier). This is exactly the instantaneous impedance it would have seen if the machine had been represented in the EMTDC program main matrix. Thus, the network current calculated in this instant is more accurate, and the spurious spikes discussed earlier do not arise. Hence, this concept of terminating the machine with its "characteristic impedance" and then compensating for this in the current injection is a suitable way for assuring accurate solutions [36].

Chapter 6

Simulations of Synchronous Condensers

In this chapter, different cases are studied to verify the model in detail

6.1 Case study - Terminal voltage control

To observe the effect of different solvers and different time steps in the synchronous condenser model, the following circuit is used:

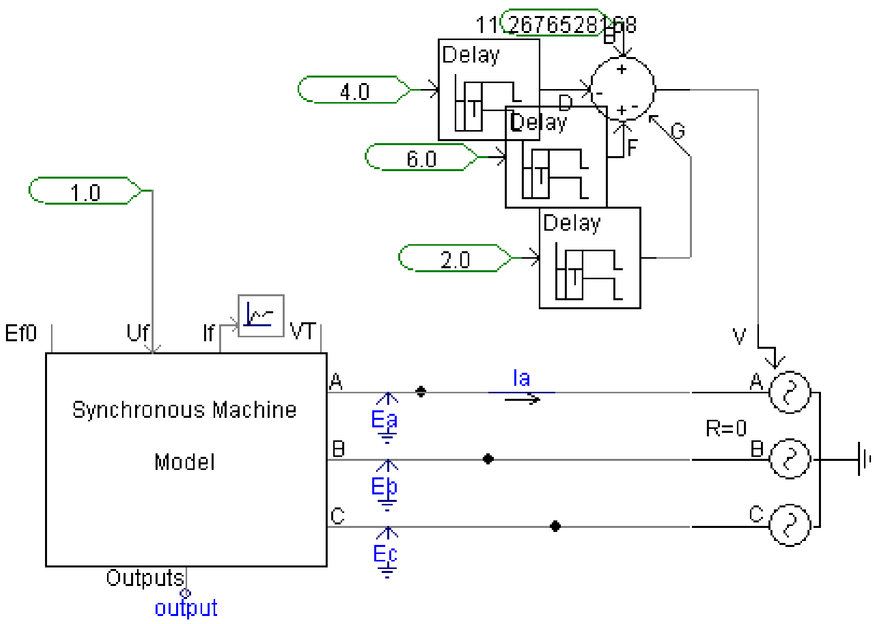

Figure 6.1: Circuit for observing the effect of different solvers and time steps in PSCAD.

After applying the V_t signal shown in Figure 6.1 to the machine terminals and using the simulation result of 5^{th} order Runge-Kutta at 1 μs as base and using the peak of the rated current as the base current for calculating the error percentage, which is $\frac{I_d - I_{d(base)}}{\widehat{I}_{rated}}100$. I_d(p.u.), I_d error (%) vs. time and I_d error (%) vs. time step (μs) figures for different solvers simulated with different time steps are obtained which are shown in Figure 6.1 (where only Euler case is shown) and Figure 6.2.

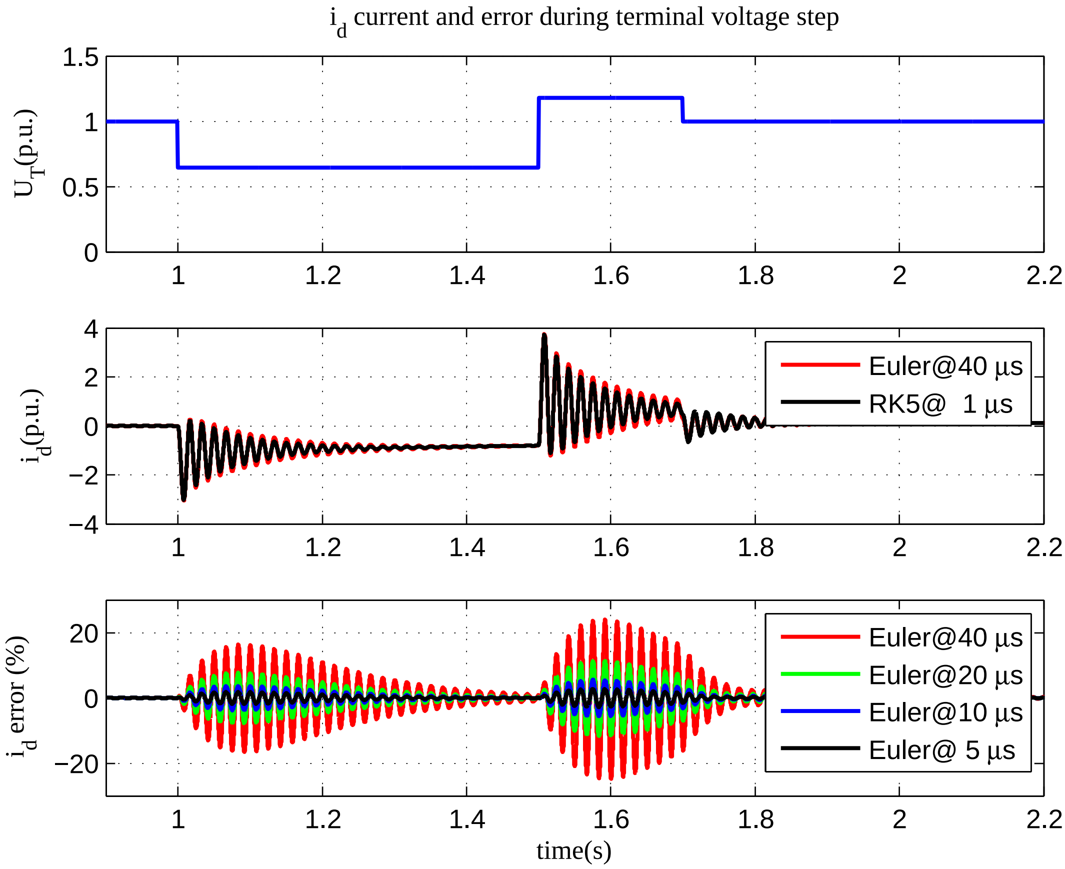

Figure 6.2: V_t (p.u.), I_d (p.u.), I_d error (%) vs. time(s) - solver comparison.

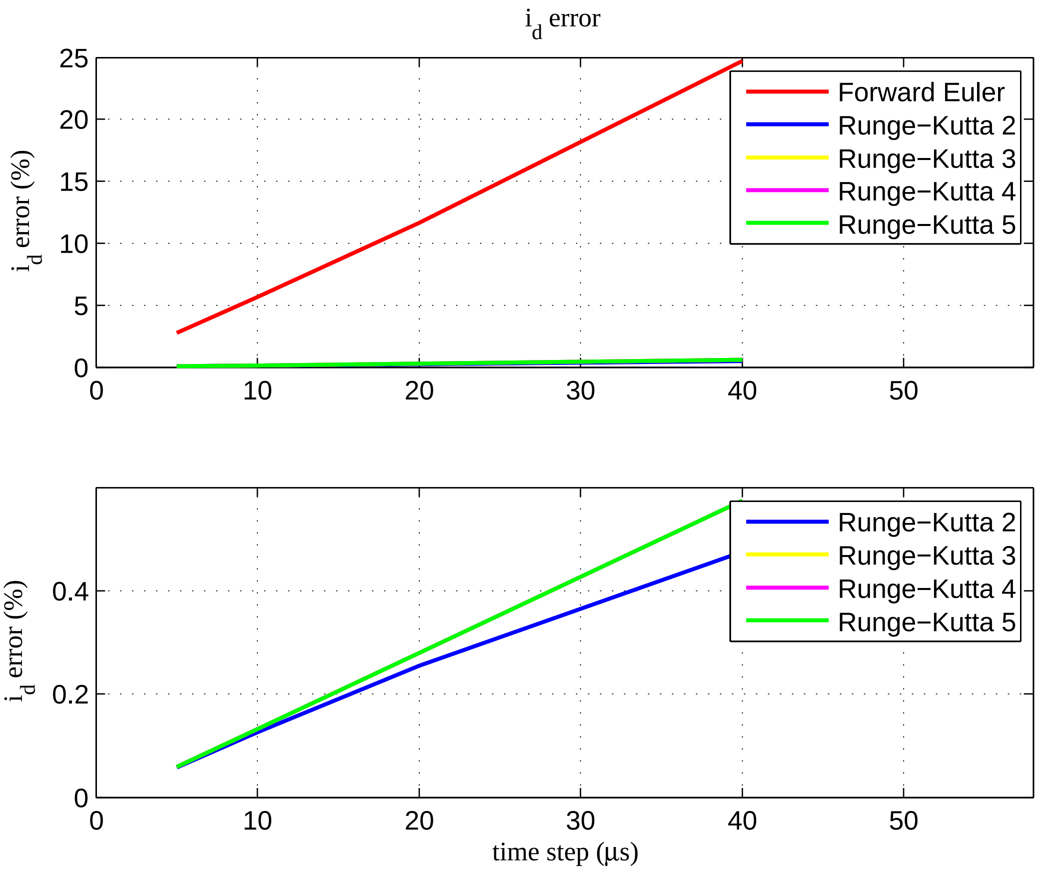

Figure 6.3: I_{d} error (%) vs. time step (μs).

As can be seen from Figure 6.3, the 3^{rd}, 4^{th} and 5^{th} order Runge-Kutta error curves overlap each other which show that they have approximately the same error.

Table 6.1 is obtained after putting the absolute maximum values for the error which are obtained from Figure 6.1 for the Euler case and from the simulation results for other cases.

Table 6.1: Time step vs. maximum error in I_{d} for different solvers

	Solver	Euler	RK2	RK3	RK4	RK5
Time Step						
5 μs		2,79 %	0,06 %	0,06 %	0,06 %	0,06 %
10 μs		5,65 %	0,13 %	0,13 %	0,13 %	0,13 %
20 μs		11,62 %	0,25 %	0,28 %	0,28 %	0,28 %
40 μs		24,71 %	0,48 %	0,57 %	0,57 %	0,57 %

Similarly, the following results shown in Figure 6.4, Figure 6.5 and Table 6.2 are obtained for I_q after simulations in PSCAD.

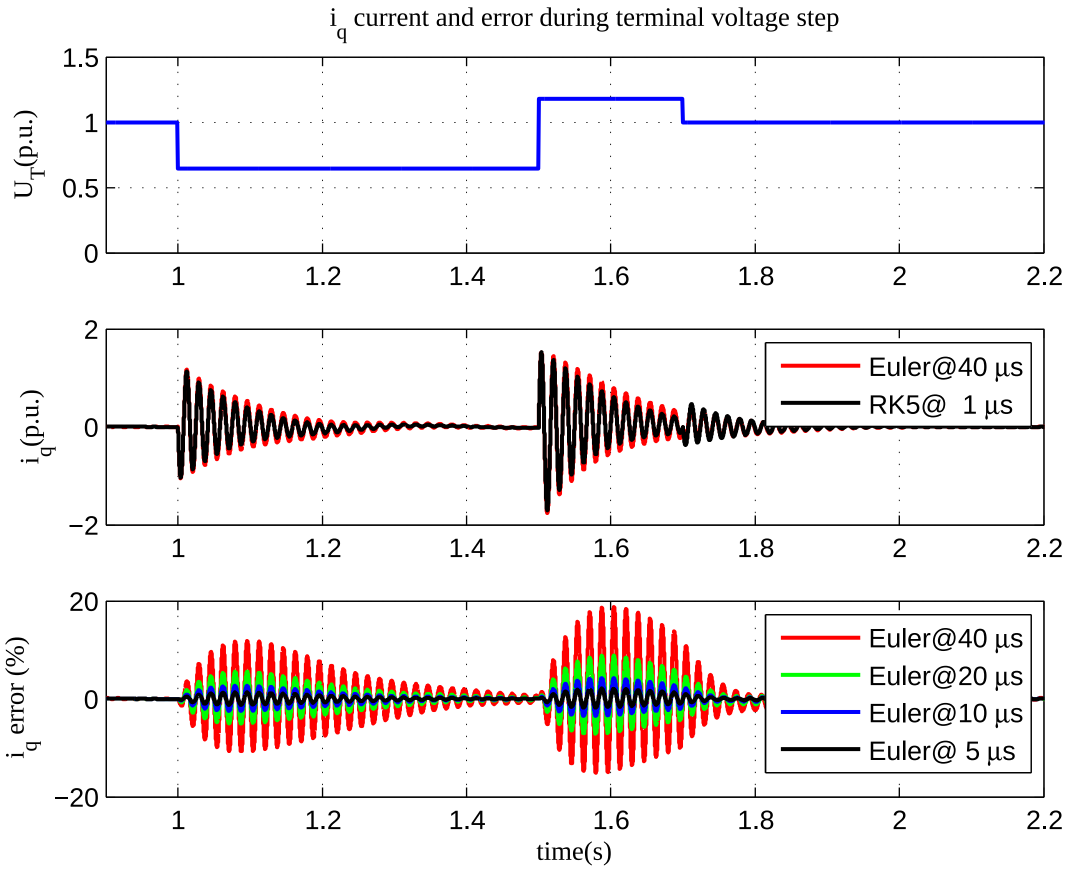

Figure 6.4: V_t (p.u.), I_q (p.u.), I_q error (%) vs. time(s) - solver comparison.

As can be seen from Figure 6.5, the 3^{rd}, 4^{th} and 5^{th} order Runge-Kutta error curves overlap each other which show that they have approximately the same error.

Table 6.2: Time step vs. maximum error in I_q for different solvers

	Solver	Euler	RK2	RK3	RK4	RK5
Time Step						
5 μs		2,10 %	0,09 %	0,09 %	0,09 %	0,09 %
10 μs		4,27 %	0,20 %	0,21 %	0,21 %	0,21 %
20 μs		8,80 %	0,42 %	0,44 %	0,44 %	0,44 %
40 μs		18,81 %	0,83 %	0,90 %	0,90 %	0,90 %

As can be seen from Table 6.1 and Table 6.2, the minimum error is obtained when the second order Rungre-Kutta method is chosen as the solver. Since there is infinite number of Runge-Kutta coefficients that can be used for the same order of solver, the final result is dependent on the choice of coefficients. Choosing coefficients c_1= $1/2$, c_2=$1/2$ and a_2=1, the second order Runge-Kutta method is resulting in the modified Euler method, which is the only method given above that is not splitting the time step into smaller pieces. Hence, this leads to increased accuracy.

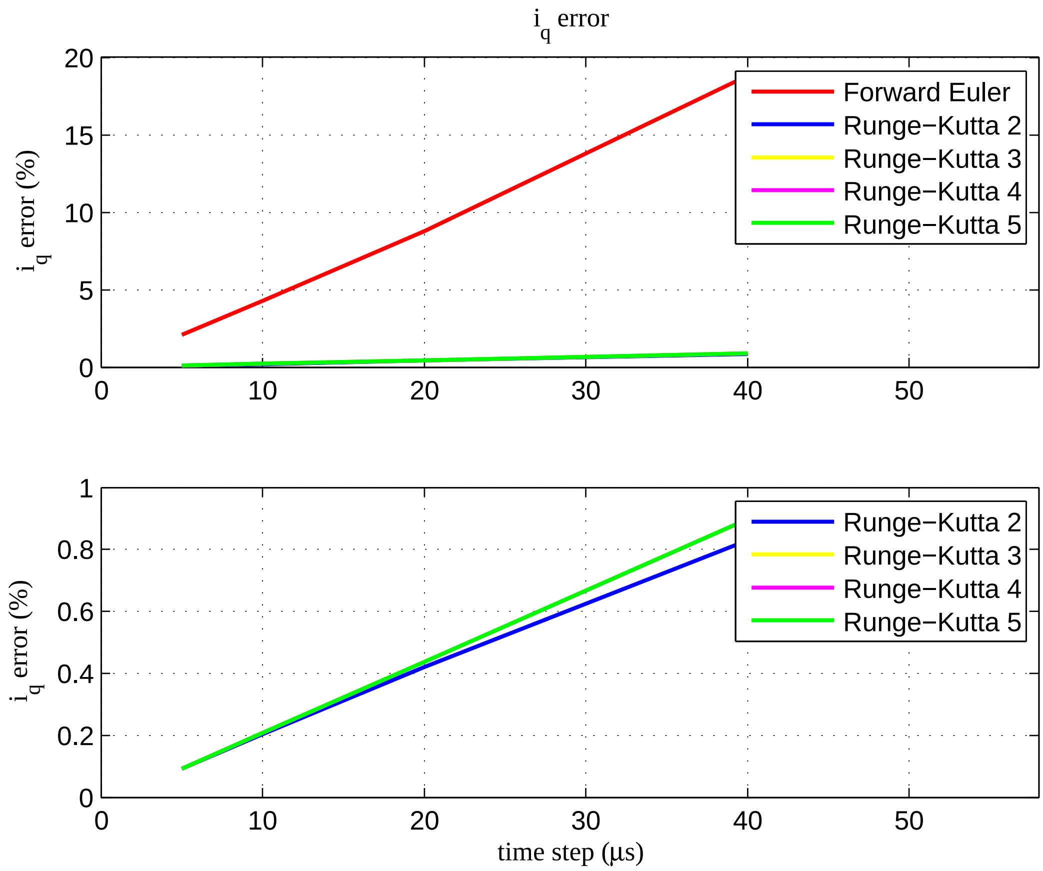

Figure 6.5: I_q error (%) vs. time step (μs).

To compare the saturation in steady state, first, the accuracy of the implemented synchronous condenser model is compared to the extrapolated saturation curve taken from the built-in PSCAD model (see Appendix D). To obtain these results, open-circuit test is conducted. In this test, a voltage step to the field winding is applied and the terminal voltage is measured. Also another test is conducted, in which the field winding voltage is kept at nominal value, while a voltage step at machine terminals is applied. This leads to expected deviation from the saturation curve, since the leakage flux is added. The deviation between the two models is shown in Figure 6.6.

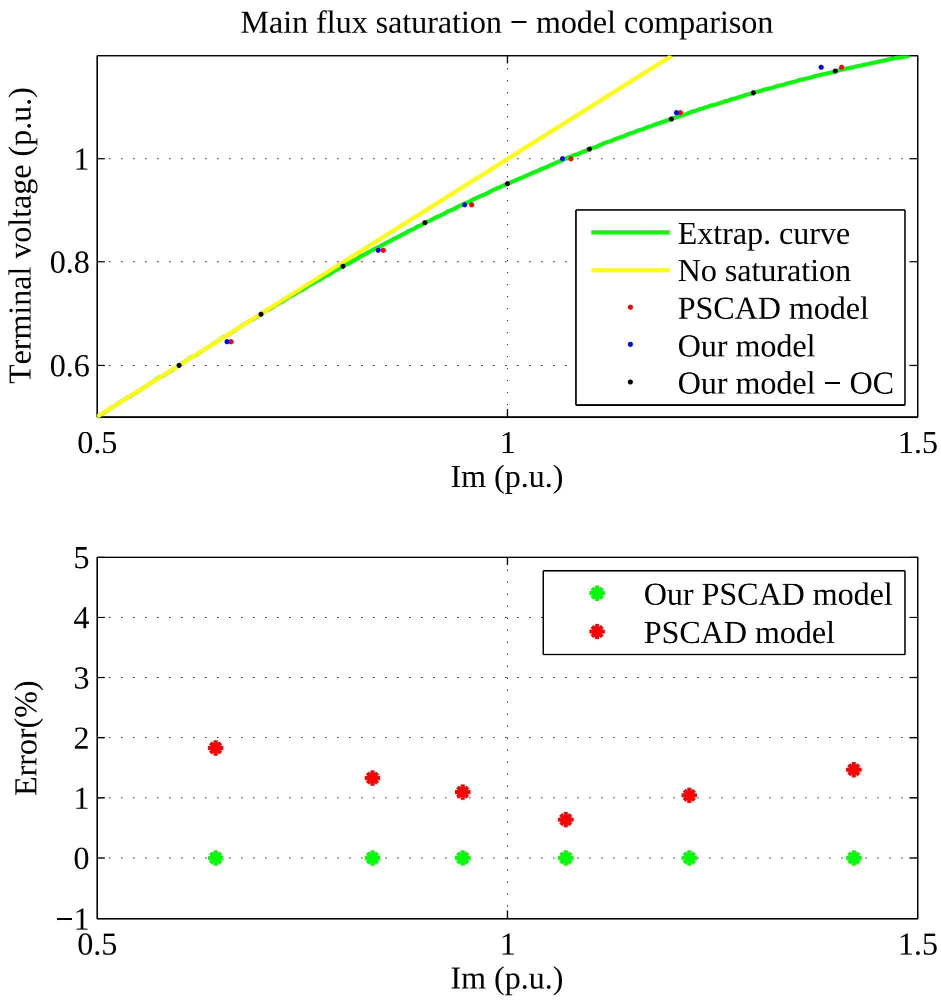

Figure 6.6: Terminal voltage, error vs. magnetizing current.

From Figure 6.6, it is seen that the deviation between the two models is less than 2 %. This deviation is mainly due to different approach in saturation curve representations.

For comparison of the implemented synchronous condenser model and the built-in PSCAD model, a Matlab model has been developed using the state space equations given in Chapter 3. In this Matlab model, which is taken as reference, the 4^{th} order Runge-Kutta solver is used.

As can be seen from Figure 6.7, the maximum error is less than 3 % for I_d obtained from the built-in PSCAD model, and less than 1 % from the implemented synchronous condenser.

Similarly, Figure 6.8 is obtained after simulations which show that the maximum error is less than 3 % for I_q obtained from the built-in PSCAD model, and less than 1 % from the implemented synchronous condenser model.

After enabling saturation, an error of maximum 10 % for I_d is obtained from the built-in PSCAD model, and an error of less than 5 % from the implemented synchronous condenser model shown in Figure 6.9. The maximum error for the PSCAD built-in model is obtained in the beginning of the transients when I_d has its minimum and maximum values and when the terminal voltage measured in steady state has its maximum error, which is shown in Figure 6.6.

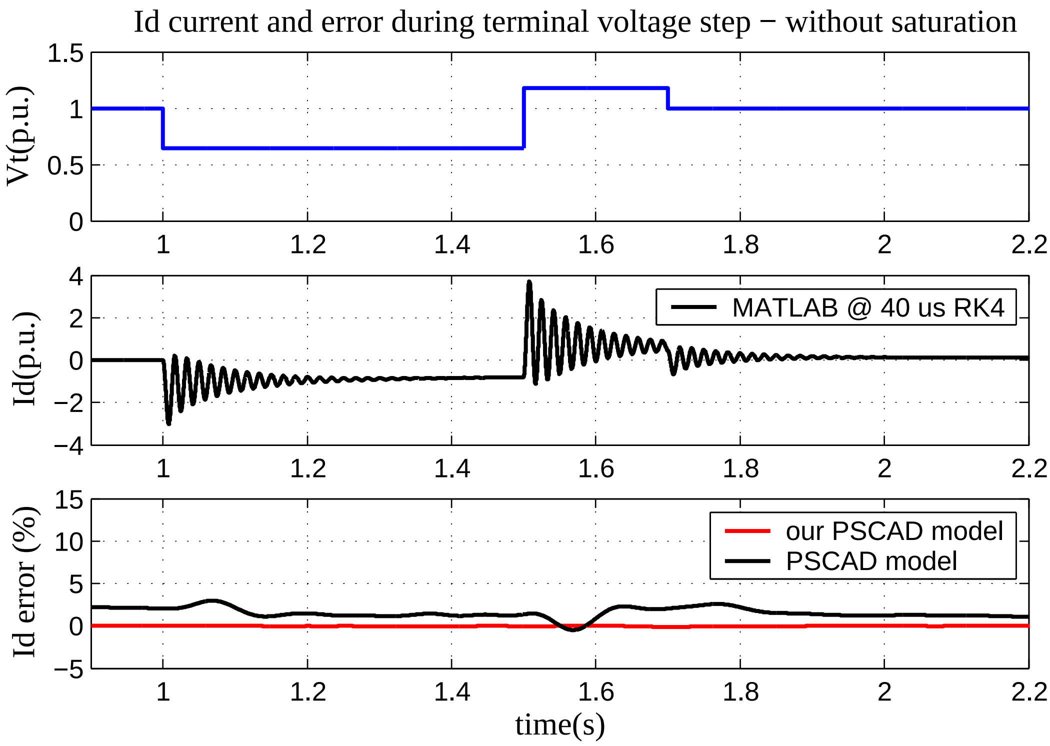

Figure 6.7: V_t (p.u.), I_d (p.u.), I_d error (%) vs. time(s) - model comparison without saturation.

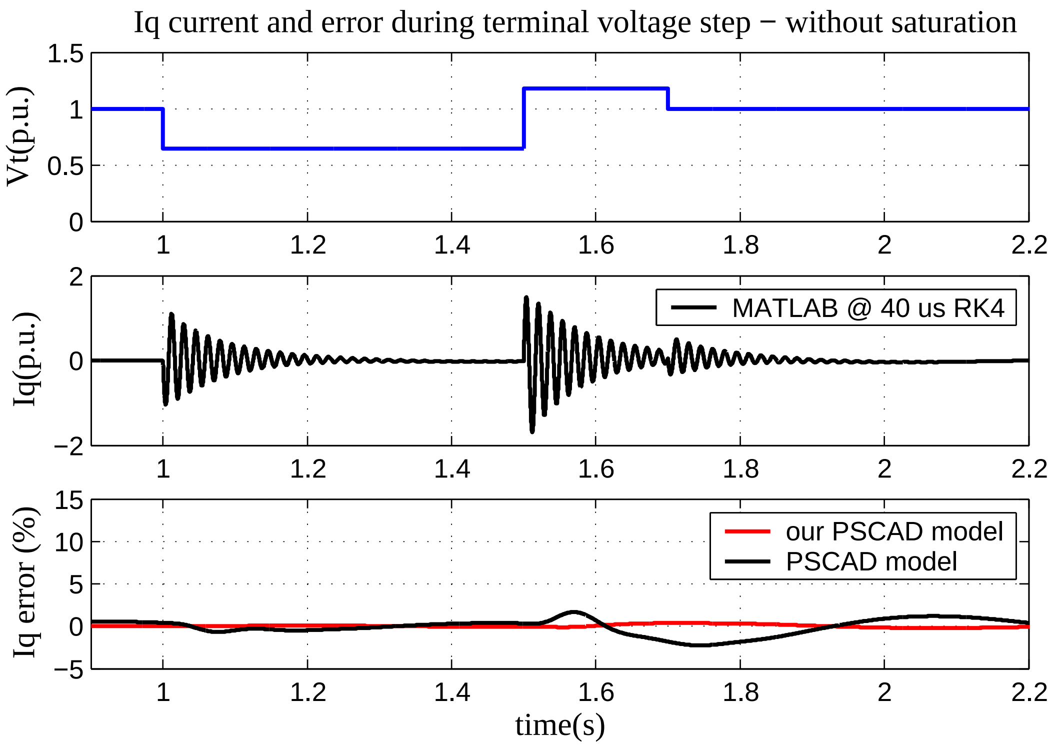

Figure 6.8: V_t (p.u.), I_q (p.u.), I_q error (%) vs. time(s) - model comparison without saturation.

As there is no saturation in the q-axis for the built-in PSCAD model, no comparison is made for I_q with saturation.

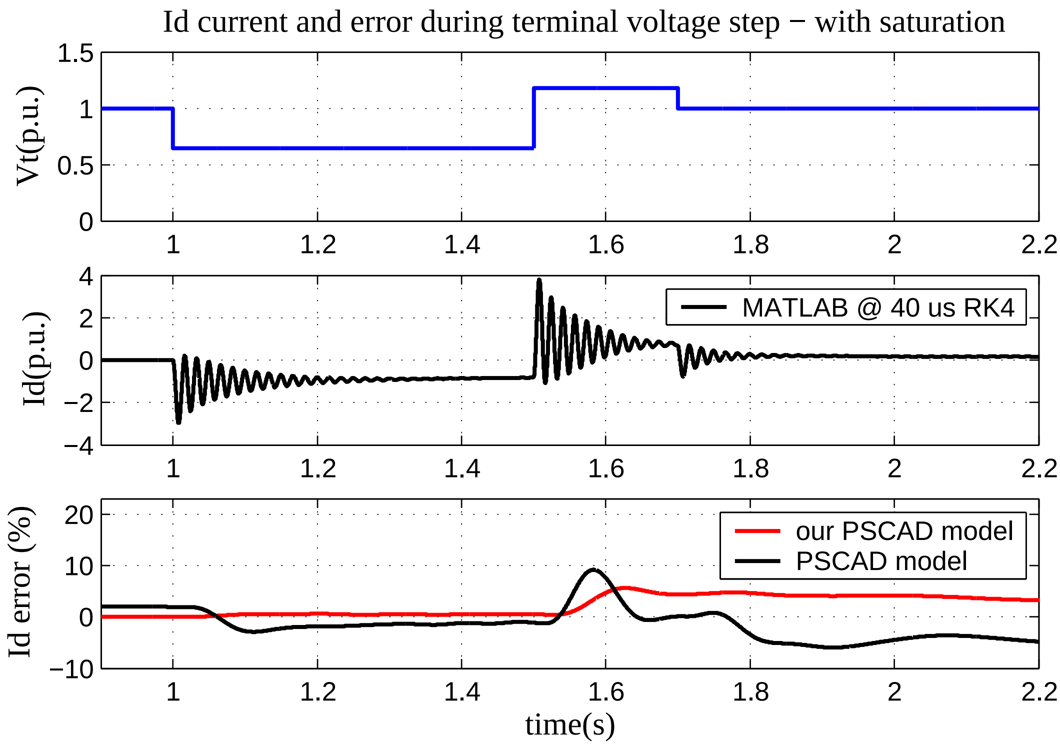

Figure 6.9: V_t (p.u.), I_d (p.u.), I_d error (%) vs. time(s) - model comparison with saturation.

To observe the effect of d-axis flux saturation more clearly and accurately, the saturation curve is normalized which is shown in Figure 6.10. This means that at nominal value of the field current, the machine will have the same parameters with and without saturation.

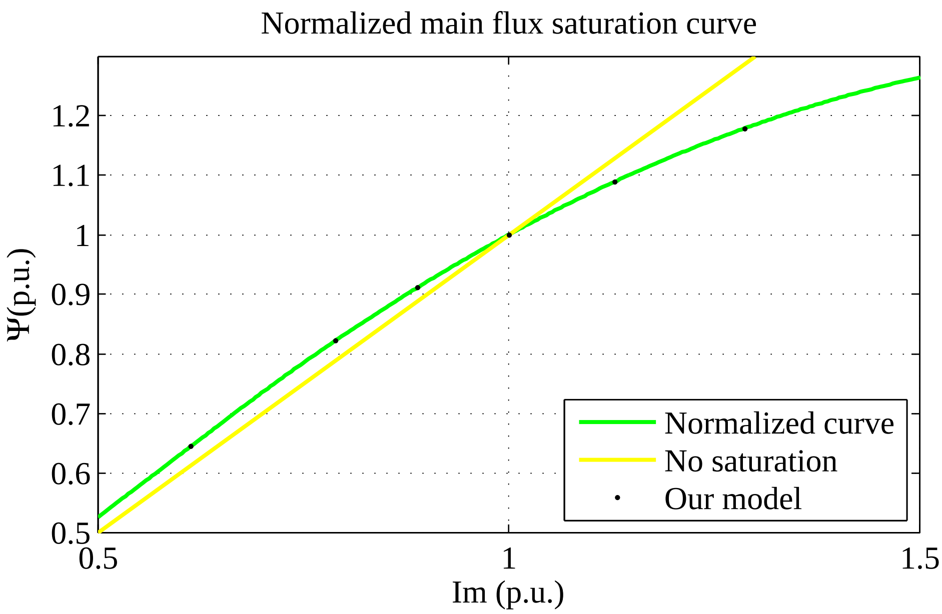

Figure 6.10: Flux (p.u.) vs. I_m (p.u.) - normalized curve.

The effect of saturation on I_d is observed in Figure 6.11. It can be seen that up to 20 % increase in current occurs with saturation.

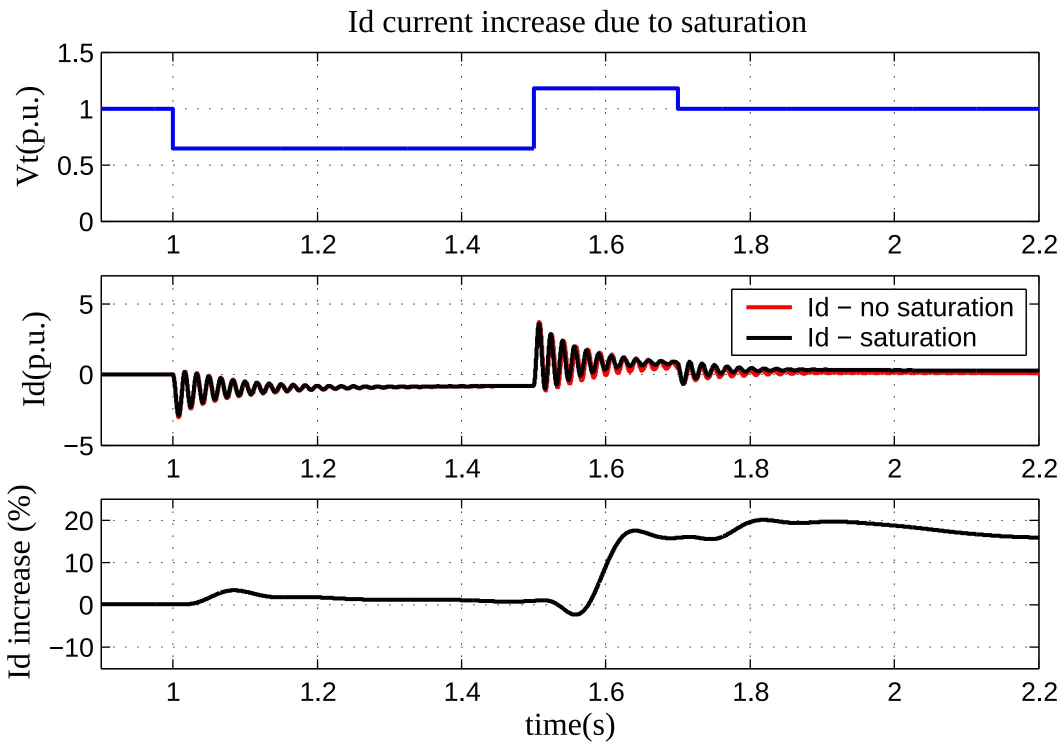

Figure 6.11: V_t (p.u.), I_d (p.u.), I_d increase (%) vs. time(s) - comparison with and without saturation in the implemented synchronous condenser model.

6.2 Case study - short circuit

To minimize the influence of the terminating resistance to machine transients and to calculations of currents, its value is calculated from the equations given in Chapter 5. This prevents oscillations in the currents during transients because of the impedance matching between the machine and the terminating resistance. Minimizing the time step increases the value of the terminating resistance and decreases the influence of the added resistance to the network, since resistances and reactances in the network will have much lower values than the terminating resistance.

To observe the effect of the terminating resistance on the calculated results, a short-circuit test is applied. In the first test, a resistor of 0.01 Ω is connected between the machine terminals and ground, in the second test, resistance is increased to 100 Ω. The first test is conducted with a 40 μs time step using the 2^{nd} order Runge-Kutta method and the second one with 10, 20 and 40 μs time step using the same numerical method. The reference signal for both tests is taken as the one obtained without the added terminating resistor and using the same solver properties.

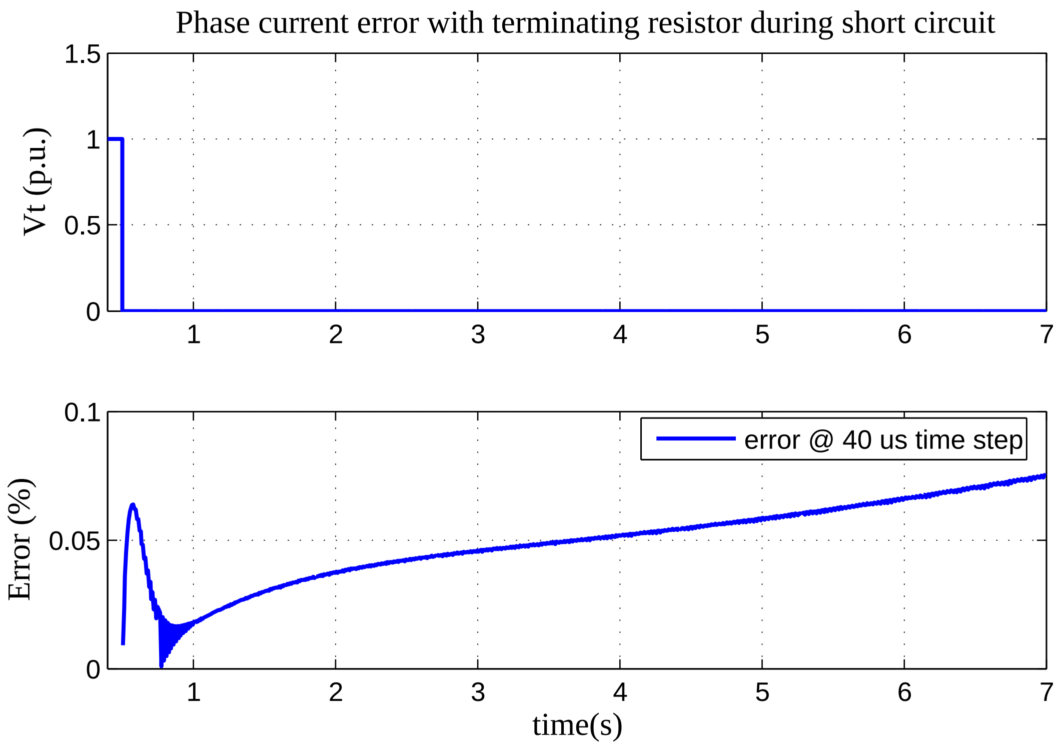

Figure 6.12: Error introduced to the phase current with the terminating resistance (R=0.01 Ω).

In Figure 6.12, it can be observed that during the short-circuit test with a resistor of 0.01 Ω, the error is less than 0.1 %. It can also be noticed that the phase current error during the beginning of the transient has a high value. This is because the terminating resistance is calculated using the subtransient inductance in d-axis direction and not in q-axis direction. During this test, the current in q-axis direction is very high which results in a higher error during the very beginning of the transient.

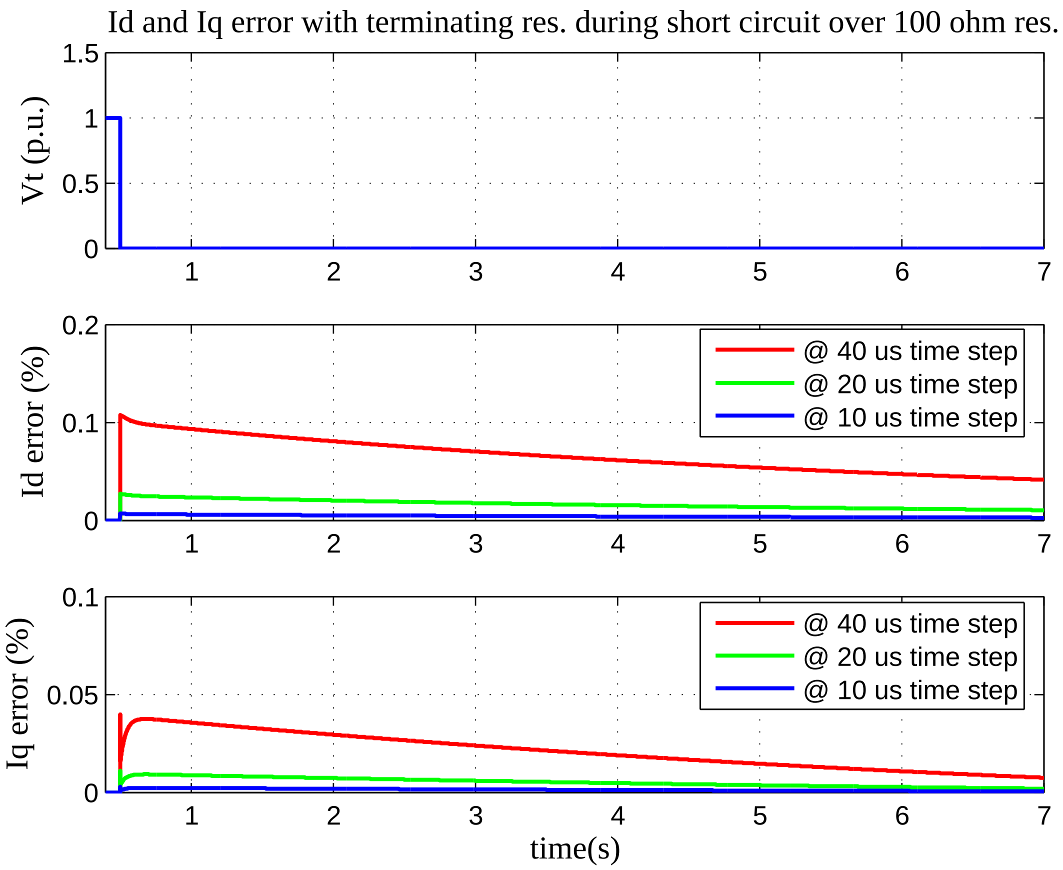

Figure 6.13: Error introduced to I_{d} and I_{q} current with the terminating resistance (R=100 Ω).

In Figure 6.13, the influence of the terminating resistance during the short-circuit test with a resistor of 100 Ω is observed. Since the calculated value of the terminating resistance for a time step of 40 μs is in the order of hundreds of Ohms, higher error is obtained. In this test, the maximum error for the currents in *d*-axis and *q*-axis direction is slightly higher than 0.1 %. However, decreasing the time step to 20 μs brings the value of the error below 0.03 %. This error is acceptable for the test.

The phase current waveform for the same test setup is investigated in Figure 6.14. It can be observed that the current angle error that is increasing during the test influences significantly the value of the phase currents. This error is negligible if the transients last no longer than the period of the transient time constant, but if the longer transients are observed, a decreased time step is recommended. For test setups where the machine has active load, it is strongly recommended to decrease the time step if the terminating resistance is used. A time step of 10 μs will keep the error within 1 % for simulations that are less than one minute long.

The amount of the error measured at different time instants vs. time step plot is obtained in Figure 6.15. The error is measured at the instants of T'_{d}, T''_{d} and at the end of the simulation. It can be noticed that decreasing the time step to 20 μs decreases the phase current error below 1 % which is satisfactory for most of the test setups.

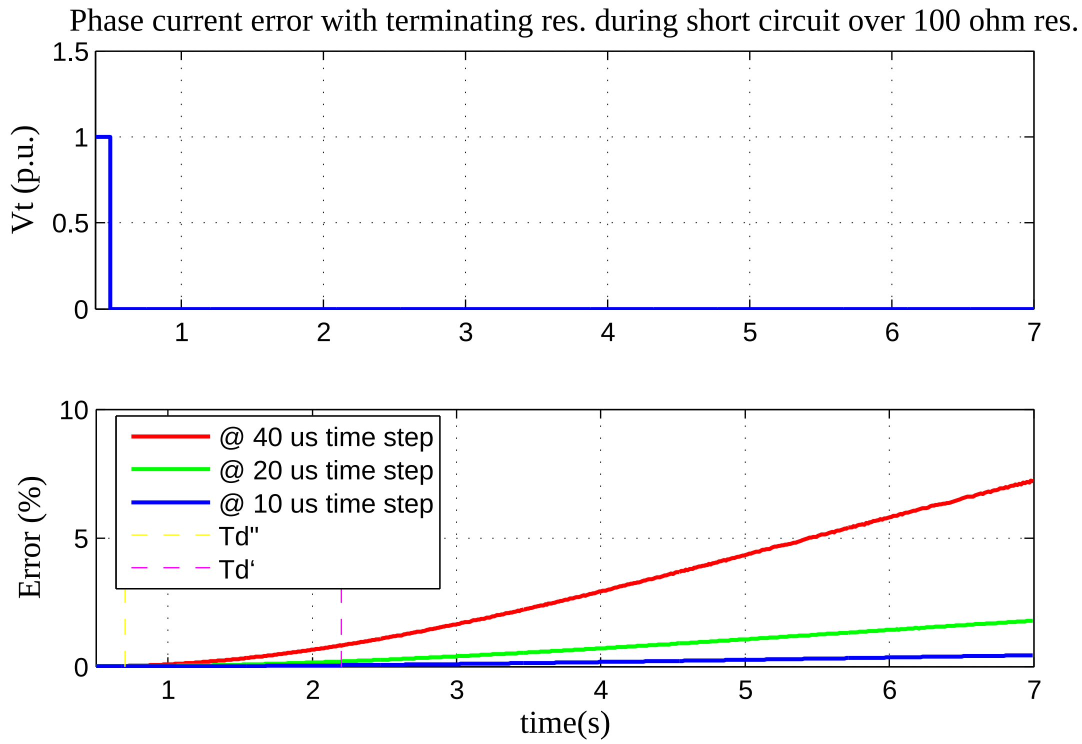

Figure 6.14: Error introduced to the phase current with terminating resistance (R=100 Ω).

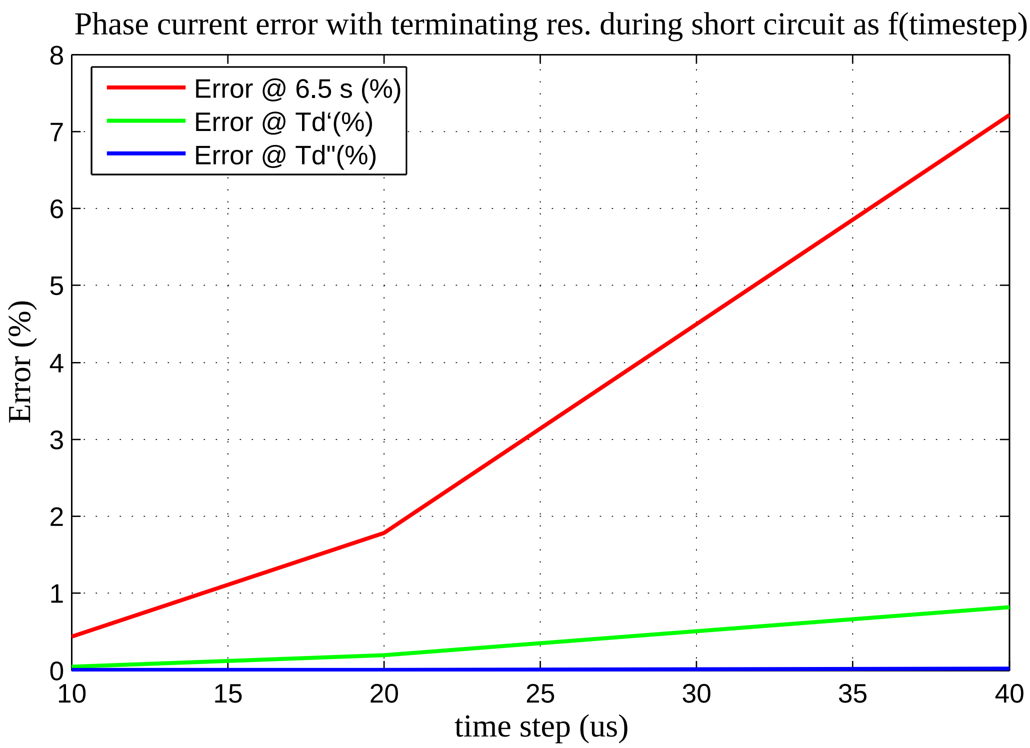

Figure 6.15: The phase current error (%) vs. time step (μs).

6.3 Summary

After the simulations, it was seen that the difference between the implemented synchronous condenser model and PSCAD built-in model is less than 5 %. Moreover, increasing the order of the solver gave more accurate results. The effect of saturation on the synchronous condenser models was also observed. Furthermore, it was seen that the error introduced by terminating resistance can be neglected when using time step less than 20 μs.

Chapter 7

Comparison of Superconducting Synchronous Condenser and Conventional Synchronous Condenser

In this chapter, the comparison of a superconducting synchronous condenser with a conventional synchronous condenser is done with a grid setup.

7.1 Grid setup

To compare the performance of the superconducting synchronous condenser and the conventional synchronous condenser, single line grid setup shown in Figure 7.1 is used.

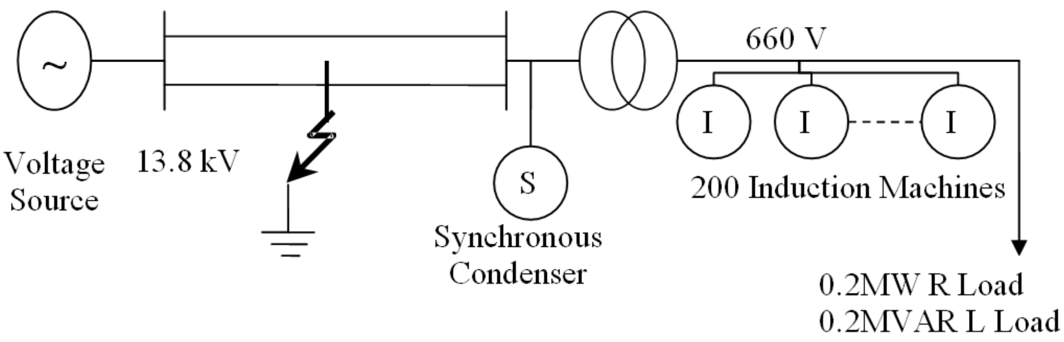

Figure 7.1: Single line diagram of the grid setup.

The detailed figure for the same grid used in PSCAD is shown in Figure 7.2.

In this grid setup, a factory, where the main load of the factory consists of 200 induction machines of 50 HP with 0.85 power factor. 660 V with inertia constant of 1 s, is connected to a substation of 13.8 kV via its own 10 %, 13.8/0.660 kV, 10 MVA transformer. A resistive and an inductive load of 0.2 MW and 0.2 MVAr are used to represent the other electronic components in the factory. A capacitor bank of 5.25 MVAr is used to keep the 660 V bus within 95 %-100 % of the bus voltage during the full load operation. The short circuit ratio

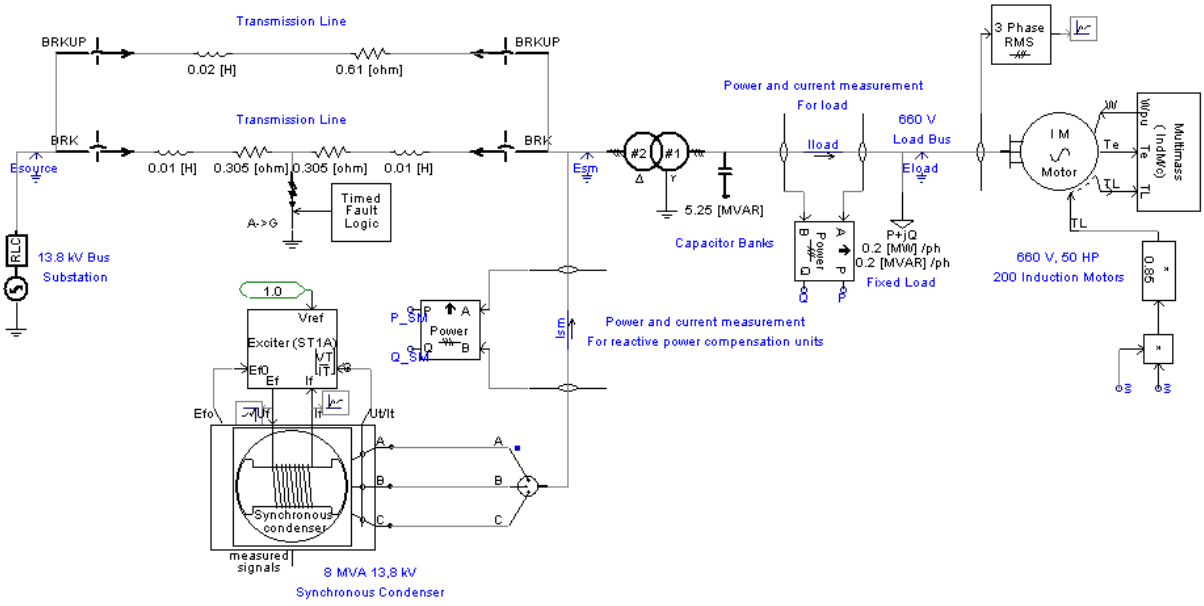

Figure 7.2: Grid setup used in PSCAD.

(SCR) at the synchronous condenser terminals, which is the ratio of short circuit power measured at the synchronous condenser terminals to the load total apparent power, is 4.2 which represents a medium system.

The 8 MVA synchronous condenser is connected to 13.8 kV bus to provide reactive power compensation especially in case of faults that can occur in the lines that transfers power from the substation to the factory. The power is transferred from the substation to the factory via two 20 km lines with an X/R ratio of 12 where the fault occurs in one of the lines which will cause the breakers to open after 200 ms delay and make the faulted line out of operation during the rest of the simulation.

The 13.8 kV substation has a short circuit capacity of 150 MVA with an X/R ratio of 11 which is kept constant during the simulations.

During the simulations, the tuning of type DC2A exciter which is used for the conventional synchronous condenser and type ST1A exciter which is used for the superconducting synchronous condenser are done according to provide the same power output from the exciters. During steady state, the field current is calculated using Eq.(7.1)

$$I_{\mathrm{f}} = \frac{E_{\mathrm{f}}}{L_{\mathrm{md}}\omega_{\mathrm{s}}} \tag{7.1}$$

Where E_{f} is the induced EMF of the synchronous condenser which is equal to peak of the synchronous condenser phase voltage. As the d-axis magnetizing inductance L_{md} of the superconducting synchronous condenser is approximately 3.8 times smaller than L_{md} of the conventional synchronous condenser, Eq.(7.2) which shows the relation between field currents can be written for the same turn ratio between rotor and stator.

$$I_{\mathrm{f,sco}} = 3.8 I_{\mathrm{f,con}} \tag{7.2}$$

Where, $I_{\mathrm{f,sco}}$ is the rated field current of the superconducting synchronous condenser, $I_{\mathrm{f,con}}$ is the rated field current of the conventional synchronous condenser during steady state. Moreover, to give the rated reactive power at steady state, using Eq.(7.3), it is found that the field current of the superconducting synchronous condenser should be increased approximately to 1.5 p.u., whereas the field current of the conventional synchronous condenser should be increased approximately to 2.6 p.u..

$$I_{\mathrm{n}} = \frac{E_{\mathrm{f}} - U_{\mathrm{t}}}{X_{\mathrm{d}}} \tag{7.3}$$

Where, I_{n} is the nominal stator phase current of the synchronous condenser, X_{d} is the d-axis synchronous reactance of the synchronous condenser and U_{t} is the peak of the nominal stator phase voltage of the synchronous condenser. Using Eqs.(7.1) to (7.3), Figure 7.3 is obtained.

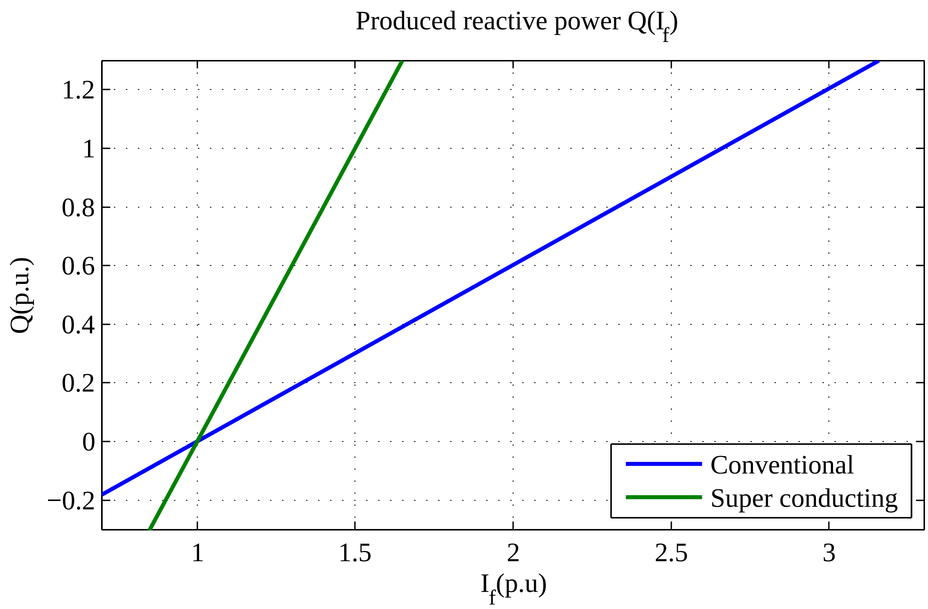

Figure 7.3: Reactive power (p.u.) vs. field current (p.u.).

Therefore, to give the rated reactive power, the field current given by the exciter of the superconducting synchronous condenser should be $\frac{3.8 I_{\mathrm{f,con}} 1.5 I_{\mathrm{f,con}}}{2.6 I_{\mathrm{f,con}}}$ which is equal to $2.2 I_{\mathrm{f,con}}$. Hence, to provide the same power output, the maximum voltage limit of the ST1A exciter should be which is 45 % of the maximum voltage limit of the DC2A exciter. As the field resistance of the superconducting synchronous condenser is approximately zero, the rated field voltage is much smaller compared to the conventional synchronous condenser rated field voltage which results in a very high regulator gain and upper and lower output voltage limits in p.u. for the ST1A exciter. The other parameters of the exciters such as regulator time constants and lead-lag compensator constants are tuned in order to make the exciter response fast as well as stable during the operation.

7.2 Simulation results

In order to compare the superconducting synchronous condenser with the conventional synchronous condenser, different cases are studied by changing the parameters in the grid. In the following figures, WOC represents configuration without any synchronous condenser connected to 13.8 kV bus, CON represents configuration with the conventional synchronous condenser connected to 13.8 kV bus and SCO represents configuration with the superconducting synchronous condenser connected to 13.8 kV bus.

7.2.1 Different Fault Type

To observe the performance of the superconducting synchronous condenser and the conventional synchronous condenser, a single phase to ground fault in the middle of one of the lines is simulated on the grid setup described in the previous section. First, the simulation is done without any synchronous condenser connected to 13.8 kV bus, then in the next simulation, the conventional synchronous condenser is connected to the 13.8 kV bus and in the final simulation, the superconducting synchronous condenser is connected to the 13.8 kV bus.

As can be seen from Figure 7.4, without compensation the system collapses after the fault whereas, the connection of the synchronous condenser (either conventional or superconducting) helps the system to survive after the fault. Also, it can be seen that the superconducting synchronous condenser keeps the minimum voltage level higher than the conventional synchronous condenser in the faulted phase, whereas the overvoltage in the other phases is higher with the superconducting synchronous condenser than the conventional synchronous condenser.

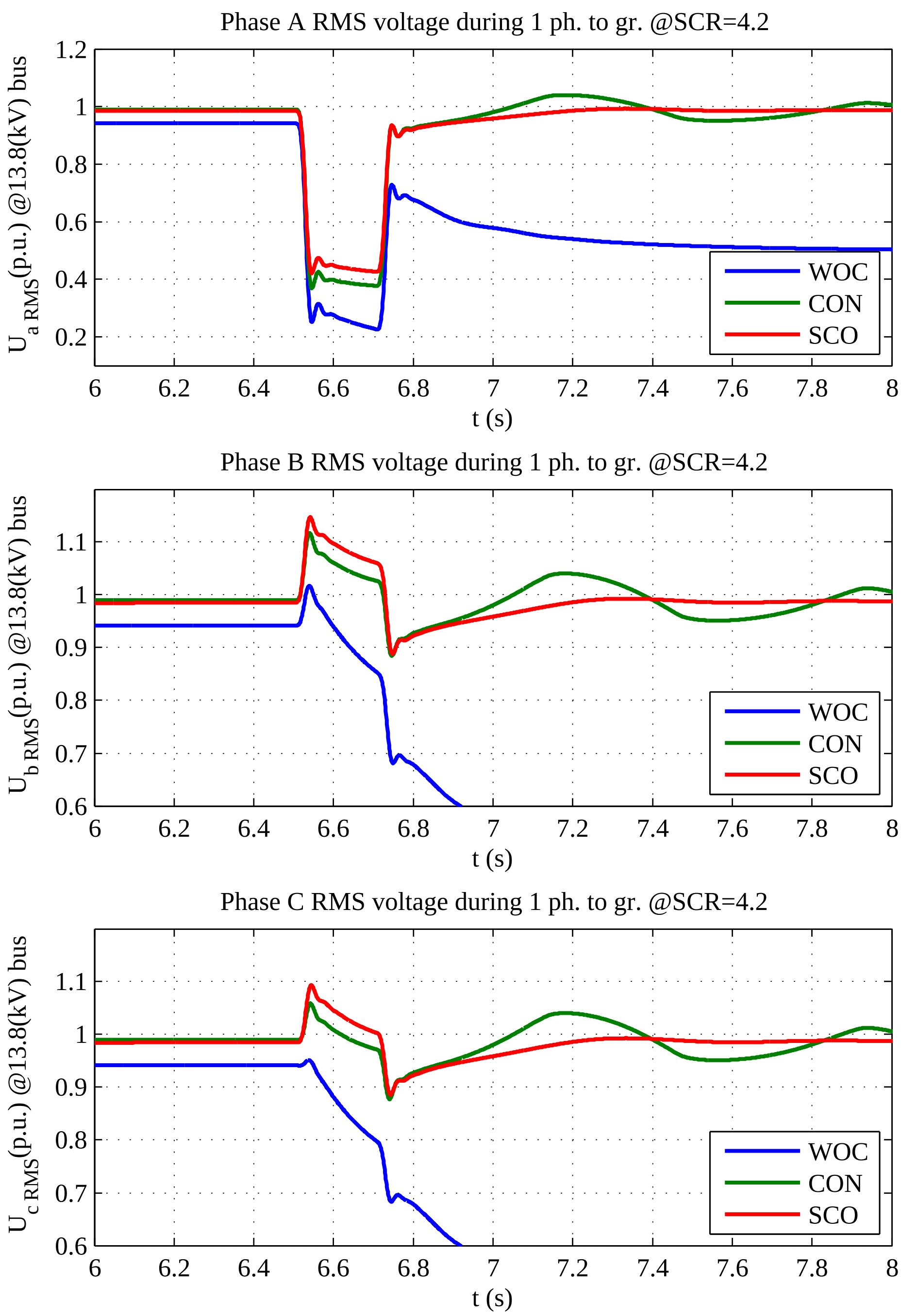

Figure 7.4: Phase voltages of synchronous condensers - single phase to ground fault.

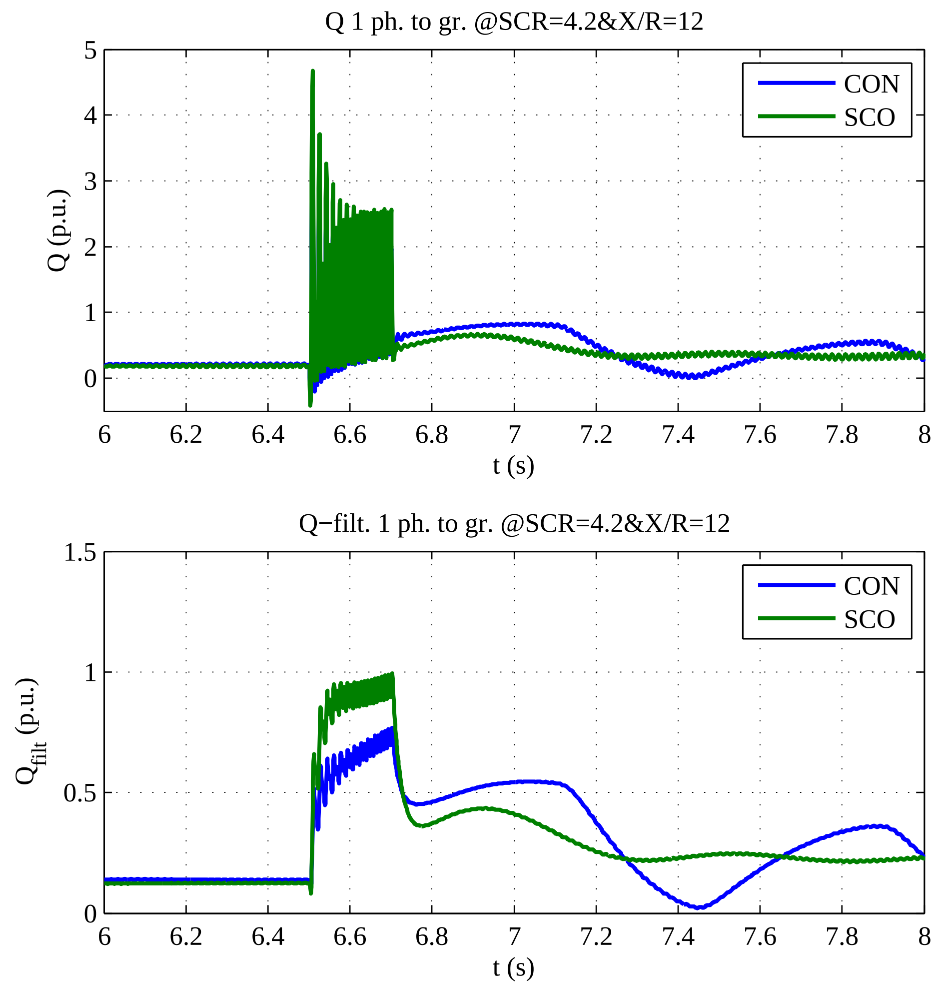

Figure 7.5: Reactive power injected (without filtering and filtered using low pass filter with 20 Hz cut-off frequency) by synchronous condensers - single phase to ground fault.

It can be noticed from Figure 7.5 that the reactive power injected from the superconducting synchronous condenser is higher than the conventional one during the fault which creates the difference between the minimum voltage level in the faulted phase and the overvoltage in other phases during the fault shown in Figure 7.4.

As can be noticed from Figure 7.6, the injected phase currents by the superconducting synchronous condenser are higher during the fault which explains the reason of having higher reactive power injection by the superconducting synchronous condenser during the fault. Also, it can be seen that the current injected in the phase where there is a fault is higher.

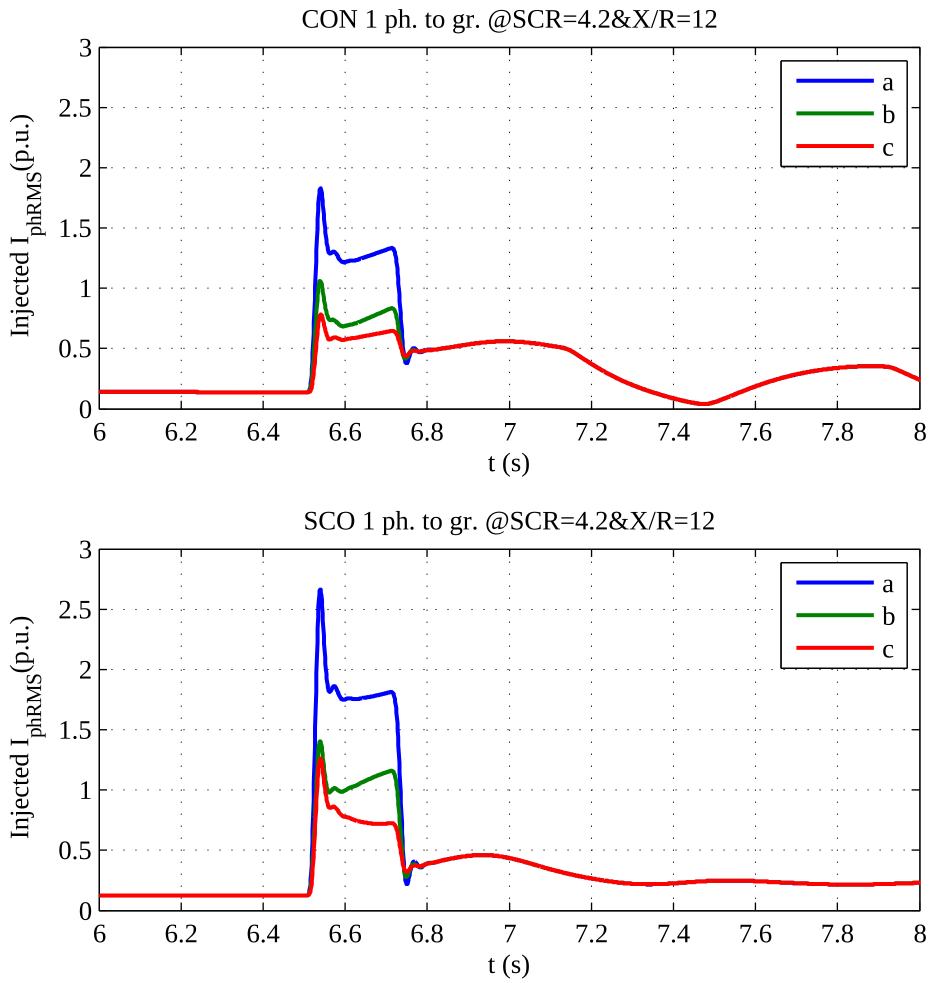

Figure 7.6: RMS values of phase currents injected by synchronous condensers - single phase to ground fault.

As can be observed from Figure 7.7, the sequence voltages drop more with the conventional synchronous condenser.

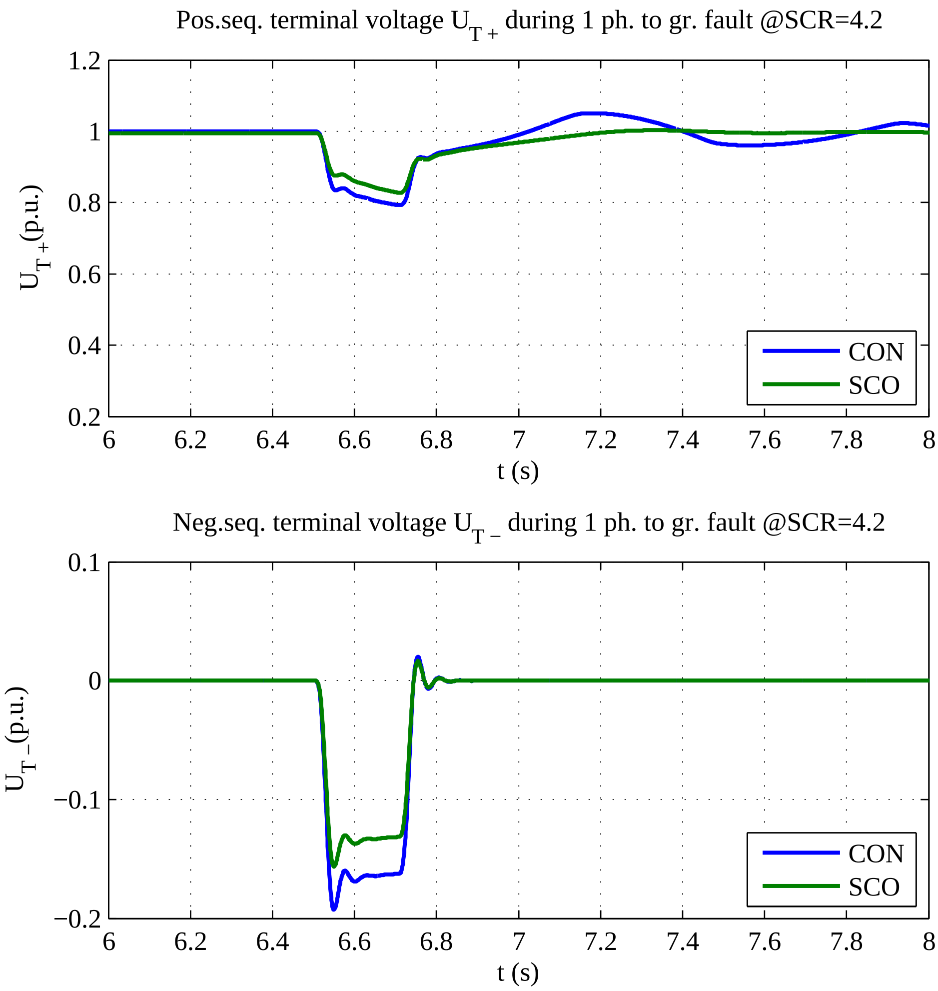

Figure 7.7: Positive and negative sequence voltages of synchronous condensers - single phase to ground fault.

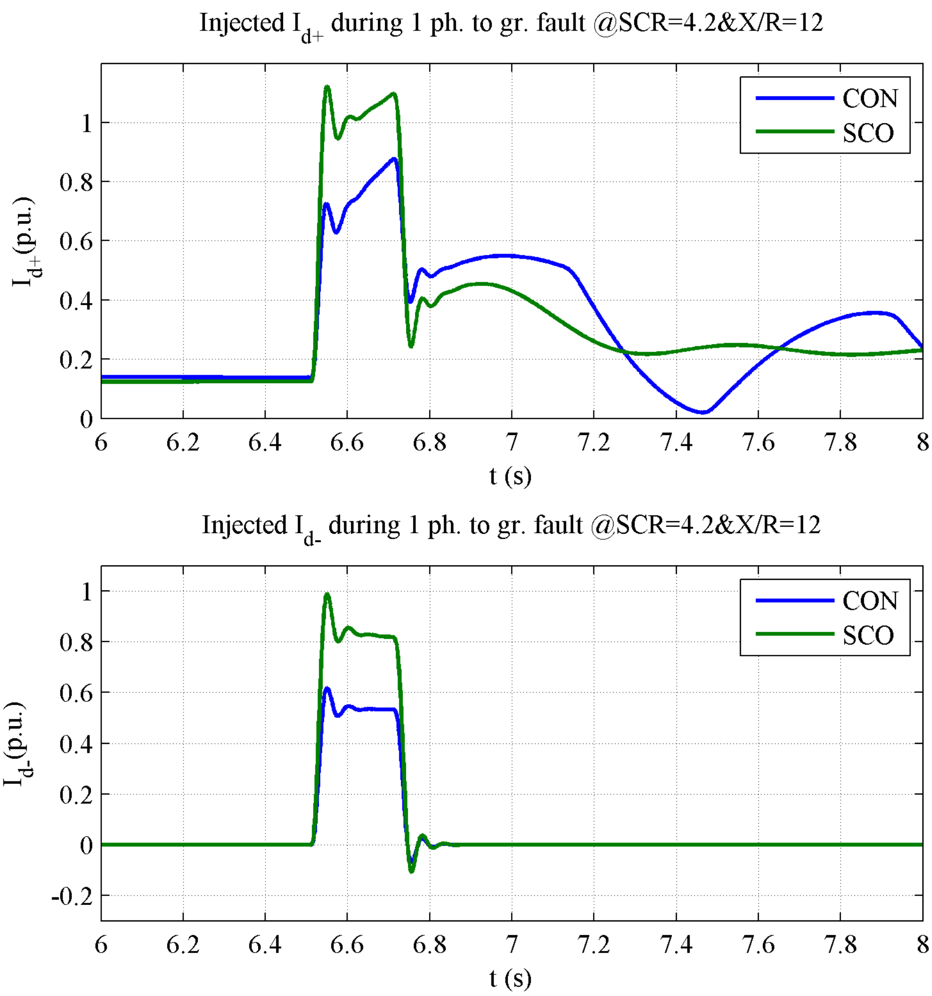

Figure 7.8: Positive and negative sequence currents of synchronous condensers - single phase to ground fault.

As can be seen from Figure 7.8, the superconducting synchronous condenser injects more positive and negative sequence current. The oscillations with twice the grid frequency seen in the reactive power curve which is shown in Figure 7.5 can be explained due to the negative sequence current injection shown in Figure 7.8.

It can be seen that the speed of induction machines drops more with the conventional synchronous condenser due to bigger positive sequence voltage drop during the fault.

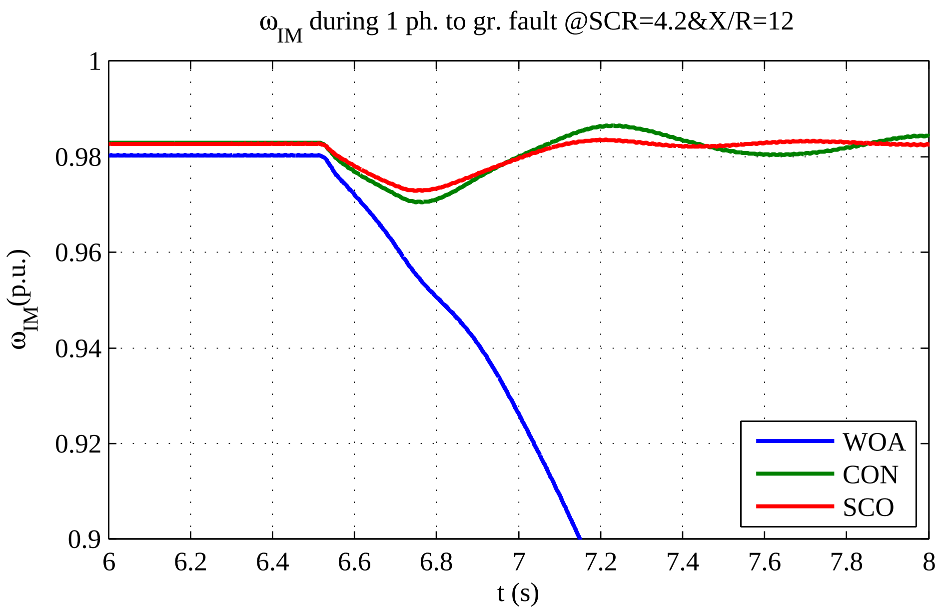

Figure 7.9: Speed of induction machines - single phase to ground fault.

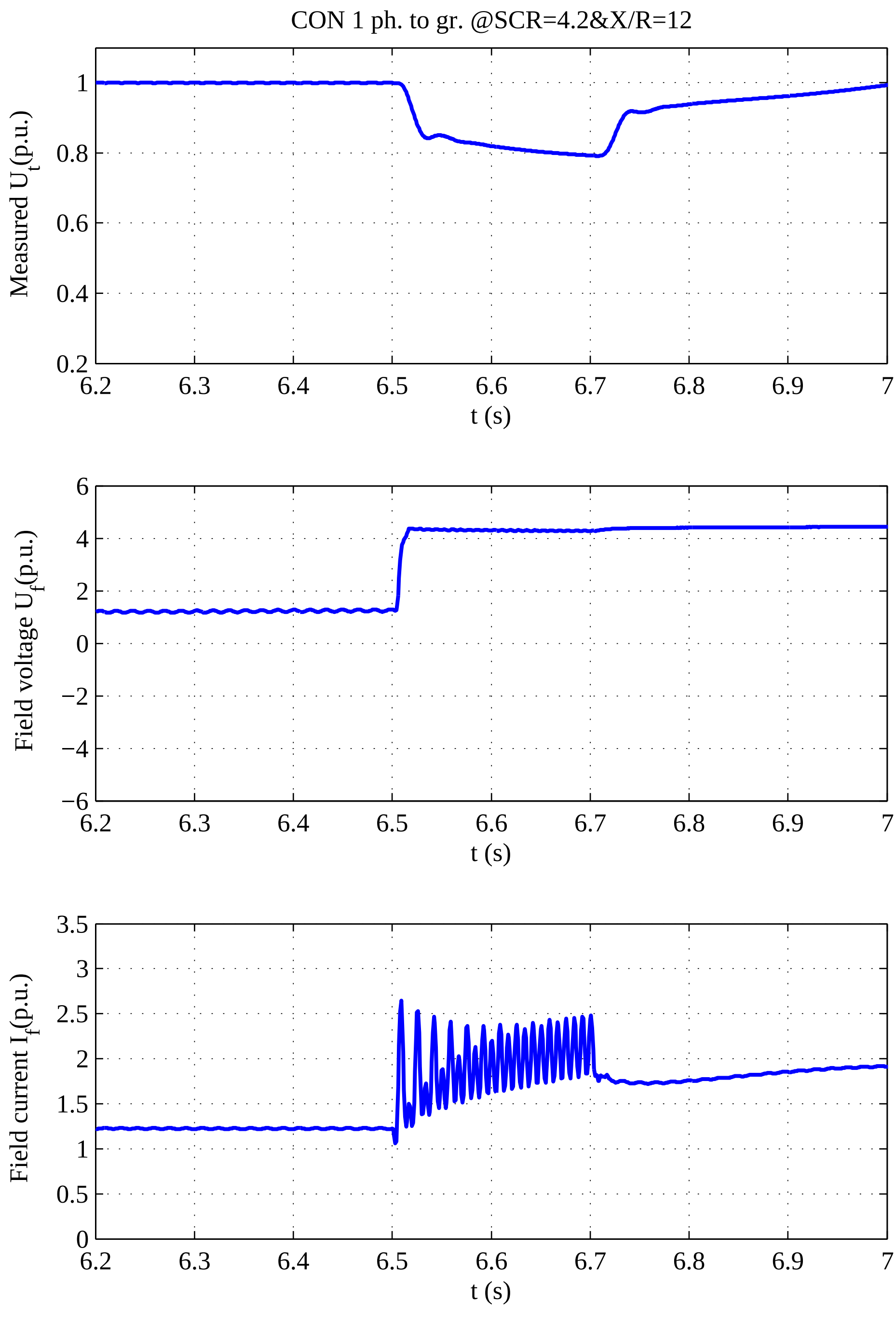

Figure 7.10: Measured voltage that is provided to the exciter, exciter field voltage and field current response for the conventional synchronous condenser - single phase to ground fault.

It can be observed from Figure 7.10 that when the exciter sees a voltage drop which creates an error signal, the exciter voltage output increases to its upper limit. As the exciter time constant is very small, it can reach to its upper limit in a very short time and hence, improving the dynamic performance of the synchronous condenser. However, this creates oscillations and increases the time to reach steady state after the fault is cleared. Also, it can be seen that the field current raises its magnitude twice of the rated field current during the fault.

Due to the mutual inductance between stator and field windings, stator negative sequence current caused oscillations can be observed on the field current

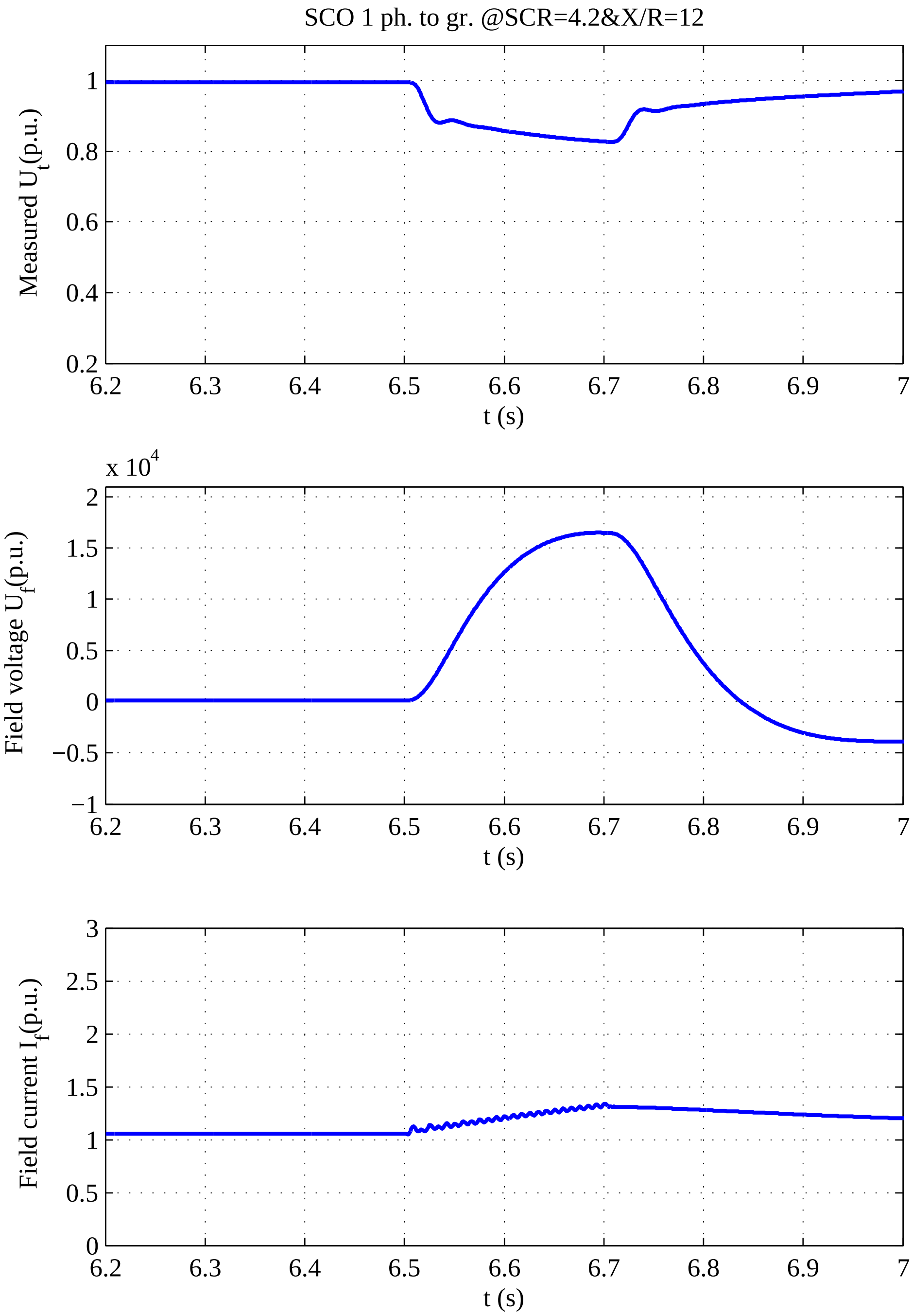

Figure 7.11: Measured voltage that is provided to the exciter, exciter field voltage and field current response for the superconducting synchronous condenser - single phase to ground fault.

It can be seen from Figure 7.11 that the field voltage rises up to approximately 18000 p.u. which is too high for conventional synchronous condensers but since the superconducting field winding has almost zero resistance, resulting field voltage in magnitude corresponds to the same voltage level obtained with conventional synchronous condensers. Also, it can be seen that the field current increase is lower compared to the conventional synchronous condenser due to the smaller synchronous reactance of the superconducting synchronous condenser.

After changing the fault type to two phase to ground and keeping other parameters same as before, Figure 7.12, which shows phase voltages of synchronous condensers and Figure 7.13, which shows the reactive power injected by synchronous condensers, are obtained

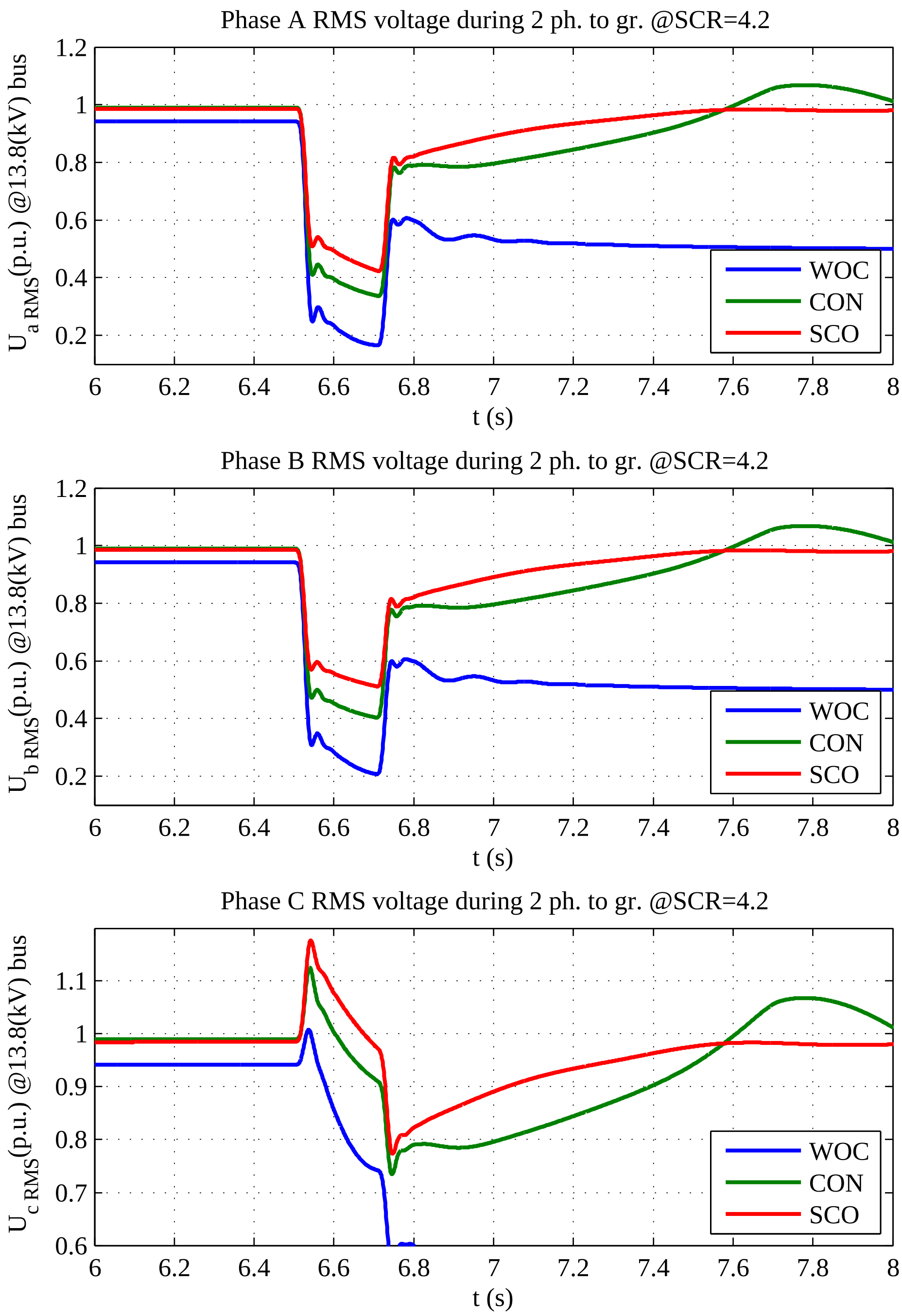

Figure 7.12: Phase voltages of synchronous condensers - two phase to ground fault.

From Figure 7.12 and Figure 7.13, it is seen that the system without compensation collapses whereas with reactive power compensation, it survives after the fault. Also, it can be noticed that the superconducting synchronous condenser keeps the minimum voltage level higher than the conventional synchronous condenser in the faulted phases, whereas the overvoltage in the other phase is higher with the superconducting synchronous condenser than the conventional synchronous condenser due to more reactive power injection by the superconducting synchronous condenser.

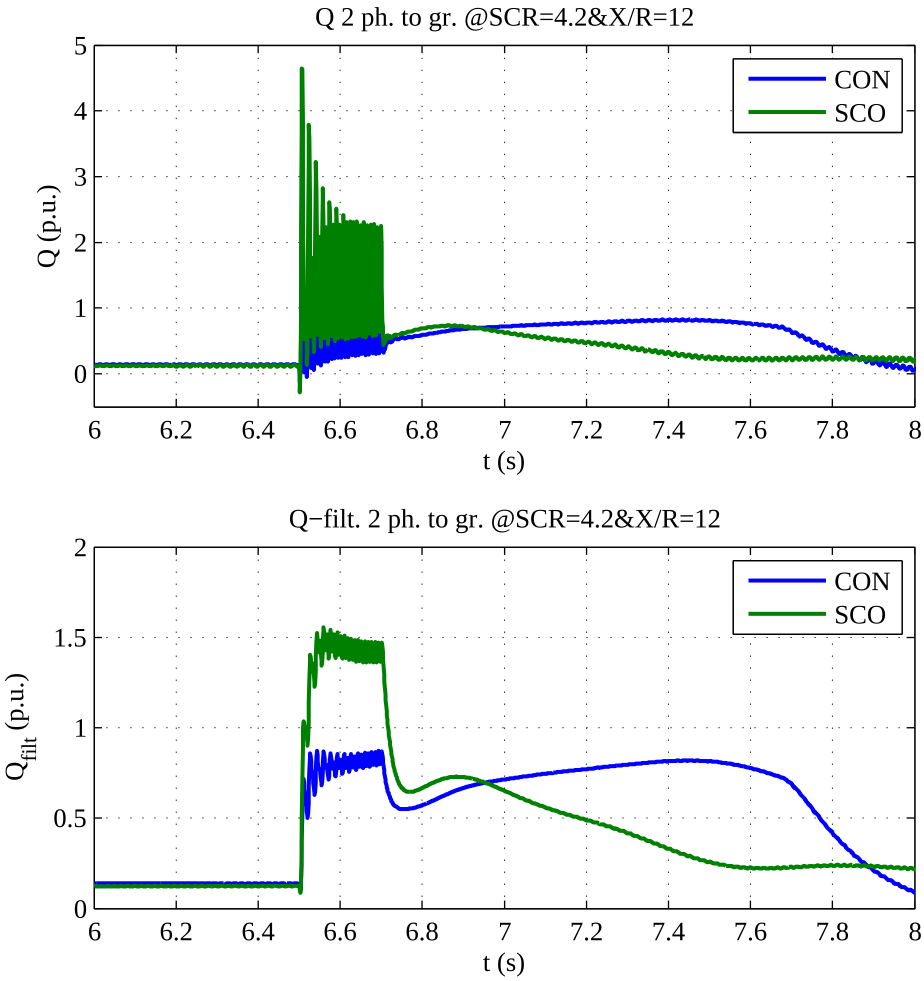

Figure 7.13: Reactive power injected (without filtering and filtered using low pass filter with 20 Hz cut-off frequency) by synchronous condensers - two phase to ground fault.

Simulating the setup with a three phase to ground fault and keeping other parameters same as before, Figure 7.14, which shows positive sequence voltages of synchronous condensers, Figure 7.15, which shows the speed of induction machines and Figure 7.16, which shows the reactive power injected by synchronous condensers, are obtained:

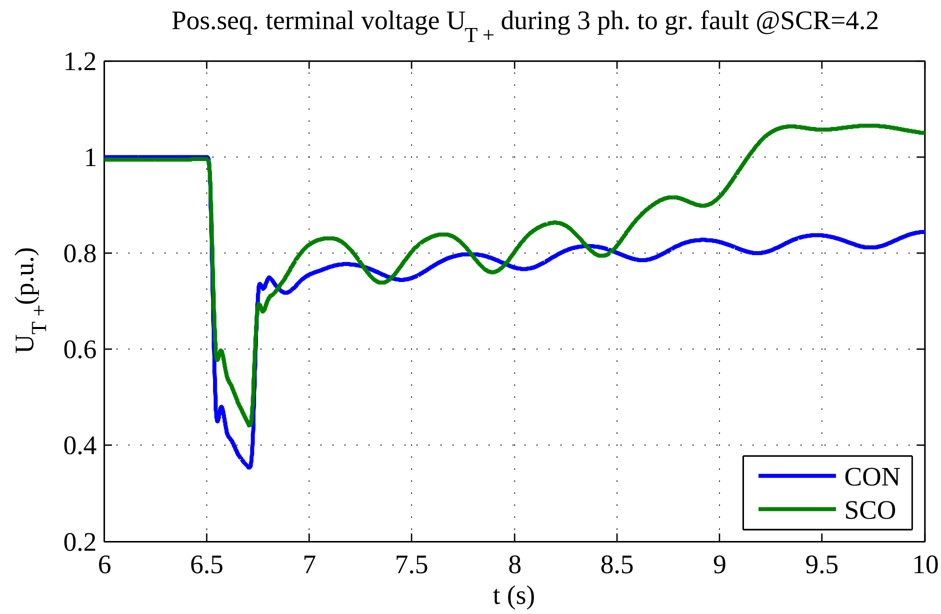

Figure 7.14: Positive sequence voltages of synchronous condensers - three phase to ground fault.

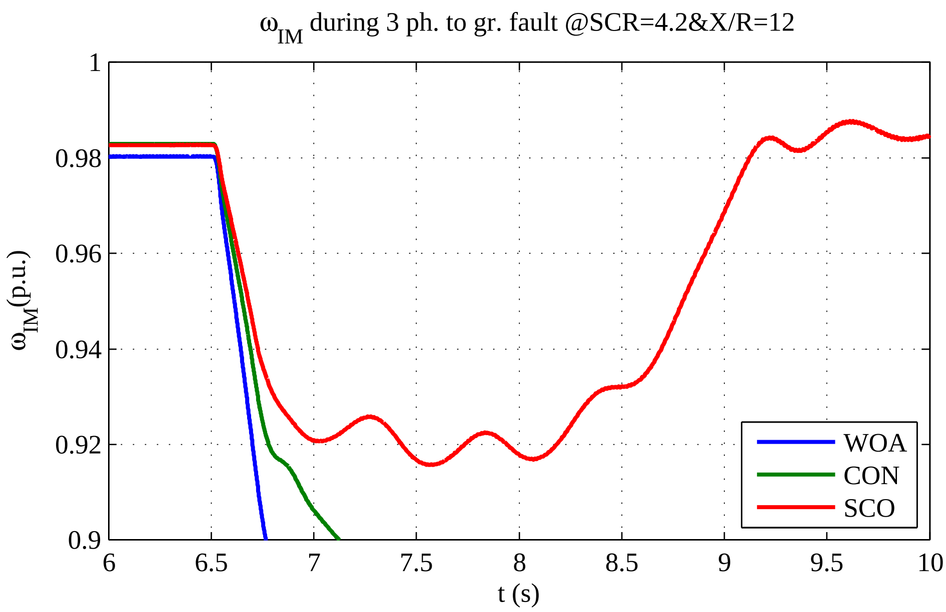

Figure 7.15: Speed of induction machines - three phase to ground fault.

From Figure 7.14, Figure 7.15 and Figure 7.16, it can be noticed that during a three phase to ground fault, only with the superconducting synchronous condenser the system survives, whereas, it collapses even with the conventional synchronous condenser. This can be explained by injection of reactive power by the superconducting synchronous condenser approximately twice as much as the conventional synchronous condenser during the fault which

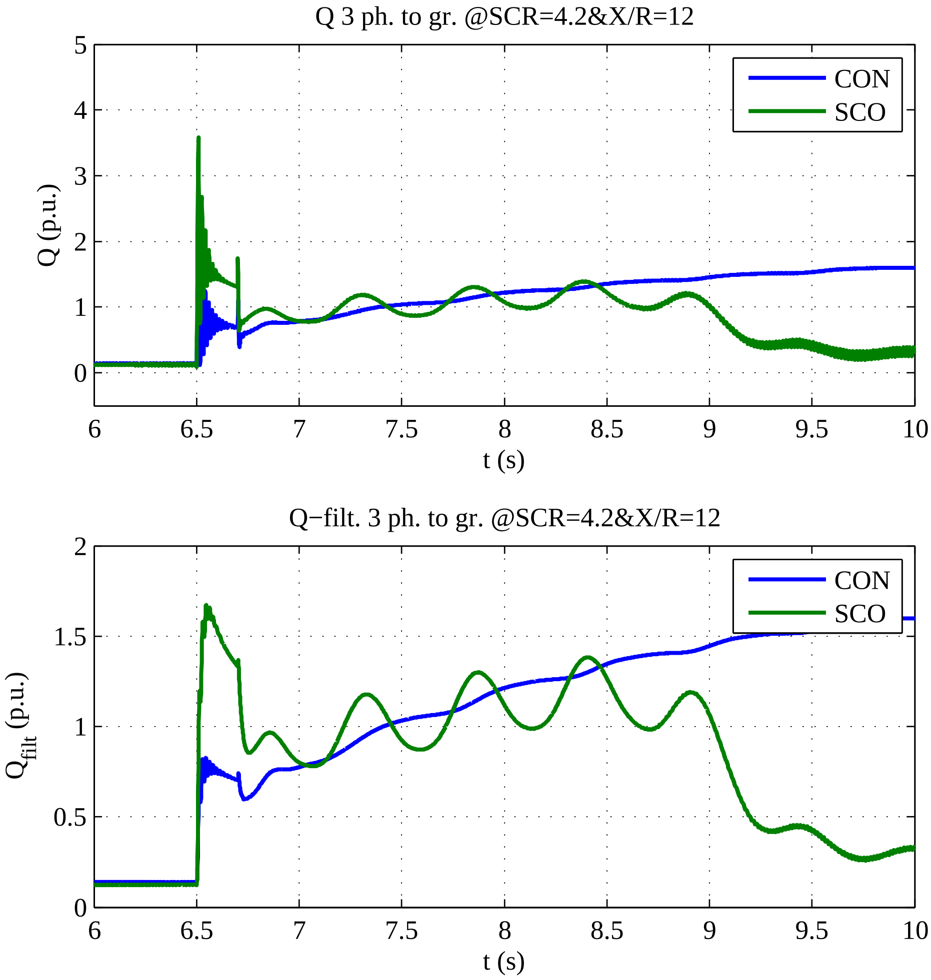

Figure 7.16: Reactive power injected (without filtering and filtered using low pass filter with 20 Hz cut-off frequency) by synchronous condensers - three phase to ground fault.

keeps the minimum positive sequence voltage and therefore, the speed of induction machines higher.

To observe the effect of reactive power compensation on minimum voltage levels more clearly during different fault types, minimum positive sequence voltage levels at 660 V bus during the fault are put on the following table:

Table 7.1: Minimum positive sequence voltage during the fault at 660 V bus.

	Fault type	1ph	2ph	3ph
Min.ter. V(p.u.)				
No comp.		0.61	0.35	0.15
With Conv. S.C.		0.78	0.52	0.32
With Super. S.C.		0.82	0.62	0.43

The maximum injected reactive power during the fault for the conventional and the superconducting synchronous condensers can be observed in the following table:

Table 7.2: Maximum injected reactive power by synchronous condensers during the fault.

	Fault type	1ph	2ph	3ph
Injected Q(p.u.)				
Conv. S.C.		0.73	0.84	0.78
Super. S.C.		0.95	1.42	1.63

As can be seen from Table 7.1 and Table 7.2, during the fault, the superconducting synchronous condenser injects reactive power approximately twice as much as the conventional synchronous condenser in case of two phase to ground and three phase to ground faults, which in turn makes the minimum positive sequence voltage level in 660 V bus higher than the voltage level when the conventional synchronous condenser is connected.

7.2.2 Different Fault Location

To analyze the performance of the superconducting synchronous condenser and the conventional synchronous condenser more deeply, the fault location is changed to 5 km from the source which corresponds to 25 % of the line length and 15 km from the source which corresponds to 75 % of the line length and a single phase to ground fault is simulated for the grid setup explained in the previous section. Figure 7.17, which shows the minimum value of positive sequence voltage at synchronous condenser terminals, Figure 7.18, which shows the minimum speed of induction machines and Figure 7.19, which shows the maximum reactive power injected by synchronous condensers, are obtained.

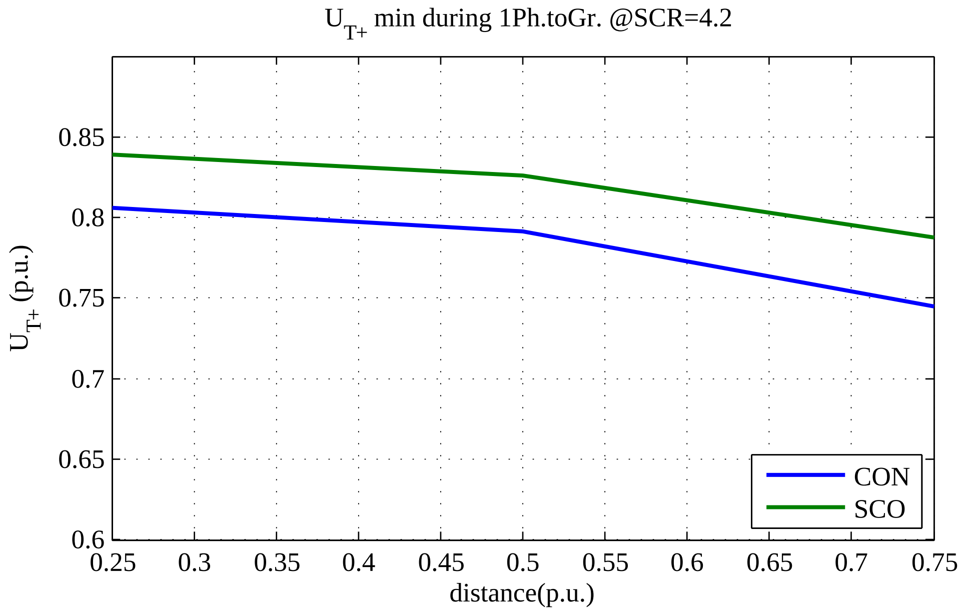

Figure 7.17: Minimum positive sequence voltage at synchronous condenser terminals - different fault location.

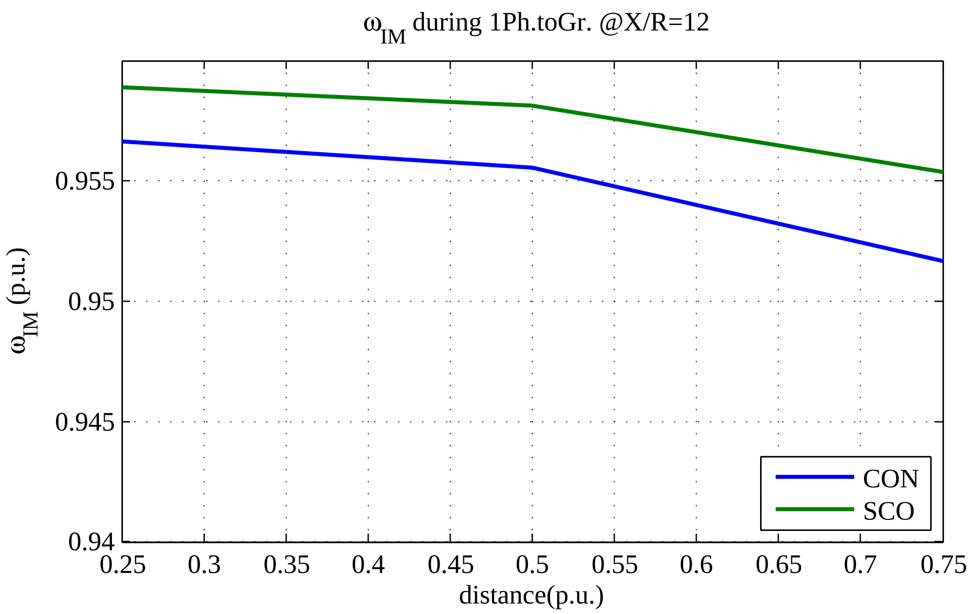

Figure 7.18: Minimum speed of induction machines - different fault location.

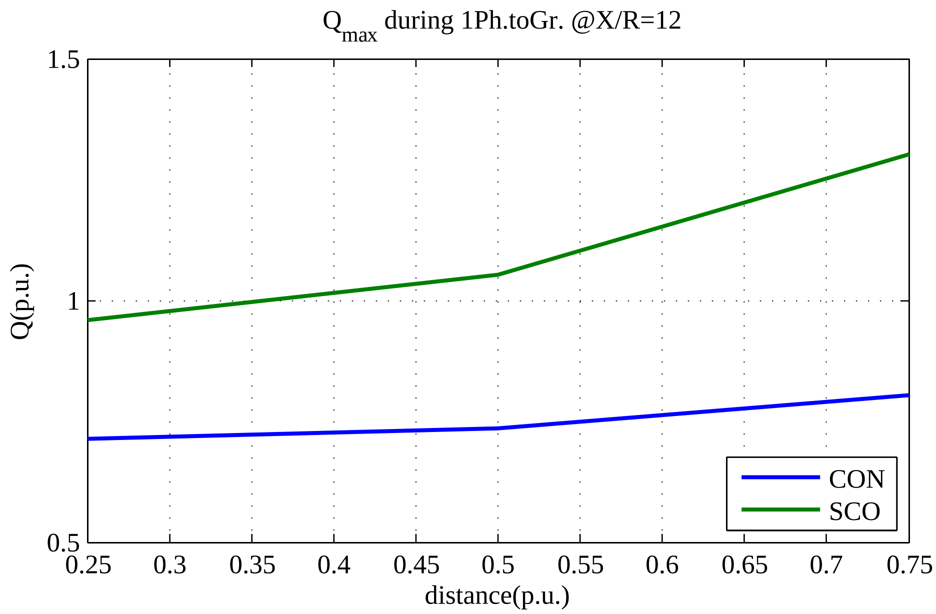

Figure 7.19: Maximum injected reactive power by synchronous condensers - different fault location.

It can be observed from Figure 7.17 that the maximum injected reactive power by the conventional synchronous condenser is lower than the superconducting synchronous condenser during the fault for all different fault locations which results in lower minimum positive sequence voltage at synchronous condenser terminals for the conventional synchronous condenser during the fault which is shown in Figure 7.18 and hence, lower minimum speed for induction machines which is shown in Figure 7.19.

7.2.3 Different SCR

To observe the effect of different SCR, the short circuit capacity seen by synchronous condensers is changed to have an SCR of 2.4 (by doubling the line length to 40 km) and 6.7 (by halving the line length to 10 km). After simulating a single phase to ground fault while keeping all other values same, Figure 7.20, which shows the minimum value of positive sequence voltage at synchronous condenser terminals and Figure 7.21, which shows the maximum reactive power injected by synchronous condensers, are obtained:

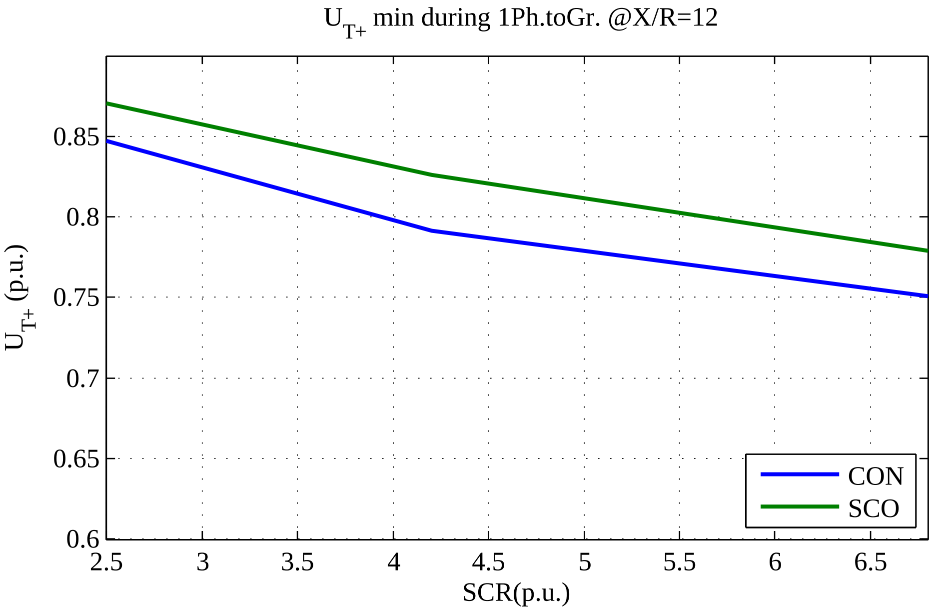

Figure 7.20: Minimum positive sequence voltage at synchronous condenser terminals - different SCR.

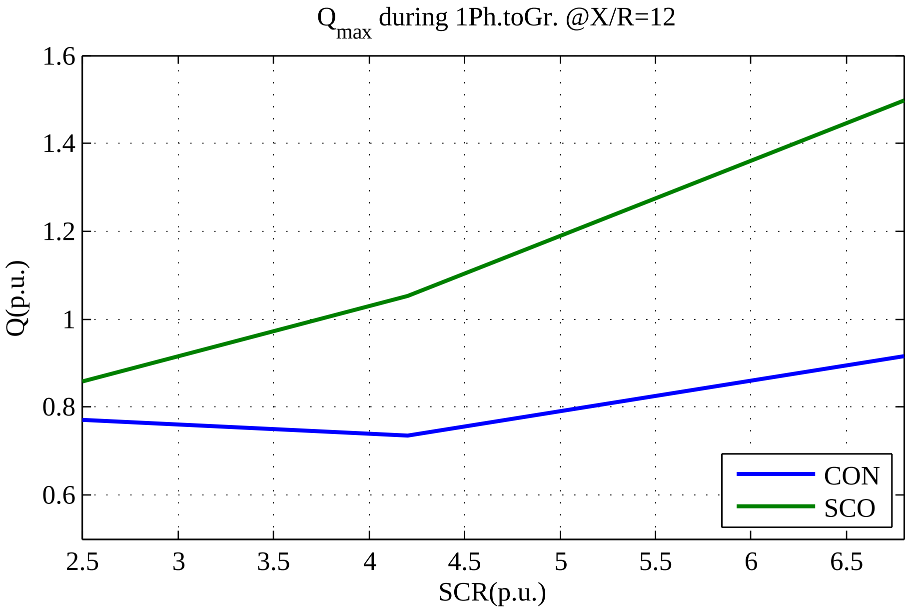

Figure 7.21: Maximum injected reactive power by synchronous condensers - different SCR.

As can be seen from Figure 7.20 and Figure 7.21, the minimum voltage level decreases due to the increase in short circuit capacity of the system, and hence, this results in more reactive power injection by the superconducting synchronous condenser due to its low synchronous reactance and bigger voltage drop on machine terminals. Also, it can be seen that, again the superconducting synchronous condenser keeps the minimum voltage level higher compared to the conventional synchronous condenser.

7.2.4 Different Inertia of Synchronous Condensers

To observe the effect of different inertia of the synchronous condenser, the inertia constant of the superconducting synchronous condenser varied from 0.05 s to 5 s. Resistance of the lines is doubled decreasing X/R ratio to 6, while the other parameters are kept the same. Results are obtained performing three phase to ground fault in the middle of the line. Figure 7.22, Figure 7.23, Figure 7.24, Figure 7.25 and Figure 7.26 are obtained:

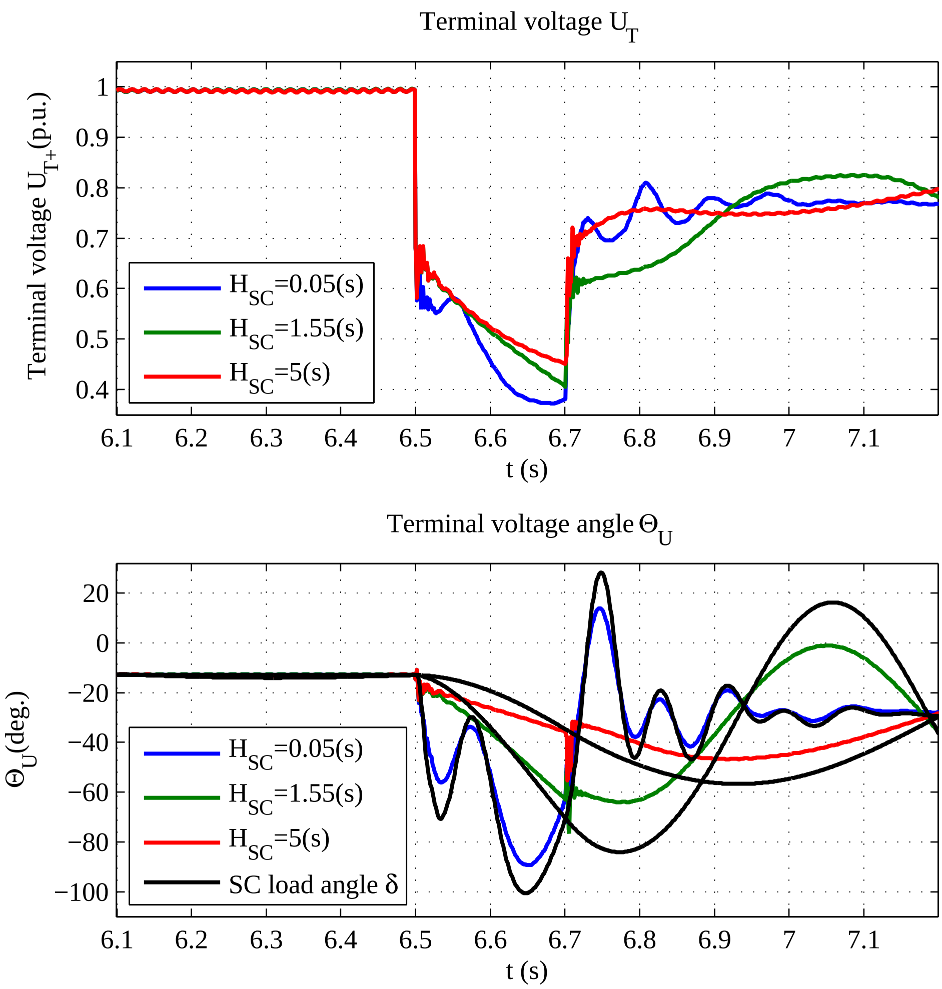

Figure 7.22: Synchronous condenser terminal voltage and phase difference between source and synchronous condenser terminals - different inertia.

It can be observed that the synchronous condenser terminal voltage drops less with increasing inertia of the synchronous condenser during the fault. Also, during the fault, it is seen that the voltage drop is significantly bigger and the voltage oscillates more when the inertia is close to zero. However, right after the faulted line is removed, which corresponds to the period from 6.7 s to 6.9 s, synchronous condensers with the lowest and the highest inertia have significantly higher voltage compared to synchronous condenser with medium inertia. Observing the synchronous condenser terminal voltage angle and the load angle of synchronous condenser where the angle of the voltage source is taken as reference, the synchronous condenser terminal voltage angle and the load angle of synchronous condenser deviates less with increasing inertia.

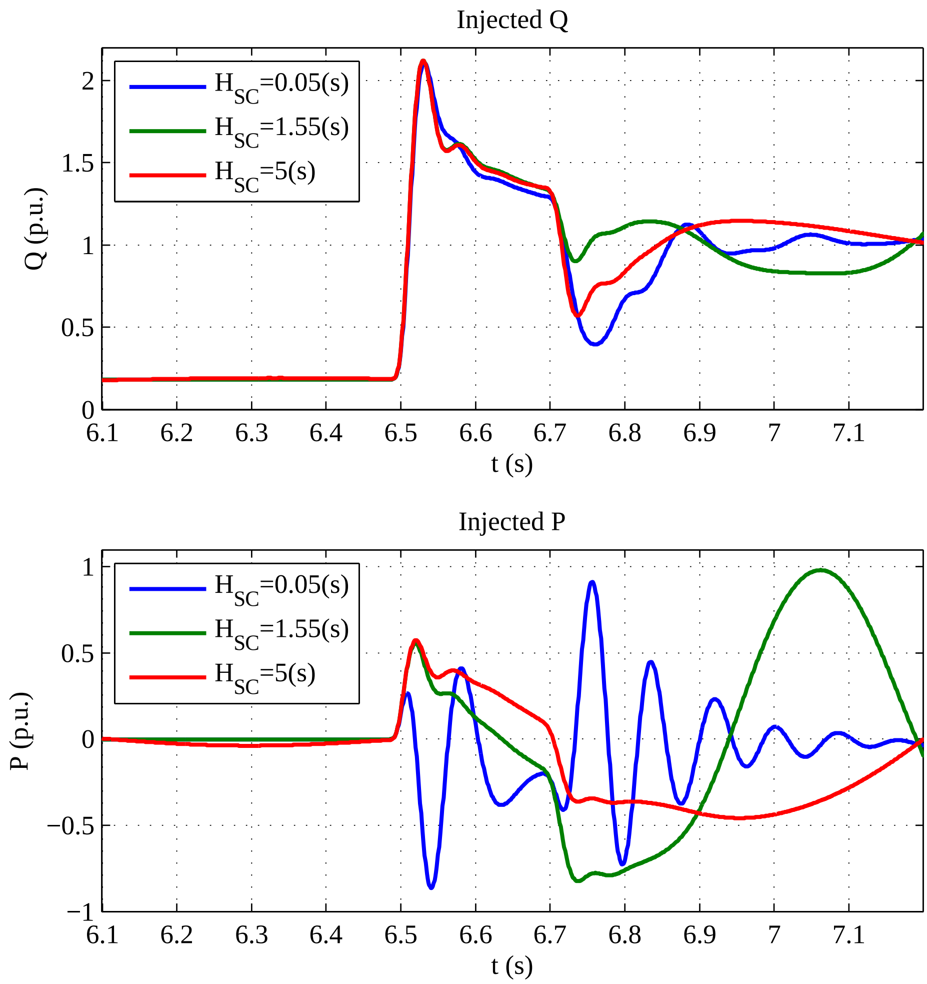

Figure 7.23: Injected reactive and active power by synchronous condenser - different inertia.

It can be noticed from Figure 7.23 that reactive power injection during the fault is not affected significantly with the change of inertia whereas, after the faulted line is removed, which corresponds to the period from 6.7 s to 6.9 s, the system with medium inertia injects more reactive power due to less voltage on its terminals. However, big difference can be noted in active power injection. During the fault, synchronous condenser with the smallest inertia starts consuming active power right after the fault initialization at the instant of 6.5 s while synchronous condensers with higher inertia initially inject active power to the grid. Synchronous condenser with highest inertia injects active power until the faulted line is disconnected. However, after the fault is cleared, synchronous condensers consume active power in order to align their load angle with the terminal voltage angle. Since the synchronous condenser with inertia of 1.55 s has deviated more its load angle in the instant of fault clearance, it consumes more active power which is supplied from the source and creates the voltage difference seen in Figure 7.22 during the period from 6.7 s to 6.9 s.

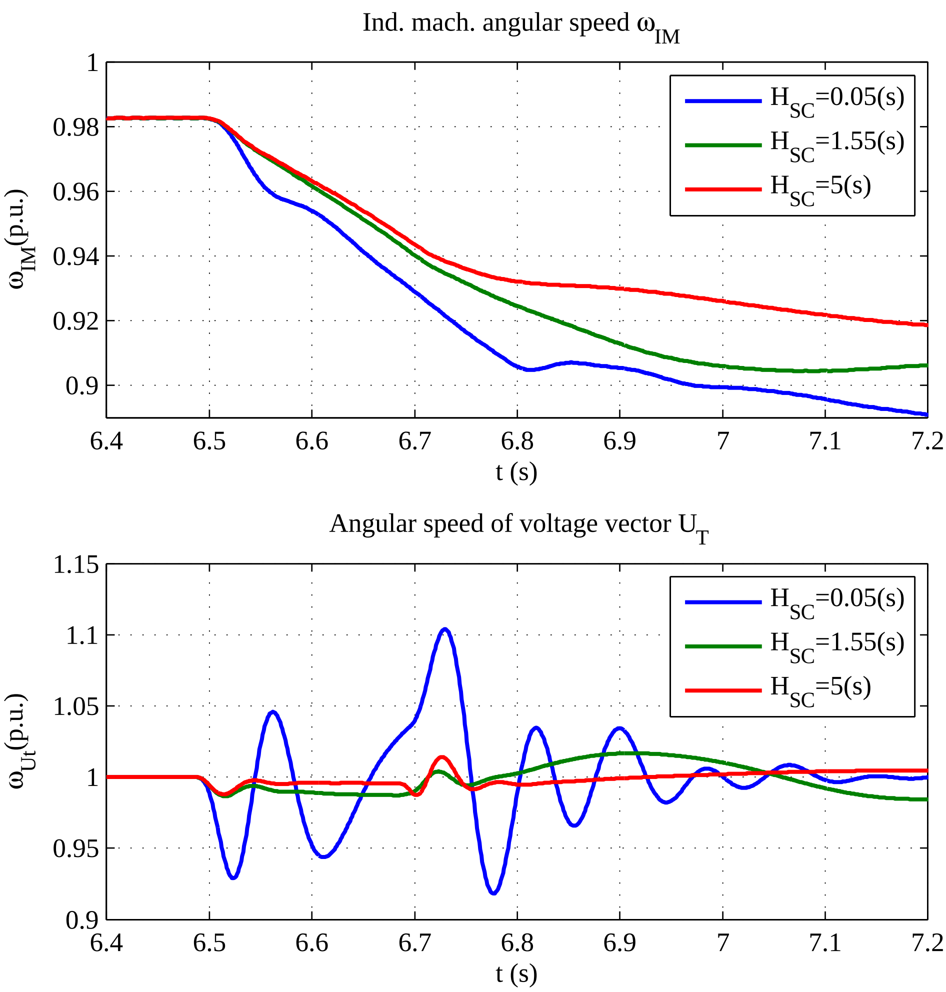

Figure 7.24: Speed of induction machines and angular speed of positive sequence synchronous condenser terminal voltage vector - different inertia.

As can be seen from Figure 7.24, the speed of induction machines drops more with decreasing inertia of synchronous condensers during the fault. This is caused by difference in active power injection by synchronous condensers with different inertia and by difference in angular speed of voltage vector which is seen in Figure 7.24. At the time instant of 6.5 s when the fault commences, synchronous condenser with inertia 0.05 s loses its speed very quickly following the angular speed of positive sequence terminal voltage. Synchronous condenser with nominal inertia 1.55 s and with big inertia is keeping the angle of positive sequence terminal voltage injecting active power. This proves to be very critical factor in keeping the speed of induction machines higher and can be observed in Figure 7.24 during the period from 6.5 s to 6.55 s. After the fault is cleared, induction machines supported by synchronous condenser with inertia of 1.55 s recover their speed slower. This is caused by lower voltage during the period from 6.7 s to 6.9 s when the synchronous condenser with nominal inertia consumes a lot of active power caused by bigger deviation of its load angle.

Observing Figure 7.25, it can be noted that with increasing inertia of the synchronous con-

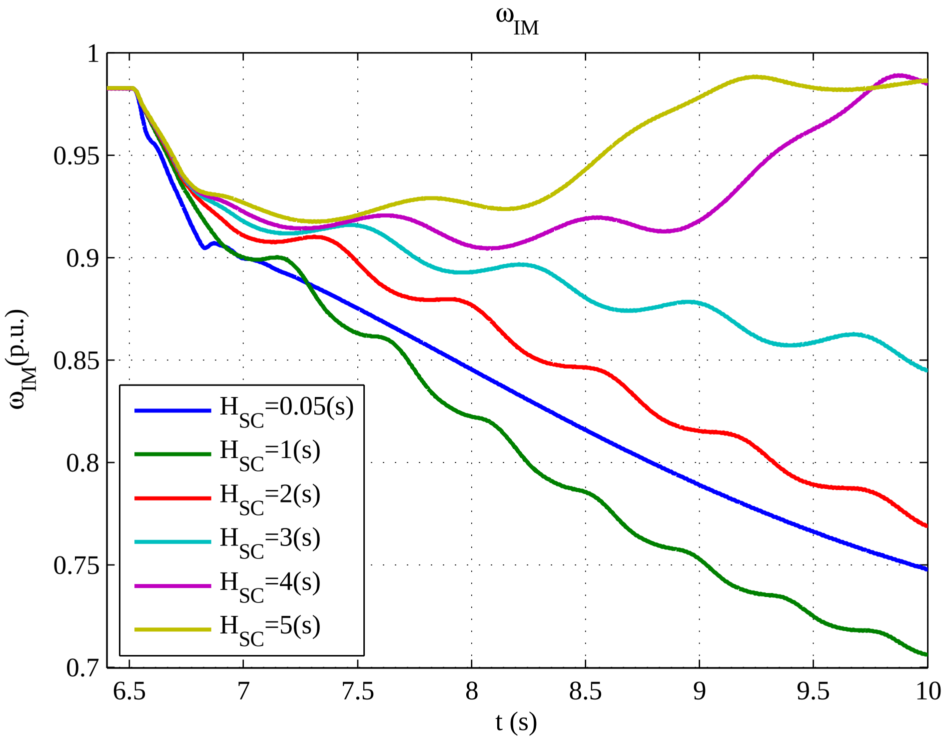

Figure 7.25: Speed of induction machines - different inertia.

denser, induction machines lose less speed and recover quicker.

It should be noted that in Figure 7.26, the IM curve corresponds to active power consumption by the load, the SC curve corresponds to active power injected by the synchronous condenser, the $line$ curve corresponds to active power injected by the healthy line, and the $line/fault$ curve corresponds to active power injected by the faulted line. Oscillations of the active power, that occur after the fault is cleared, are smaller in magnitude, have smaller frequency and are more difficult to damp for the systems protected by synchronous condensers with bigger inertia. This active power oscillates between the voltage source and synchronous condensers which can be observed in Figure 7.26. These active power oscillations will cause oscillations in the positive sequence terminal voltage which in turn create oscillations in the speed of induction machines.

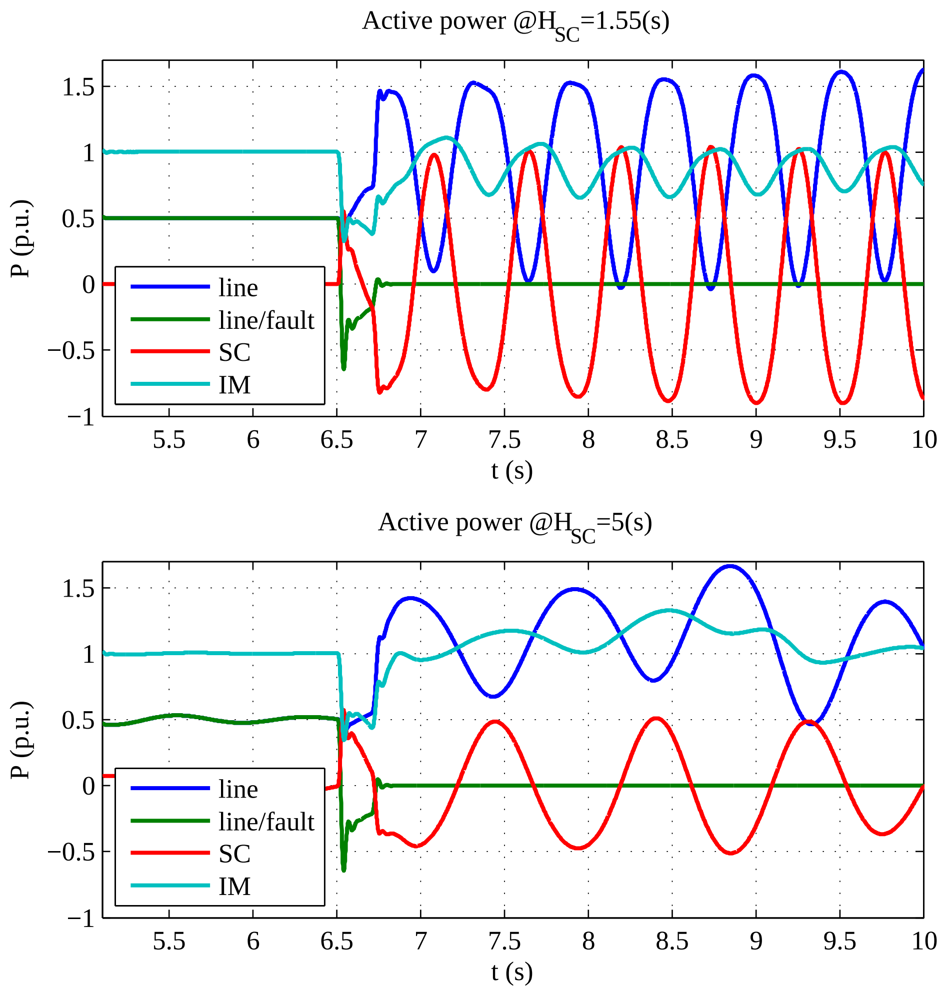

Figure 7.26: Active power balance at synchronous condenser terminals - different inertia.

7.3 Summary

In this chapter, effect of different factors on the performance of synchronous condensers was observed. Simulations, while changing different parameters on the grid setup, were made and it was seen that the superconducting synchronous condenser injects more current and hence, more reactive power compared to the conventional synchronous condenser during the faults due to its low synchronous reactance. Due to this reason, it was observed that the superconducting synchronous condenser keeps the load voltage higher compared to the conventional synchronous condenser. Also it was seen that increasing the inertia of synchronous condensers helps induction machines to recover their speed.

Chapter 8

Comparison of SVC and Synchronous Condensers

In this chapter, comparison of a superconducting synchronous condenser, a conventional synchronous condenser and an SVC is done with a grid setup.

8.1 Grid Setup

To compare the performance of the superconducting synchronous condenser, the conventional synchronous condenser and the SVC, single line grid setup shown in Figure 8.1 is used:

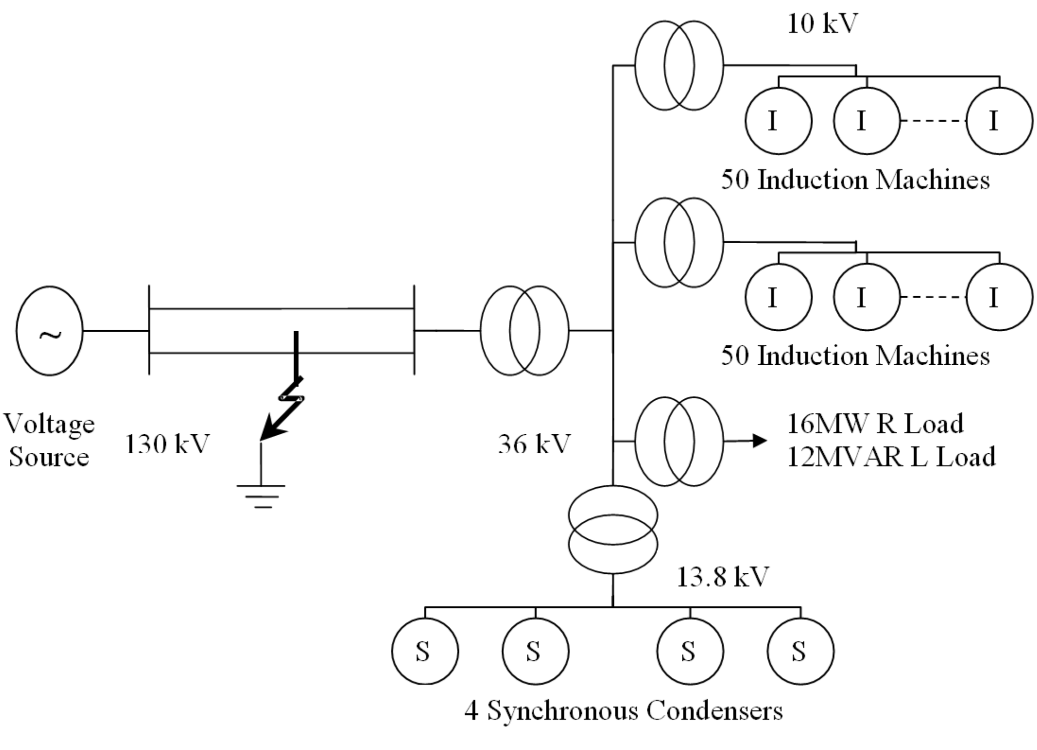

Figure 8.1: Single line diagram of the grid setup.

The detailed figure for the same grid used in PSCAD is shown in Figure 8.2.

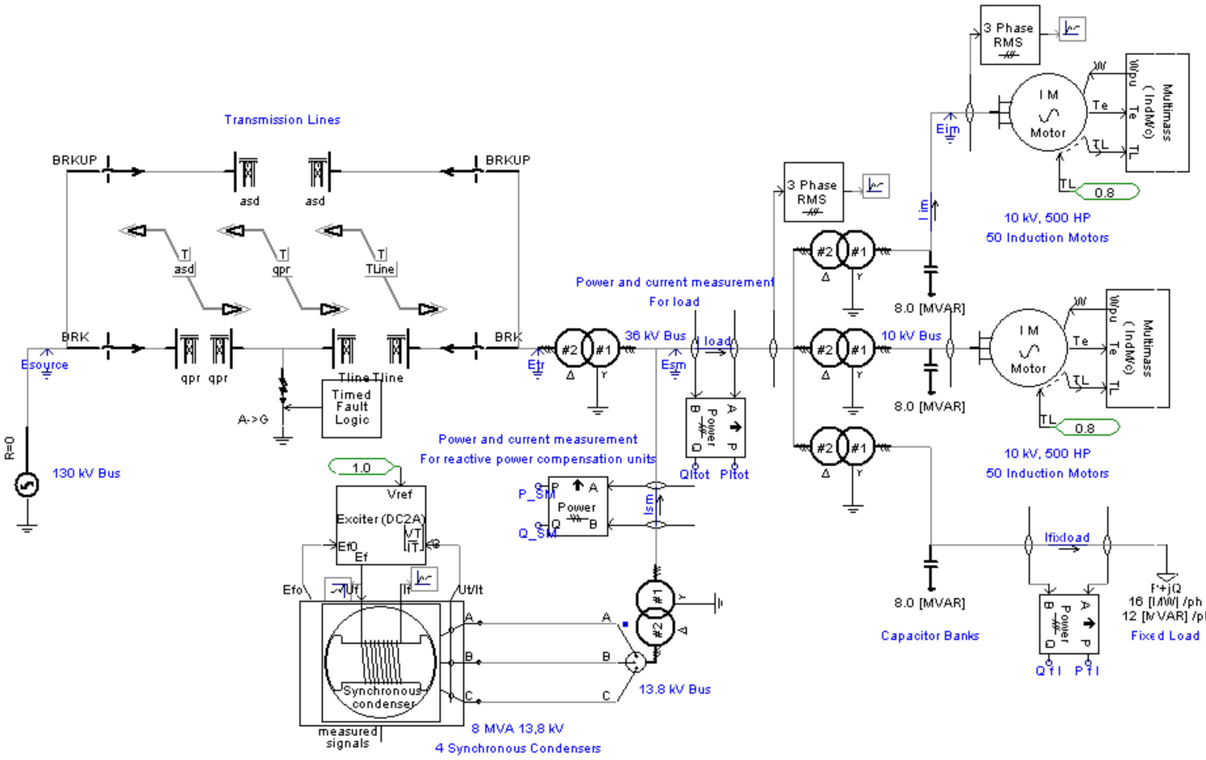

Figure 8.2: Grid setup used in PSCAD.

In this grid setup, a factory, where the main load of the factory consists of two sets of 50 induction machines of 500 HP with 0.9 power factor; 10 kV with inertia constant of 2 s, is connected to a substation of 36 kV via their own 10 %, 36/10 kV, 25 MVA transformers. Also, a resistive and an inductive load of 16 MW and 12 MVAr are connected to a substation of 36 kV via its own 10 %, 36/10 kV, 25 MVA transformer. A capacitor bank of 8 MVAr is connected to each 10 kV load bus in order to keep the 10 kV bus within 95 %-100 % of the bus voltage during the full load operation. The SCR, which is the ratio of short circuit power measured at the 36 kV bus to the load total apparent power, is 3.9 which represents a medium system.

4x8 MVA synchronous condensers (or a 32 MVA SVC without a 13.8/36 kV transformer) are connected to 36 kV bus via 10 %, 13.8/36 kV, 32 MVA transformer to provide reactive power compensation especially in case of faults that can occur in the lines that transfers power from the source to the factory. The power is transferred from the source to the factory via two 200 km lines with an X/R ratio of 15 where the fault occurs in one of the lines which will cause the breakers open after 250 ms delay, disconnect the faulted line and connect it back 500 ms after the fault is cleared. In the substation of 36 kV, there is a 10 %, 130/36 kV, 70 MVA step down transformer which brings the voltage level to the desired value for the factory.

The 130 kV source has an infinite short circuit capacity which is kept constant during the simulations.

During the simulations, type DC2A exciter is used for the conventional synchronous condenser and type ST1A exciter is used for the superconducting synchronous condenser where the parameters are tuned according to the explanation given in the previous chapter.

8.2 Simulation Results

To compare synchronous condensers with SVC, different cases are studied by changing the parameters in the grid. In the following figures, WOC represents configuration without any synchronous condenser connected to 36 kV bus, CON represents configuration with the conventional synchronous condensers connected to 36 kV bus, SCO represents configuration with the superconducting synchronous condensers connected to 36 kV bus and SVC represents configuration with the SVC connected to 36 kV bus.

8.2.1 Different Fault Type

To observe the performance of the superconducting synchronous condenser, the conventional synchronous condenser and the SVC, a single phase to ground fault in the middle of one of the lines is simulated on the grid setup described in the previous section. First, the simulation is done without any reactive power compensation unit connected to 36 kV bus, then in the next simulation, the conventional synchronous condenser is connected, after it, the superconducting synchronous condenser is connected and in the final simulation, the SVC is connected.

As can be seen from Figure 8.3, without any reactive power compensation unit, the system collapses whereas, with compensation, it survives. Also, it can be observed that after the fault, the SVC brings the voltage back to 1 p.u. quicker.

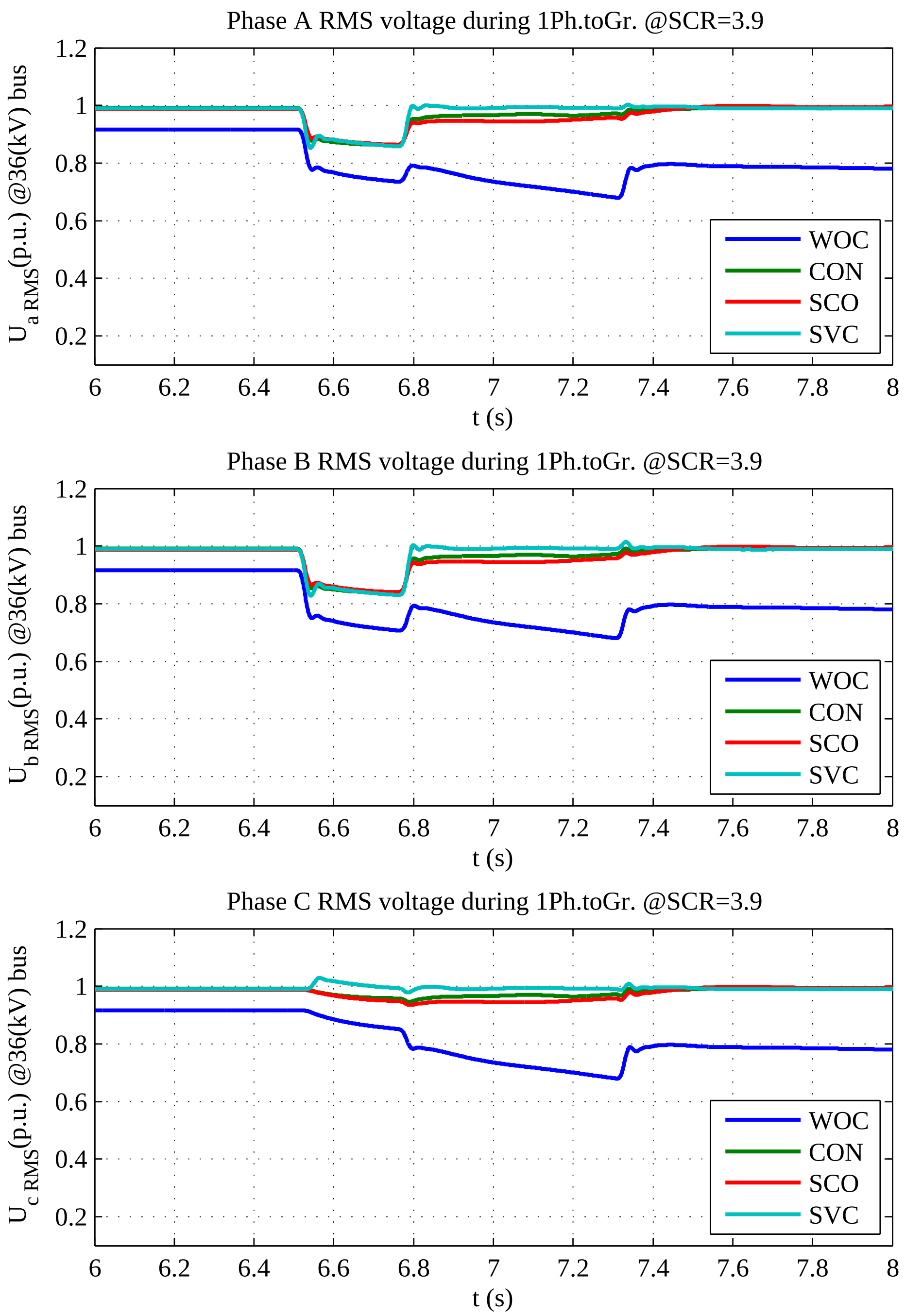

Figure 8.3: Phase voltages at 36 kV bus - single phase to ground fault.

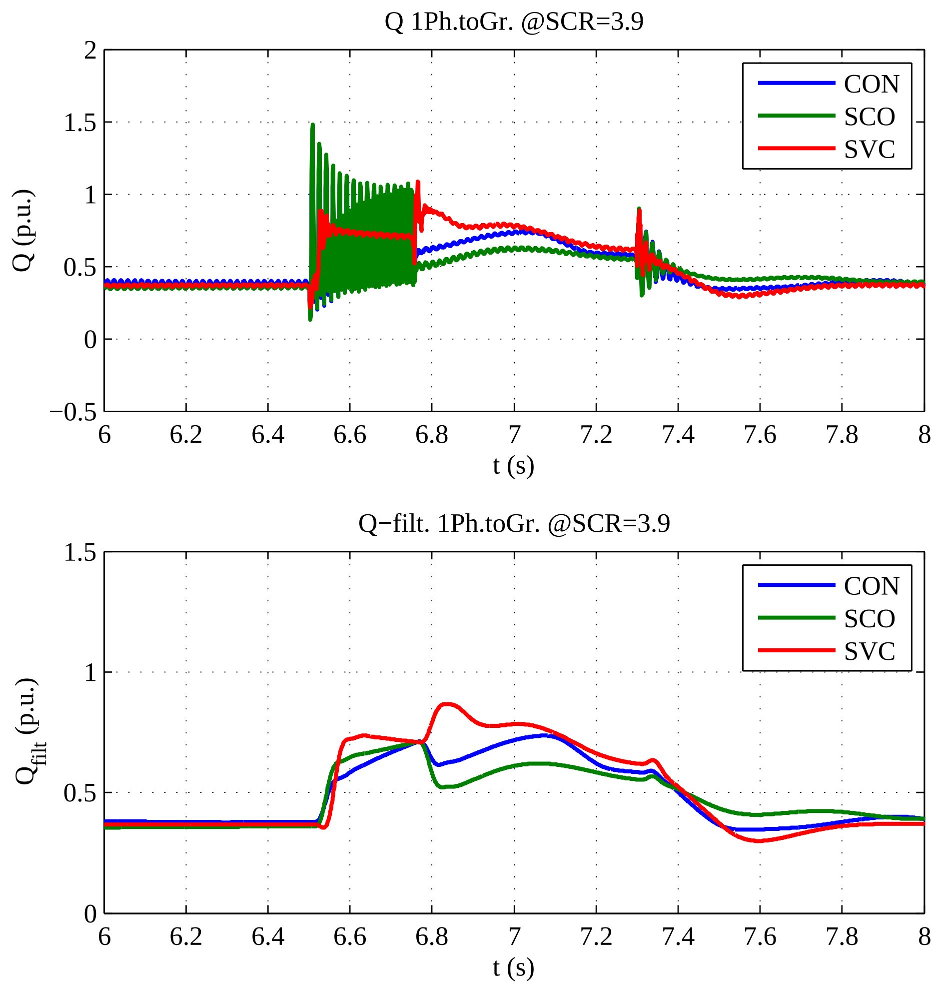

Figure 8.4: Reactive power injected (without filtering and filtered using low pass filter with 20 Hz cut-off frequency) by synchronous condensers and SVC - single phase to ground fault.

As can be noticed from Figure 8.4, the SVC begins injecting reactive power after some delay due to measurements whereas, synchronous condensers react instantaneously due to sudden change in the terminal voltage. Also, it can be observed that after an initial delay, the SVC injects more reactive power due to faster voltage control compared to synchronous condensers which have significantly bigger time constants in their field windings.

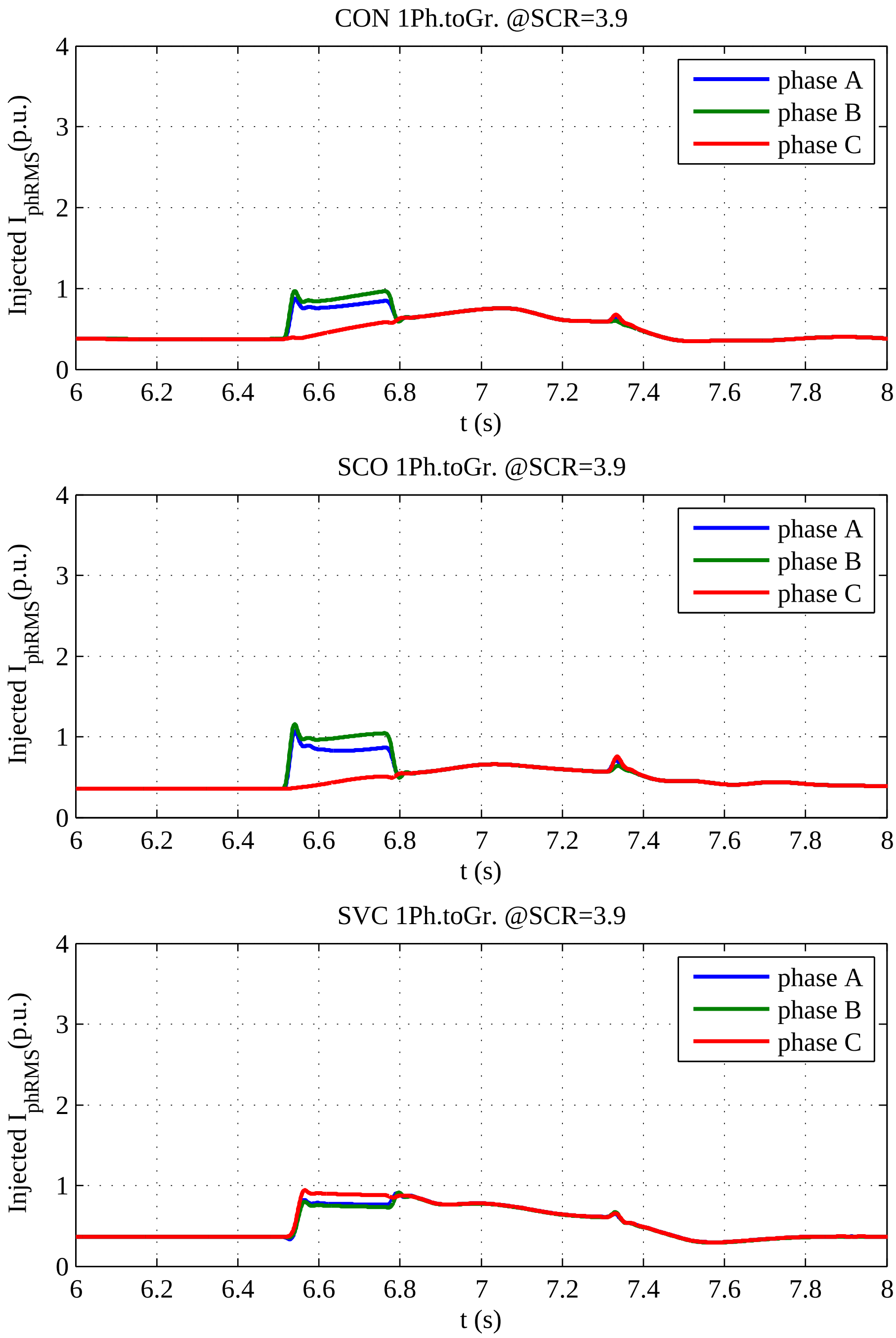

Figure 8.5: RMS values of phase currents injected by synchronous condensers and SVC - single phase to ground fault.

It can be observed from Figure 8.5 that the SVC also injects current to the phase where there is minimum voltage drop which causes higher voltage in phase C with the SVC shown in Figure 8.3.

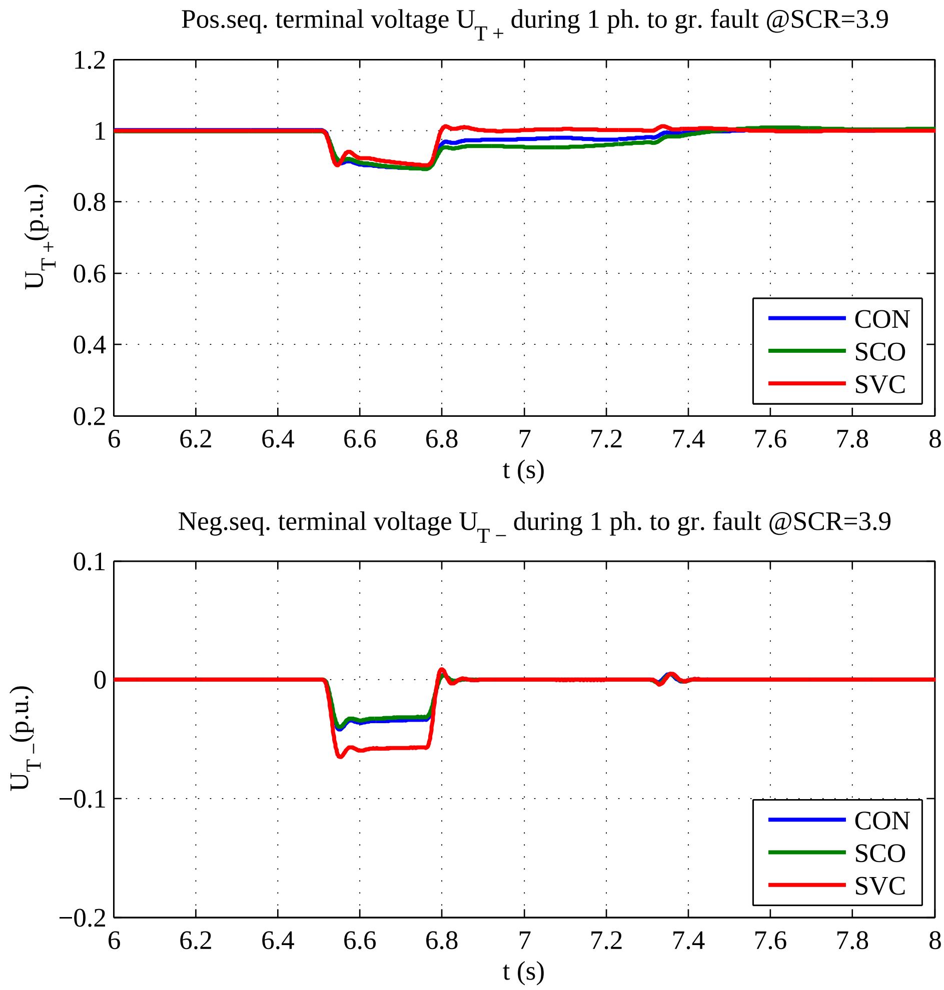

Figure 8.6: Positive and negative sequence voltages of synchronous condensers and SVC - single phase to ground fault.

It can be noticed from Figure 8.6 that injecting current to phase C makes the positive sequence voltage drop less whereas the magnitude of the negative sequence voltage is higher.

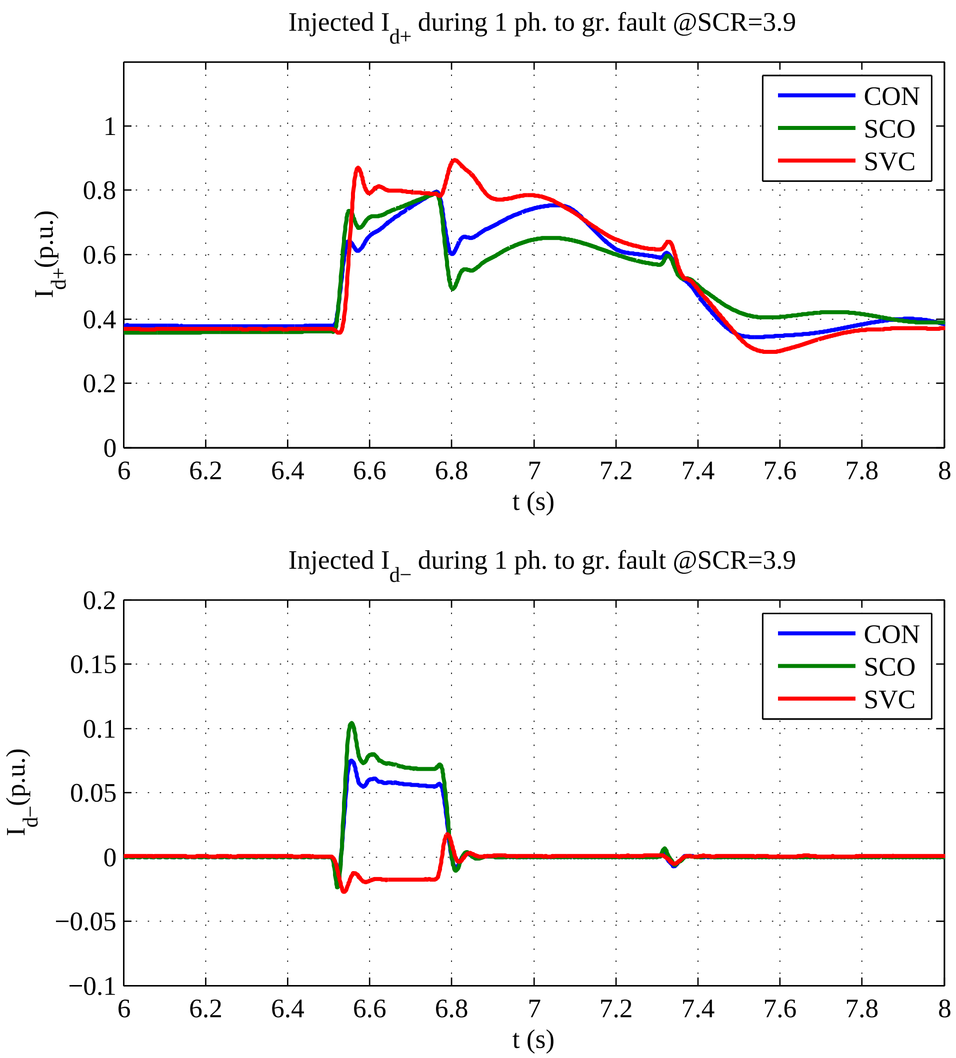

Figure 8.7: Positive and negative sequence currents of synchronous condensers and SVC - single phase to ground fault.

As it can be seen from Figure 8.7, the SVC injects more positive sequence current which in turn makes the positive sequence voltage shown in Figure 8.6 higher than synchronous condensers. Also it is observed that the SVC draws negative sequence current which results in increased magnitude of the negative sequence voltage shown in Figure 8.6.

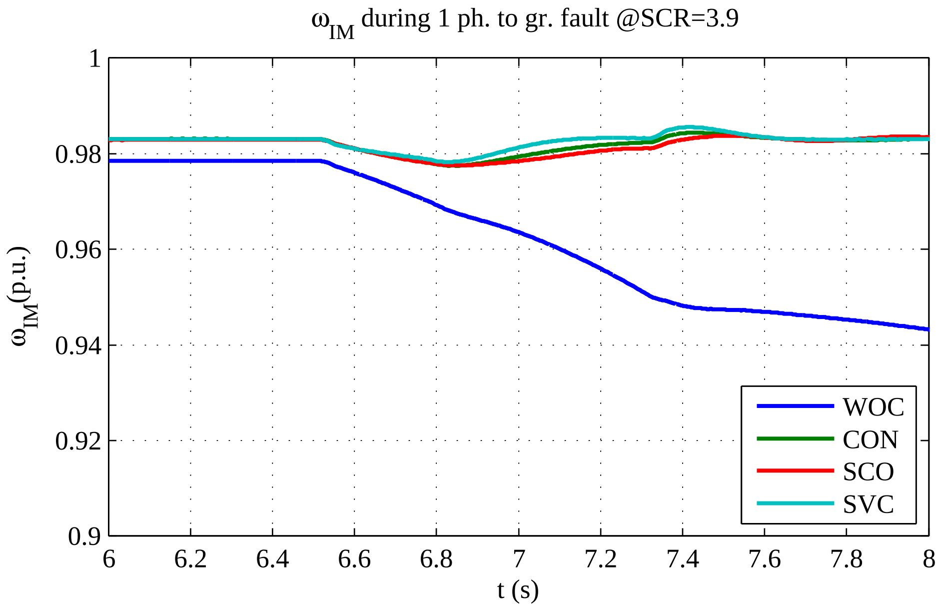

Figure 8.8: Speed of induction machines - single phase to ground fault.

It can be noticed from Figure 8.8 that induction machines collapses without any reactive power compensation unit. Also it can be observed that the speed of induction machines recover quicker with the SVC.

After changing the fault type to two phase to ground and keeping other parameters same as before, Figure 8.9, which shows phase voltages of synchronous condensers and the SVC, Figure 8.10, which shows positive sequence voltages of synchronous condensers and the SVC, Figure 8.11, which shows the reactive power injected by synchronous condensers and the SVC and Figure 8.12, which shows the speed of induction machines are obtained.

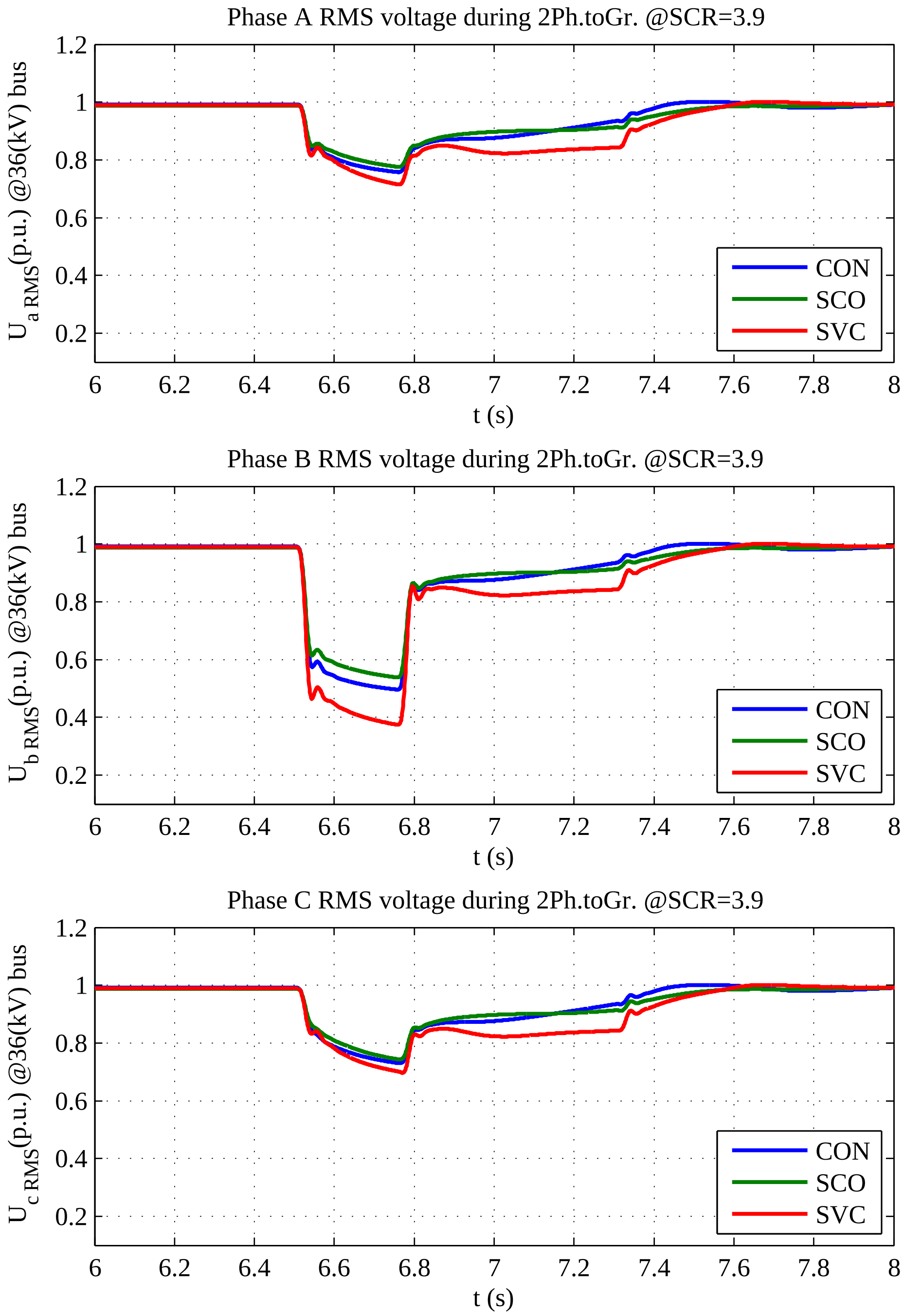

Figure 8.9: Phase voltages of synchronous condensers and SVC - two phase to ground fault.

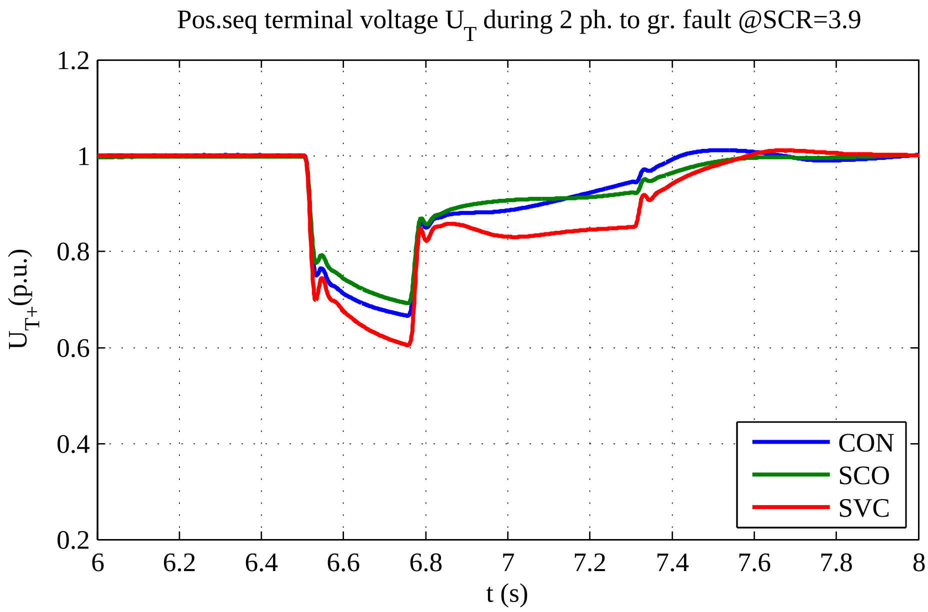

Figure 8.10: Positive sequence voltages of synchronous condensers and SVC - two phase to ground fault.

As can be observed from Figure 8.9 and Figure 8.10, phase voltages and hence the positive sequence voltage drops more with the SVC compared to synchronous condensers. Also, it can be seen that the positive sequence voltage reaches to the nominal value quicker with synchronous condensers.

From Figure 8.11, it is seen that the SVC injects less reactive power during and after the fault until the line is connected back. As the SVC provides reactive power proportional to the square of its terminal voltage, severe voltage drop on its terminals limits its reactive power injection.

As can be noticed from Figure 8.12, the speed of induction machines drops more with the SVC due to the lower positive sequence voltage.

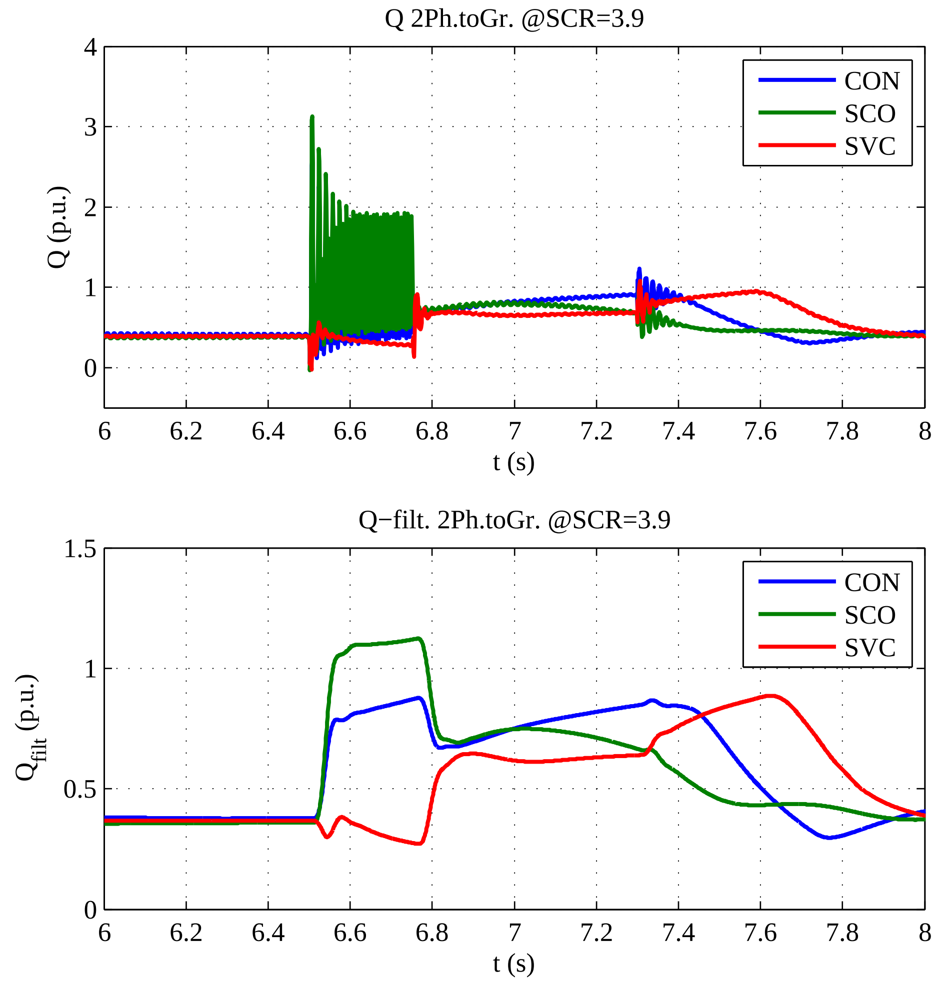

Figure 8.11: Reactive power injected (without filtering and filtered using low pass filter with 20 Hz cut-off frequency) by synchronous condensers and SVC - two phase to ground fault.

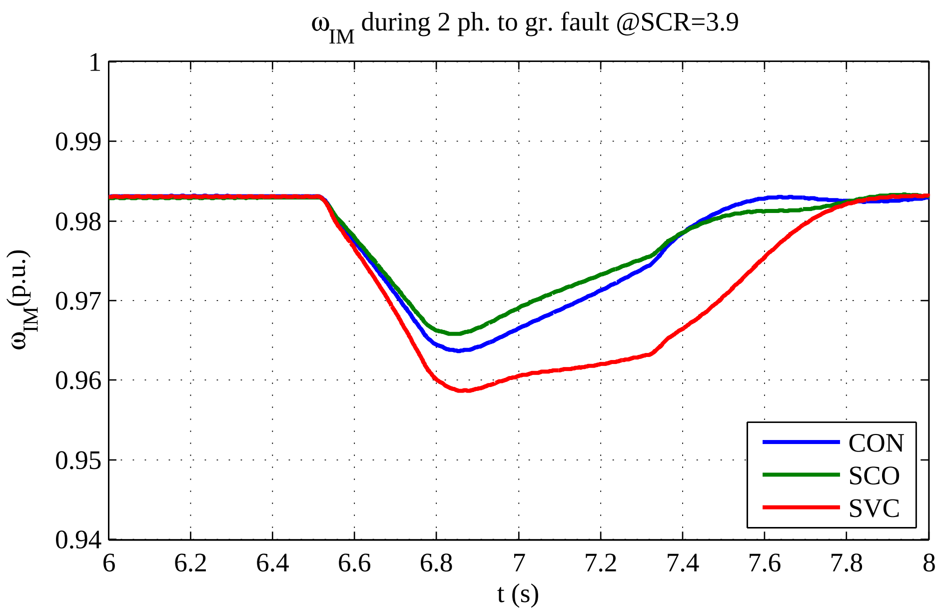

Figure 8.12: Speed of induction machines - two phase to ground fault.

Simulating the setup with a three phase to ground fault and keeping other parameters same as before, Figure 8.13, which shows positive sequence voltages of synchronous condensers and the SVC, Figure 8.14, which shows the reactive power injected by synchronous condensers and the SVC, Figure 8.15, which shows the speed of induction machines, are obtained:

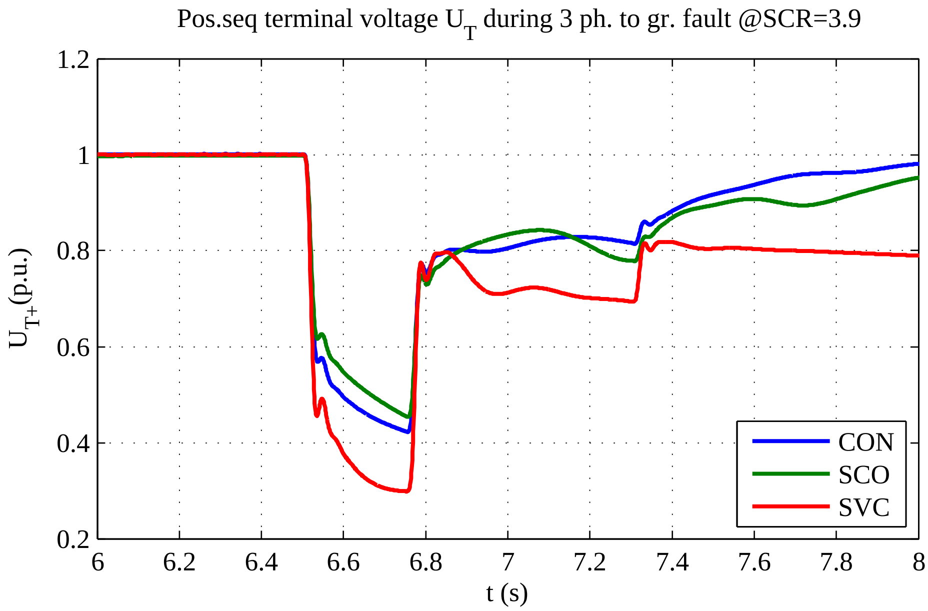

Figure 8.13: Positive sequence voltages of synchronous condensers and SVC - three phase to ground fault.

As can be seen from Figure 8.13, the positive sequence voltage drops even more with the SVC. Also it can be noticed that the system collapsed with the SVC.

It can be noticed from Figure 8.14, due to more voltage drop, the reactive power injected by the SVC decreases while the reactive power injected by synchronous condensers increases.

From Figure 8.15, it is observed that the speed of induction machines drops more with the SVC and hence induction machines can not recover their speed after the fault is cleared.

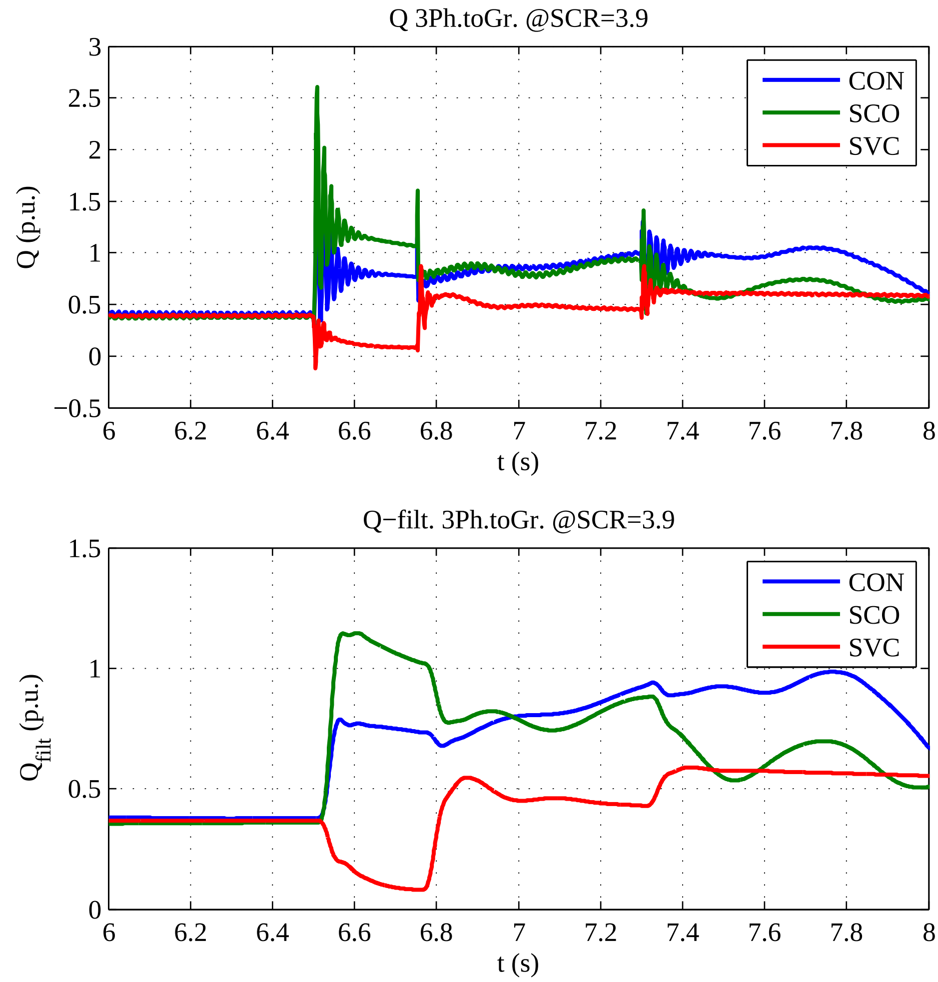

Figure 8.14: Reactive power injected (without filtering and filtered using low pass filter with 20 Hz cut-off frequency) by synchronous condensers and SVC - three phase to ground fault.

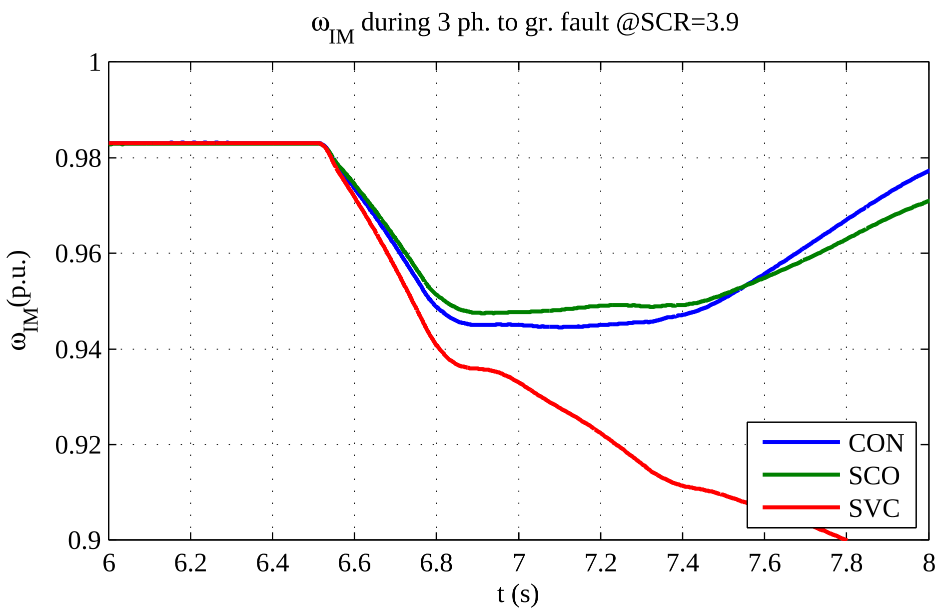

Figure 8.15: Speed of induction machines - three phase to ground fault.

To observe the effect of reactive power compensation on minimum voltage levels more clearly during different fault types, minimum positive sequence voltage levels at 36 kV bus during the fault are put on the following table:

Table 8.1: Minimum positive sequence voltage during the fault at 36 kV bus.

	Fault type	1ph	2ph	3ph
Min.ter. V(p.u.)				
With SVC		0.89	0.60	0.30*
With Conv. S.C.		0.89	0.67	0.42
With Super. S.C.		0.89	0.70	0.45

The maximum injected reactive power during the fault for the conventional synchronous condenser, the superconducting synchronous condenser and the SVC can be observed in the following table:

Table 8.2: Maximum injected reactive power by synchronous condensers and SVC during the fault

	Fault type	1ph	2ph	3ph
Injected Q(p.u.)				
SVC		0.67	0.48	0.10*
Conv. S.C.		0.54	0.69	0.74
Super. S.C.		0.54	0.93	1.07

It should be mentioned that the values marked with * are obtained with a 40 MVA SVC (where the system did not collapse) due to collapse with a 32 MVA SVC during the three phase to ground fault. It can be seen from Table 8.1 and Table 8.2 that the SVC injects more reactive power when there is less voltage drop on 36 kV bus whereas, when the voltage drops more, such as the case observed in two phase and three phase to ground faults, synchronous condensers inject more reactive power than the SVC.

8.2.2 Different Fault Location

To analyze the performance of the superconducting synchronous condenser, the conventional synchronous condenser and the SVC more deeply, the fault location is changed to 50 km from the source which corresponds to 25 % of the line length and 150 km from the source which corresponds to 75 % of the line length and a single phase to ground fault is simulated for the grid setup explained in the previous section. Figure 8.16, which shows the minimum value of positive sequence voltage at 36 kV bus, Figure 8.17, which shows the maximum reactive power injected by synchronous condensers and the SVC and Figure 8.18, which shows the minimum speed of induction machines, are obtained:

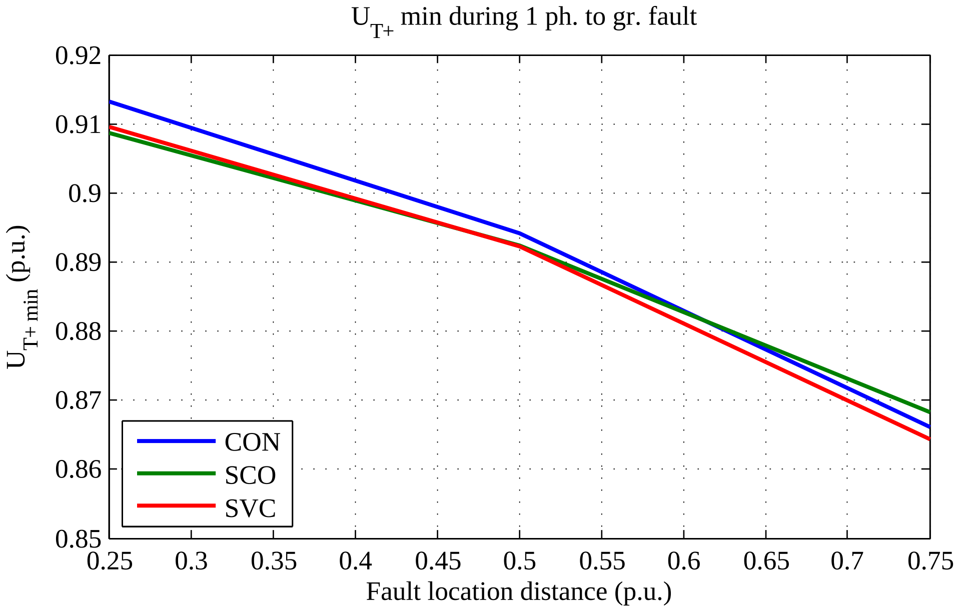

Figure 8.16: Minimum positive sequence voltage at 36kV bus - different fault location.

As can be noticed from Figure 8.16, the minimum positive sequence voltage drops more when the fault location gets far away from the source.

It can be seen from Figure 8.17 that the SVC injects more reactive power during and after the fault for all different fault locations.

The minimum speed of induction machines drops more when the fault is closer to the load which is seen in Figure 8.18. Also the speed with the SVC is higher due to bigger reactive power injection by the SVC.

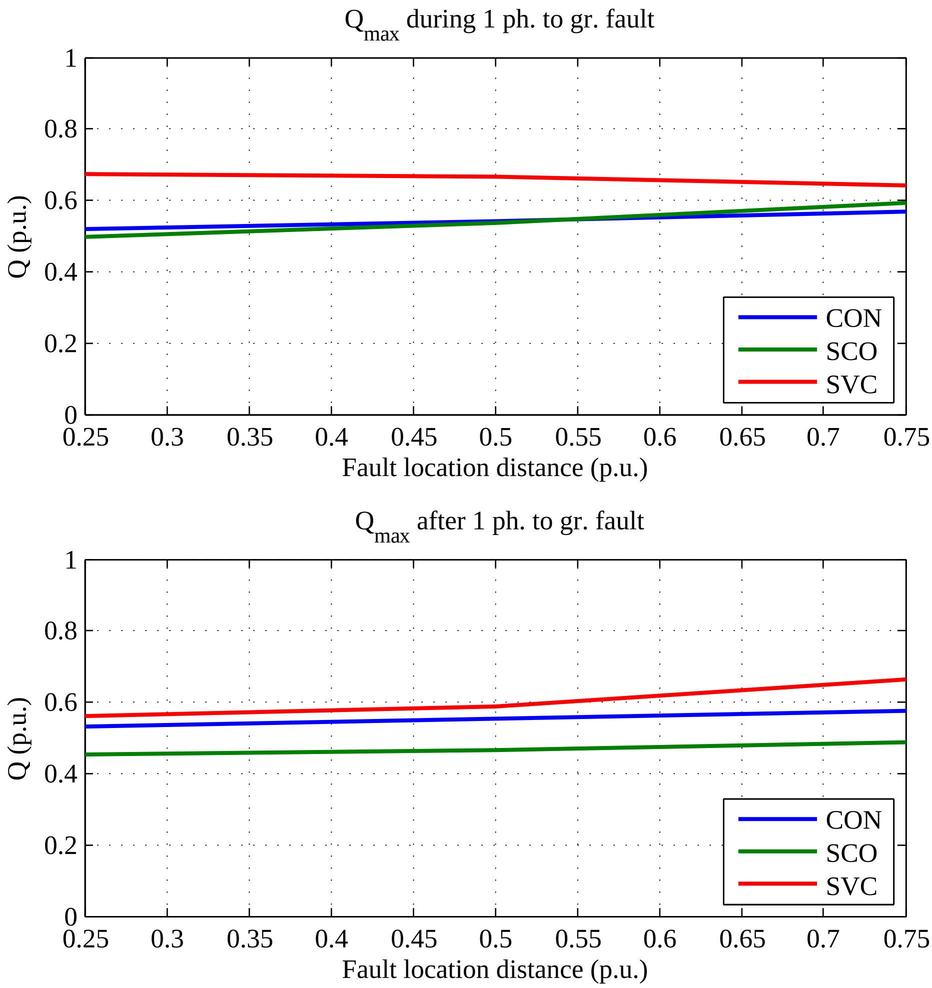

Figure 8.17: Maximum injected reactive power by synchronous condensers and SVC - different fault location.

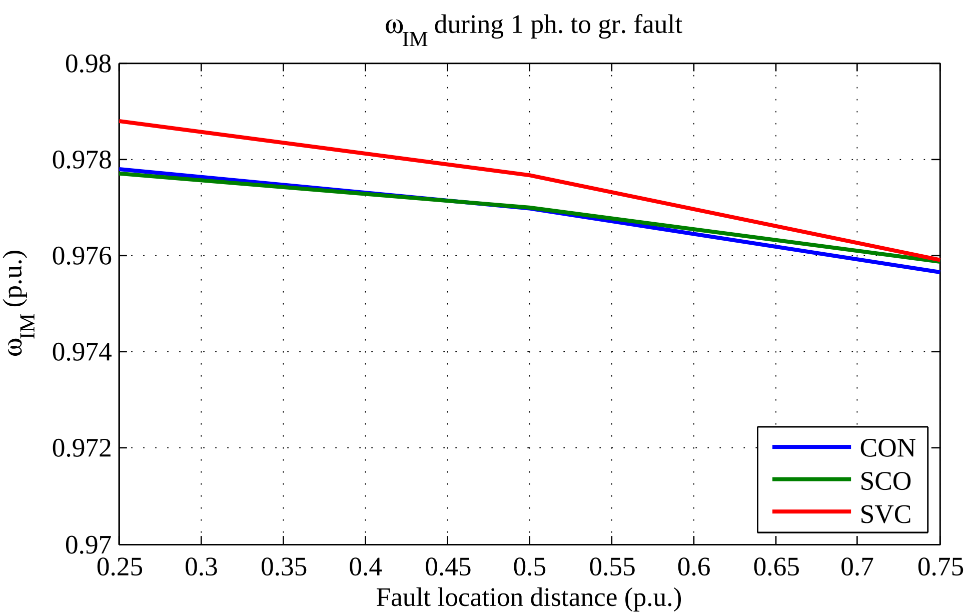

Figure 8.18: Minimum speed of induction machines - different fault location.

8.2.3 Different SCR

To observe the effect of different SCR, the short circuit capacity seen at 36 kV bus is changed to have an SCR of 2.4 (by doubling the line length to 400 km) and 5.8 (by halving the line length to 100 km). After simulating a single phase to ground fault while keeping all other values same, Figure 8.19, which shows the positive sequence voltage at 36 kV with an SCR of 2.4, Figure 8.20, which shows the positive sequence voltage at 36 kV with an SCR of 5.8 and Figure 8.21, which shows the maximum reactive power injected by synchronous condensers and the SVC, are obtained:

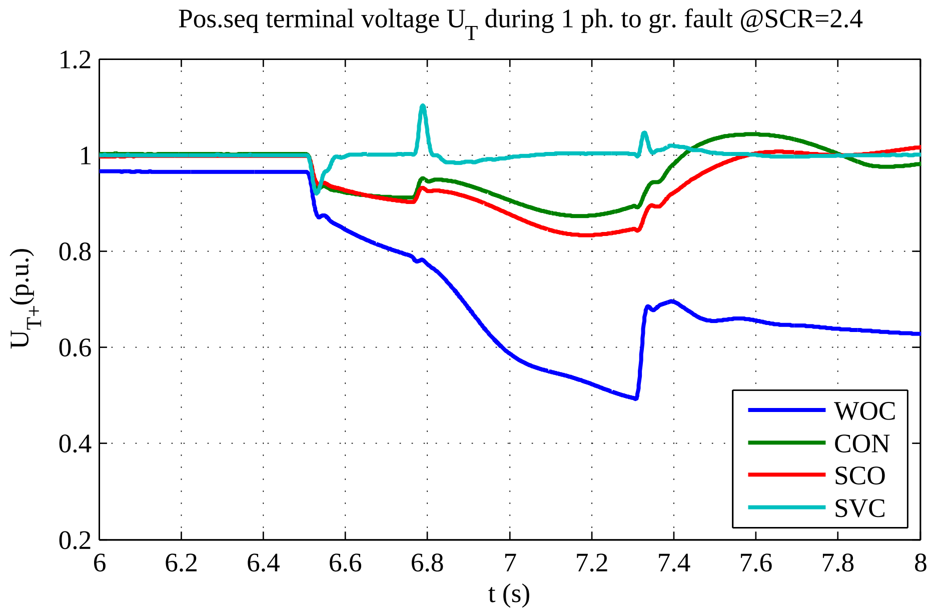

Figure 8.19: Positive sequence voltage at 36 kV bus - short circuit ratio=2.4.

Decreasing the SCR to 2.4 shows that it takes more time for synchronous condensers to bring the voltage level back to the nominal value, which is observed in Figure 8.19. Also it can be seen that the voltage during the fault drops only 10 % which represents small error for exciters resulting in very small increase in the field current. When the fault is cleared, induction machines begin to consume a lot of reactive power. Due to this and slow response of synchronous condensers for low voltage changes, the voltage continues to drop and it takes more time with synchronous condensers to bring the voltage back to the nominal value.

Again, it can be observed from Figure 8.20 that the SVC brings the voltage to the nominal value quicker. Also it is seen that the system without reactive power compensation also survives unlike other cases when the SCR is 5.8.

Injection of more reactive power by the SVC during and after the fault, which is seen in Figure 8.21, explains the reason for bringing of the voltage back to the nominal value quicker with the SVC which is seen in Figure 8.19 and Figure 8.20.

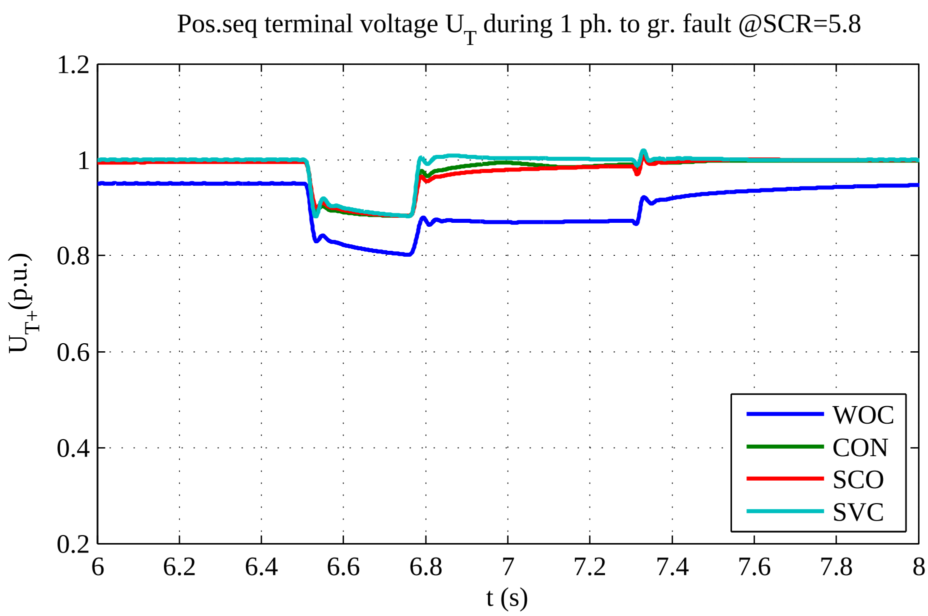

Figure 8.20: Positive sequence voltage at 36 kV bus - short circuit ratio=5.8.

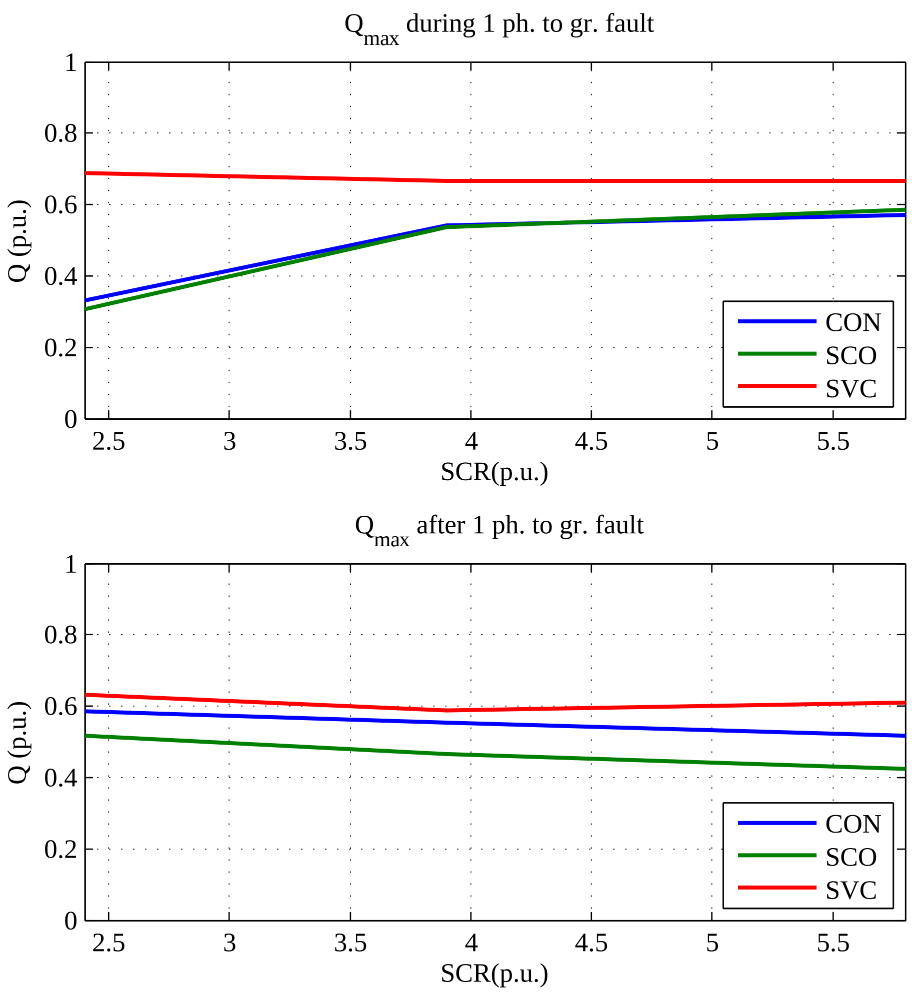

Figure 8.21: Maximum injected reactive power by synchronous condensers and SVC - different SCR.

8.2.4 Different Loading on Induction Machines

To observe the effect of different loading on induction machines on the performance of synchronous condensers and the SVC, the load torque of induction machines is decreased to 25 % of the rated load torque and Figure 8.22 and Figure 8.23 is obtained after simulations.

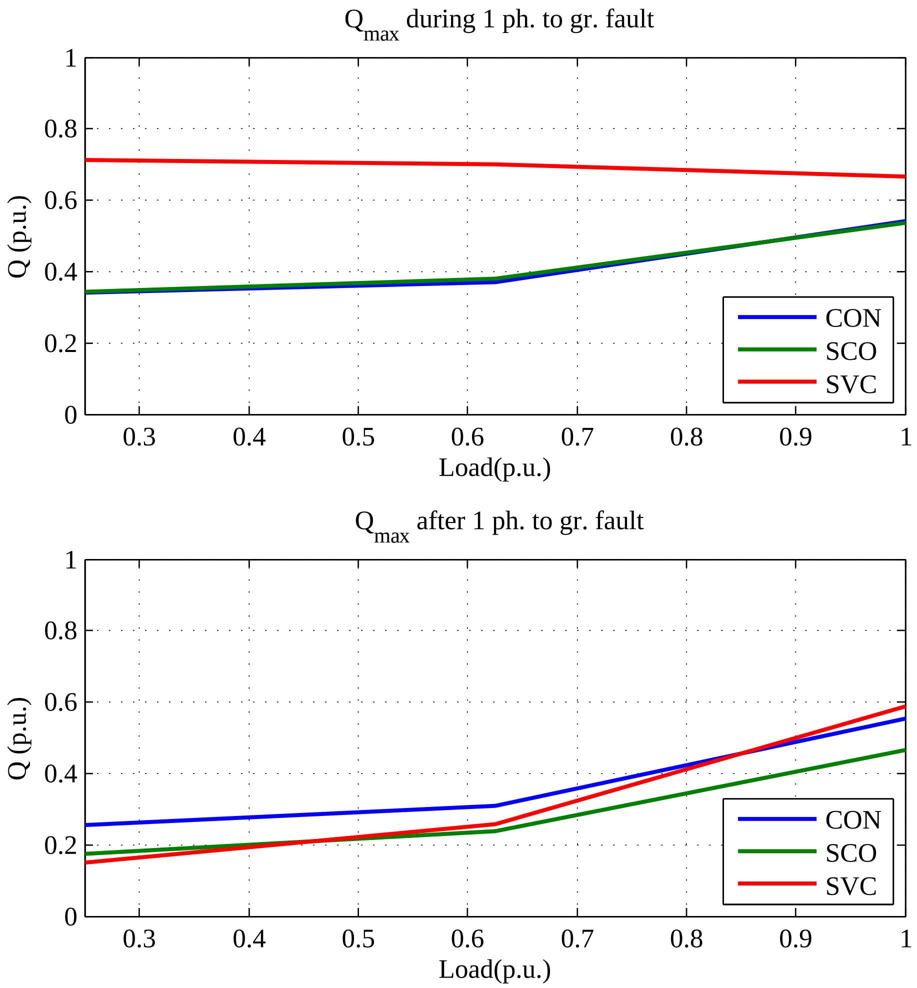

Figure 8.22: Maximum injected reactive power by synchronous condensers and SVC - different loading on induction machines.

For decreased loading, less voltage drop is obtained during the fault and therefore, the SVC injects more reactive power during the fault.

It can be noticed from Figure 8.23 that reactive power compensation units need to inject more reactive power with increasing loading.

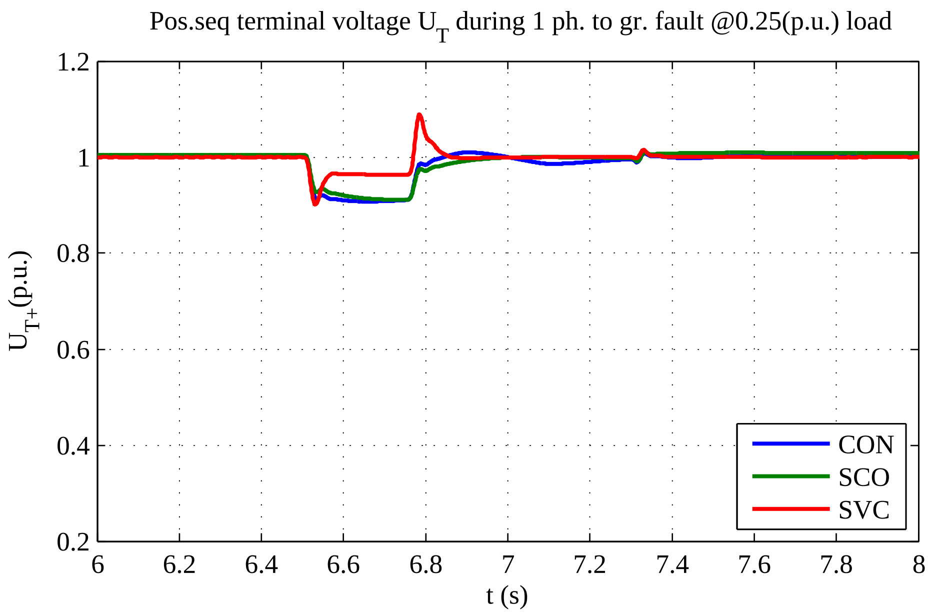

Figure 8.23: Positive sequence terminal voltage at 36 kV bus - 25 % loading on induction machines.

8.2.5 Different Load Type

To observe the effect of different load types on the performance of reactive power compensation units, the load torque characteristics of induction machines is changed from constant torque to ω^2 dependent torque, and for the other case, induction machines are replaced by a resistance and an inductance of 20.6 MW and 0.1 MVAr respectively to have mainly a resistive load. After simulating a three phase to ground fault, Table 8.3 and Table 8.4 are obtained:

Table 8.3: Minimum positive sequence voltage during the fault at 36 kV bus.

	Fault type	Resistive	$T = k\omega^2$	$T = k$
Min.ter. V(p.u.)				
With SVC		0.28	0.30	0.30*
With Conv. S.C.		0.45	0.42	0.42
With Super. S.C.		0.50	0.45	0.45

Table 8.4: Maximum injected reactive power by synchronous condensers and SVC during the fault

	Fault type	Resistive	$T = k\omega^2$	$T = k$
Injected Q(p.u.)				
SVC		0.11	0.10	0.10*
Conv. S.C.		0.68	0.74	0.74
Super. S.C.		1.10	1.07	1.07

It should be mentioned that the values marked with * are obtained with a 40 MVA SVC (where the system did not collapse) due to collapse with a 32 MVA SVC during the three phase to ground fault. From Table 8.3, it is seen that synchronous condensers keep the minimum voltage level higher due to the injection of more reactive power during the fault which is observed in Table 8.4.

8.3 Summary

Analyzing studies after simulating different parameters on the grid, it was observed that as SVC injects reactive power proportional to square of its terminal voltage, during faults that caused less voltage drop on its terminals, such as the case observed in single phase to ground faults, SVC showed a better performance, whereas during severe faults, such as two phase and three phase to ground faults, synchronous condensers brought the load voltage to the nominal value quicker.

Chapter 9

Conclusions and Suggestions

In this thesis, a synchronous condenser model is implemented into PSCAD/EMTDC and compared with the PSCAD built-in model. After verifying the model, a comparison between a conventional synchronous condenser and a superconducting synchronous condenser is made by simulating different type of faults, fault locations, short circuit ratios and other factors that affect the performance in a grid setup. Finally, a comparison between a conventional synchronous condenser, a superconducting synchronous condenser and an SVC is made in a grid setup by simulating different cases that affect the performance of reactive power compensation units.

9.1 Conclusions

From the results of the simulations, it is observed that:

- The difference between the implemented synchronous condenser model and PSCAD built- in model is less than 5 %, moreover, increasing the order of solver gives more accurate results, and the error introduced by terminating resistance can be neglected when using a time step less than 20 μs;
- During the faults, the superconducting synchronous condenser injects more reactive power than the conventional synchronous condenser due to its low synchronous reactance compared to the conventional synchronous condenser and hence, keeps the load voltage higher;
- As the SVC injects reactive power proportional to square of its terminal voltage, during faults that cause less voltage drop on its terminals, such as the case observed in single phase to ground faults, it shows a better performance, whereas during severe faults, such as two phase and three phase to ground faults, the synchronous condensers bring the voltage to the nominal value quicker;
- The performance of reactive power compensation units depend on several factors such as load type, short circuit ratio, fault type, fault location.

9.2 Suggestions

During simulations, several changes in the grid setup are made and effects of these changes are observed. For future study, other changes such as different fault duration, different X/R ratio of the source can be simulated in order to see effects on reactive power compensation units. Also, different case studies with different applications of reactive power compensation units can be studied. Furthermore, a detailed analysis including factors such as cost and reliability can be studied.

Bibliography

[1] S. Kalsi, "Development Status of Superconducting Rotating Machines", *IEEE PES Meeting*, New York, 27-31 January 2002

[2] T. J. Miller, *Reactive Power Control in Electric Power Systems*, New York,Wiley, 1982.

[3] E. Wanner, R. Mathys, and M. Hausler, "Compensation systems for industry," Brown Boveri Rev., vol. 70, pp. 330-340, Sep. /Oct. 1983.

[4] G. Bonnard, "The problems posed by electrical power supply to industrial installations," Proc. IEE Part B, vol. 132, pp. 335-340,Nov. 1985.

[5] A. Hammad and B. Roesle, "New roles for static VAR compensators in transmission systems," Brown Boveri Rev., vol. 73, pp. 314-320, Jun. 1986.

[6] N. Grudinin and I. Roytelman, "Heading off emergencies in large electric grids," IEEE Spectr., vol. 34, no. 4, pp. 43-47, Apr. 1997.

[7] C. W. Taylor, "Improving grid behavior," *IEEE Spectr.*, vol. 36, no. 6, pp. 40-45, Jun. 1999.

[8] Canadian Electrical Association, *Static compensators for reactive power control*, 1984.

[9] L. Gyugyi, "Reactive power generation and control by thyristor circuits," *IEEE Trans. Ind. Appl.*, vol. IA-15, no. 5, pp. 521-532,Sep./Oct. 1979.

[10] L. Gyugyi, R. Otto, and T. Putman, "Principles and applications of static, thyristor-controlled shunt compensators," *Trans. Power App. Syst.*, vol. PAS-97, no. 5, pp. 1935-1945, Oct. 1980.

[11] Y. Sumi, Y. Harumoto, T. Hasegawa, M. Yano, K. Ikeda, and T.Mansura, "New static VAR control using force-commutated inverters," *IEEE Trans. Power App. Syst.*, vol. PAS-100, no. 9, pp.4216-4223, Sep. 1981.

[12] C. Edwards, K. Mattern, E. Stacey, P. Nannery, and J. Gubernick, "Advanced static VAR generator employing GTO thyristors," *IEEE Trans. Power Del.*, vol. 3, no. 4, pp. 1622-1627, Oct. 1988.

[13] L. Walker, "Force-commutated reactive power compensator," *IEEE Trans. Ind. Appl.*, vol. IA-22, no. 6, pp. 1091-1104, Nov./Dec. 1986.

[14] K. E. Stahlkopf and M. R. Wilhelm, "Tighter controls for busier systems," *IEEE Spectr.*, vol. 34, no. 4, pp. 48-52, Apr. 1997.

[15] R. Grünbaum, Å. Petersson, and B. Thorvaldsson, *"FACTS, improving the performance of electrical grids"*, ABB Rev., pp. 11-18, Mar. 2003.

[16] N. Hingorani and L. Gyugyi, *Understanding FACTS, Concepts and Technology of Flexible AC Transmission Systems,* New York: IEEE Press, 2000.

[17] J. Dixon, L. Moran, E. Rodriguez, R. Domke, "Reactive power compensation technologies: state-of-the-art review," *IEEE Trans. Ind. Appl.*, vol. 93, no. 12, pp. 2144-2164, Dec. 2005.

[18] S. Kalsi et al., "Development status of rotating machines employing superconducting field windings," *Proc. IEEE,* vol. 92, no. 10, pp. 1688-1704, Oct. 2004.

[19] P. Kundur, *Power system stability and control,* McGraw-Hill, Inc. 1994

[20] IEEE Power Engineering Society, "IEEE Recommended Practice for Excitation System Models for Power System Stability Studies," *IEEE Std.* 421.5-2005.

[21] Westinghouse Electric Corporation, *Electric Transmission and Distribution Reference Book,* East Pittsburgh, Pa., 1964.

[22] E.W. Kimbark, *Power System Stability, Vol. 3: Synchronous Machines*, John Wiley & Sons, 1956.

[23] L. Gyugyi, *Solid-State Synchronous Voltage Sources for Dynamic Compensation and Real-Time Control of AC Transmission Lines*, IEEE Press, New Jersey, 1993.

[24] M.H. Rashid, *Power Electronics Handbook*, Academic Press, 2001

[25] M.H. Rashid, *Power Electronics Circuits, Devices, and Applications*, Pearson Education, Inc. 2004

[26] T. Thiringer, "Measurements and Modeling of Low-Frequency Disturbances in Induction Machines," Nov. 1996.

[27] IEEE Power Systems Engineering Committee, "Application of SVC for System Dynamic Performance," IEEE Special Publication 87TH0187-5-PWR. 1987.

[28] I. A. Erinmez, "Static Var Compensators", CIGRE working group 38-01, Task Force No.2 on SVC, 1986.

[29] Y. H. Song and A. T. Johns, *Flexible AC Transmission Systems (FACTS),* IEE Press, London, U.K., 1999.

[30] R. Mathur and K. Varma, *Thyristor-Based FACTS Controllers for Electrical Transmission Systems,* IEEE Press, USA, 2002.

[31] R.T. Byerly, D.T. Pozniak, E.R. Taylor, "Static Reactive Compensation for Power Transmission Systems," *IEEE PES Winter Power Meeting*, 1982.

[32] H. Frank and S. Ivner, "Thyristor Controlled Shunt Compensation in Power Networks", ASEA Journal, Volume 54, No. 5-6, 1981.

[33] L. Gyugyi, "Fundamentals of Thyristor Controlled Static Var Compensators in Electric Power System Applications," *IEEE Special Publication*, Application of Static Var Systems for System Dynamic Performance, 1987, pp. 8-27.

[34] N. G. Hingorani and L. Gyugyi, *Understanding FACTS,* IEEE Press, New York, 1999

[35] H.J. Lee, W.E. Schiesser, *Ordinary and Partial Differential Equation Routines in C, C++, Fortran, Java, Maple, and MATLAB*, Chapman & Hall/CRC,2004.

[36] Manitoba HVDC Research Centre Inc., *EMTDC User's Guide*, 2004.

[37] J. Luomi, *Transient Phenomena in Electrical Machines*, Chalmers University of Technology, 1998.

Appendix A

Coordinate Transformations

To transform three phase stator quantities to two axis stationary quantities following equations are used (ignoring zero sequence component):

$$\begin{bmatrix} u_\alpha \\ u_\beta \end{bmatrix} = \begin{bmatrix} \frac{2}{3} & \frac{-1}{3} & \frac{-1}{3} \\ 0 & \frac{1}{\sqrt{3}} & \frac{-1}{\sqrt{3}} \end{bmatrix} \times \begin{bmatrix} u_\mathrm{a} \\ u_\mathrm{b} \\ u_\mathrm{c} \end{bmatrix} \tag{A.1}$$

To transform stationary two phase quantities to two phase quantities rotating with synchronous speed following equations are used:

$$\begin{bmatrix} u_\mathrm{d} \\ u_\mathrm{q} \end{bmatrix} = \begin{bmatrix} \cos\theta & \sin\theta \\ -\sin\theta & \cos\theta \end{bmatrix} \times \begin{bmatrix} u_\alpha \\ u_\beta \end{bmatrix} \tag{A.2}$$

To obtain abc quantities from dq quantities following equations are used:

$$\begin{bmatrix} u_\alpha \\ u_\beta \end{bmatrix} = \begin{bmatrix} \cos\theta & -\sin\theta \\ \sin\theta & \cos\theta \end{bmatrix} \times \begin{bmatrix} u_\mathrm{d} \\ u_\mathrm{q} \end{bmatrix} \tag{A.3}$$

$$\begin{bmatrix} u_\mathrm{a} \\ u_\mathrm{b} \\ u_\mathrm{c} \end{bmatrix} = \begin{bmatrix} 1 & 0 \\ \frac{-1}{2} & \frac{\sqrt{3}}{2} \\ \frac{-1}{2} & \frac{-\sqrt{3}}{2} \end{bmatrix} \times \begin{bmatrix} u_\alpha \\ u_\beta \end{bmatrix} \tag{A.4}$$

Appendix B

Per Unit Calculations

Per unit values are commonly used in the analysis of electrical machines such as synchronous machines. The parameters of different electrical machines of the same machine type vary in a narrow range when p.u. values are used. Hence, it is easy to compare machines with different nominal voltage, power and speed [26].

Per unit values are calculated by dividing each quantity by a base value. The base values used are chosen as follows:

- The amplitude of the nominal phase voltage, $\sqrt{2}U_{\mathrm{nph}}$.
- The peak value of the nominal stator current, $\sqrt{2}I_{\mathrm{n}}$.
- The impedance corresponding to nominal voltage and current, $U_{\mathrm{nph}}/I_{\mathrm{n}}$
- The apparent power corresponding to the nominal voltage and current, $3U_{\mathrm{nph}}I_{\mathrm{n}}$
- The torque corresponding to nominal apparent power and frequency, $3U_{\mathrm{nph}}I_{\mathrm{n}}/(\omega_{\mathrm{n}}/p)$
- The field current $I_{\mathrm{f}b} = \sqrt{2}U_{\mathrm{n}ph}/(\omega_{\mathrm{s}}L_{\mathrm{m}d})$
- The field voltage $U_{\mathrm{f}b} = I_{\mathrm{f}b}R_{\mathrm{f}}$

Using these base values, per unit resistances and inductances are calculated as follows:

$$r_{\mathrm{s}} = \frac{I_{\mathrm{n}}R_{\mathrm{s}}}{U_{\mathrm{nph}}} \tag{B.1}$$

$$l_{\mathrm{m}} = \frac{\omega_{\mathrm{n}}I_{\mathrm{n}}}{U_{\mathrm{nph}}}L_{\mathrm{m}} = \frac{I_{\mathrm{n}}}{U_{\mathrm{nph}}}X_{\mathrm{m}} = x_{\mathrm{m}} \tag{B.2}$$

It is observed that per unit inductances are equal to per unit reactances from the above equations.

Appendix C

Synchronous Condenser Parameters

During the simulations, values given in Table C.1 and Table C.2 are used for calculating parameters for the conventional synchronous condenser:

Table C.1: Parameters of the conventional synchronous condenser

S_{B}	8.0	MVA
$U_{\text{L-L}}$	13.8	kV
f	60.0	Hz
L_{d}	1.6	p.u
L_{q}	1.1	p.u
L''_{d}	0.2	p.u
L''_{q}	0.29	p.u
L_{sl}	0.06	p.u
R_{a}	0.008	p.u
T'_{d}	1.5	s
T'_{d0}	7.0	s
T''_{d}	0.02	s
T''_{q}	0.043	s

Table C.2: Saturation data

$i_{\mathrm{m}}(p.u.)$	0	0.5	0.8	1.0	1.2	1.5	1.8	2.2	3.2	4.2
$V_{\mathrm{t}}(p.u.)$	0	0.5	0.79	0.947	1.076	1.2	1.26	1.32	1.53	1.74

The parameters given in Table C.3 are used for the exciter of the conventional synchronous condenser (according to Figure 3.5).

Table C.3: Exciter parameters for the conventional synchronous condenser

T_{C}	0.1	s
T_{B}	0.2	s
K_{A}	300	p.u.
T_{A}	0.001	s
U_{RMAX}	6	p.u.
U_{RMIN}	-6	p.u.
T_{E}	0.001	s
K_{E}	0	p.u.
E_{FD1}	0.279	p.u.
$S_{\mathrm{E1}}(E_{\mathrm{FD1}})$	3.05	p.u.
E_{FD2}	0.117	p.u.
$S_{\mathrm{E2}}(E_{\mathrm{FD1}})$	2.29	p.u.
K_{F}	0.001	p.u.
T_{F}	0.1	s

During the simulations, values given in Table C.4 are used for calculating parameters for the superconducting synchronous condenser:

Table C.4: Parameters of the superconducting synchronous condenser

S_{B}	8.0	MVA
$U_{\mathrm{L\text{-}L}}$	13.8	kV
f	60.0	Hz
L_{d}	0.5	p.u
L_{q}	0.35	p.u
L''_{d}	0.11	p.u
L''_{q}	0.12	p.u
L_{sl}	0.1	p.u
R_{a}	0.007	p.u
T'_{d}	7.31	hr
T'_{d0}	15.55	hr
T''_{d}	0.02	s
T''_{q}	0.043	s

The parameters given in Table C.5 are used for the exciter of the superconducting synchronous condenser (according to Figure 3.6):

Table C.5: Exciter parameters for the superconducting synchronous condenser

T_{C}	0.9	s
T_{B}	0.09	s
K_{A}	60000	p.u.
T_{A}	0.1	s
K_{F}	0	p.u.
T_{F}	0	s
U_{AMAX}	18000	p.u.
U_{AMIN}	-18000	p.u.
U_{RMAX}	1E5	p.u.
U_{RMIN}	-1E5	p.u.
I_{LR}	4.4	p.u.
K_{LR}	4.54	p.u.

Appendix D

Saturation curve extrapolation

In our model extrapolation is used for the main flux saturation curve definition. This leads to simplification of equations that describe saturation curve since the saturation curve has two distinct linear regions, one before the saturation commences and another one when the flux is fully saturated. The middle part is extrapolated using 2^{nd} order polynomial. This simplification yields in following results for the tangential magnetizing inductance equations that are used for the saturated main flux calculation.

$L_{\mathrm{mt}}(i_{\mathrm{m}}) = L_{\mathrm{md}}$ unsaturated for $i_{\mathrm{m}} < i_1$

$L_{\mathrm{mt}}(i_{\mathrm{m}}) = L_{\mathrm{md}}(L_{\mathrm{msat}}/L_{\mathrm{md}} - 1)/(i_2 - i_1)i_{\mathrm{m}} + L_{\mathrm{md}}(i_2 - i_1 L_{\mathrm{msat}}/L_{\mathrm{md}})/(i_2 - i_1)$ for $i_1 < i_{\mathrm{m}} < i_2$

$L_{\mathrm{mt}}(i_{\mathrm{m}}) = L_{\mathrm{msat}}$ for $i_{\mathrm{m}} > i_2$

Where, i_1 is the value of magnetizing current at the end of first linear region, L_{msat} represents the slope of the $\Psi_{\mathrm{m}}(i_{\mathrm{m}})$ and i_{m} curve in the fully saturated region and i_2 is the value of the magnetizing current when curve enters fully saturated region.

This means that we can extrapolate saturation curve knowing only three saturation parameters, $L_{\mathrm{msat}}/L_{\mathrm{md}}$ ratio, which is equal to L_{msatpu}, i_1 and i_2.

For the saturation curve given in table C.2 following saturation parameters have been calculated

$$\begin{array}{lcll} L_{\mathrm{msatpu}} & = & 0.166 & \text{[p.u.]} \\ i_1 & = & 0.650 & \text{[p.u.]} \\ i_2 & = & 1.650 & \text{[p.u.]} \end{array}$$

Error of the extrapolated saturation curve in measured points is presented in table D.1

Table D.1: Extrapolation error

$i_{\mathrm{m}}(p.u.)$	0	0.5	0.8	1.0	1.2	1.5	1.8	2.2
$V_{\mathrm{t}}(p.u.)$	0	0.5	0.79	0.947	1.076	1.2	1.26	1.32
$V_{\mathrm{t}}(p.u.) - (extr.)$	0	0.5	0.7906	0.9489	1.0739	1.1987	1.2579	1.3243
Error (%)	0	0	0.06	0.19	0.21	0.13	0.21	0.43